Aus dem Institut für Physik der Universität Potsdam

Multistable systems under the influence of noise

Dissertation

zur Erlangung des akademischen Grades
Doktor der Naturwissenschaften
(Dr. rer. nat.)
in der Wissenschaftsdisziplin Theoretische Physik

eingereicht an der
Mathematisch–Naturwissenschaftlichen Fakultät
der Universität Potsdam

von
Suso Kraut

Potsdam, im Dezember 2001

Contents

Chapter 1

Introduction

In the present work the effects of noise on multistable nonlinear systems are analyzed, thus combining nonlinear dynamics with classical stochastic theory.

Multistable systems, i.e. systems with a large number of coexisting stable states, are very common in nature. While bistable systems have been investigated in the physical literature for a very long time, multistable systems are the subject of increasing interest only in the last two decades. It has been the discovery of multiple stable states in laser systems (Kitano et al., 1981; Agarwal, 1982; Arecchi et al., 1982; Wiesenfeld et al., 1990; Brambilla et al., 1991) that triggered the research in many other fields. As a result, multistable behavior was found in a wide range of different areas of science. These include ocean circulation (Thual & McWilliams, 1992; Rahmstorf, 1995), ecosystems (Scheffer, 1990), neuroscience (Schiff et al., 1994; Foss et al., 1996), and chemistry (Marmillot et al., 1991; Hunt et al., 1992). Multistable behavior was also reported in mechanical systems (Ryabov & Ito, 1995), semiconductor physics (Prengel et al., 1994), plasma physics (Chern & I, 1991), solid state physics (Carroll et al., 1987), for coupled oscillators (Wiesenfeld & Hadley, 1989), and time delay systems (Kim et al., 1997a). Likewise, multistability arises in the dynamics of the Duffing oscillator with a double-well potential (Arecchi et al., 1985) and in discrete maps, describing physical systems (Hénon, 1976; Ikeda, 1979; Grebogi et al., 1987a; Feudel et al., 1996). Since the phenomenon of multistability appears to be very common in nature, it is naturally to study its properties in detail.

Another important feature of physical systems is the presence of noise. Perturbations to a system, which are either of random nature or can be modeled as random, are practically inevitable. Every measurement of a macroscopic physical system is necessarily contaminated with noise. These processes are usually described by Langevin and Fokker-Planck equations (Risken, 1989). The addition of noise to a physical model has also led to several interesting phenomena (van Kampen, 1983),

most notably noise-induced transitions (Horsthemke & Lefever, 1984). With the development of the theory of nonlinear dynamical systems, the role of noise was intensively studied (Crutchfield et al., 1982), whereby main focus was laid on the smoothing of the invariant density through noise and the noise-scaling behavior of bifurcations. This has also been undertaken with mathematical rigor (Arnold, 1998). Today, noise in nonlinear dynamical systems is a well established field of research (Moss & McClintock, 1989; Millonas, 1996).

The influence of noise on dynamical systems has several, sometimes counterintuitive consequences, which could not take place, if the governing equations were linear. The most prominent phenomenon is stochastic resonance, where the addition of noise to a periodically driven system produces a maximum of the signal-to-noise ratio at a particular noise value (Benzi et al., 1981; Gammaitoni et al., 1998). Further effects are coherence resonance (Pikovsky & Kurths, 1997), noise-induced order (Matsumoto & Tsuda, 1983), noise-induced chaos (Iansiti et al., 1985), noise-induced stabilization (Wackerbauer, 1995), noise enhanced stability (Mantegna & Spagnolo, 1996; Mielke, 2000), noise-induced chaos-order transitions (Gassmann, 1997), noise-induced nonequilibrium phase transitions (Van den Broeck et al., 1994), and noise suppression by noise (Vilar & Rubí, 2001). This enumeration demonstrates, that noise introduces a plethora of phenomena in nonlinear systems that are a topic of utmost interest and the subject of ongoing research.

The present work aims at the study of the effects of noise on multistable nonlinear systems. The first investigation of the role of noise on a system exhibiting 'generalized' multistability was performed in (Arecchi et al., 1985), addressing the question of jumps between the metastable states induced by noise. The term 'generalized' is used in order to distinguish it from the bistable case. It has also been found, that noise can induce multistability in a laser system (Barbéroshie et al., 1993) and in coupled oscillators (Kim et al., 1997b). Moreover, noise-induced selection of attractors in coupled systems was detected (Kaneko, 1997). The jumping between metastable states, also called attractor-hopping, is related to the phenomenon of 'chaotic itinerancy', which occurs in laser systems (Ikeda et al., 1989; Otsuka, 1990) and has been confirmed experimentally as well (Arecchi et al., 1990).

Although a generally accepted definition of complexity is still missing, many different proposals for its definition have been put forward (Badii & Politi, 1997). One of these suggestions states, that a system is complex if it (i) is composed of many parts that are interacting in a complicated manner, (ii) possesses both ordered and random behavior, and (iii) exhibits a hierarchy of structures; that is, nontrivial structures exist over a wide range of time and/or length scales (Grassberger, 1989b). It

has been pointed out in (Poon & Grebogi, 1995), that the noise-induced attractor-hopping process in a multistable system with a fractal basin boundary separating the metastable states can be considered as complex dynamics in the above stated sense. The first point is fulfilled through the coexistence of many stable states. The second condition applies, since ordered behavior takes place close to the metastable states and random behavior on the fractal basin boundary, or, more specific, on the chaotic saddles embedded in the fractal basin boundary. Finally, the metastable states are grouped in a hierarchical manner, as they originate from a complicated bifurcation scenario. Typically, the stability with respect to random perturbations differs for the various metastable states.

In this work, the attractor-hopping process in complex systems with fractal basin boundaries is scrutinized and the crucial role of chaotic saddles, residing on the fractal basin boundary, is elucidated. They are responsible for the new phenomenon of preference of attractors. Utilizing the tools of symbolic dynamics, the importance of bifurcations of the chaotic saddles for the complexity of the attractor-hopping process is emphasized. Furthermore, the role of chaotic saddles for the noise-induced escape process out of a metastable state is exposed. This is done using the theory of quasipotentials (Graham & Tél, 1984; Graham et al., 1991; Hamm & Graham, 1992a), which defines a potential for nonequilibrium systems and maps, which were otherwise not describable in the framework of potentials. Quasipotentials allow to calculate the scaling of noise on invariant densities and escape processes. In this study, they are used to establish the novel phenomenon of enhancement of noise-induced escape through the existence of chaotic saddles. This phenomenon is remarkable since it occurs even in the case, when the chaotic saddle is completely embedded in the open neighborhood of the basin of attraction of one attractor and the basin boundary is not fractal.

This work is organized as follows: Chapter 2 introduces the dissipative standard map as a paradigmatic model for multistable behavior. After the derivation of the map from the well known standard map, its basic properties are presented. The number of coexisting stable states is very large (> 100). Addition of noise leads to several interesting consequences, in particular noise-induced chaos and attractor-hopping. Both effects are treated quantitatively with the help of Lyapunov exponents, including finite-time Lyapunov exponents. With these tools the noise-induced transition into chaos is unveiled. The existence of spectra with a $1/f$ divergence is shown, and necessary conditions for their occurrence are discussed, which have been proposed only for bistable systems up to now. Noise-induced preference of attractors is found, implying that some attractors become more likely to occur for a random initial condition. They attain a maximum probability of occurrence at a certain noise level,

to the disadvantage of other attractors, with a decreasing likelihood of appearance. By increasing the noise strength, some attractors become even extinct, completely 'hidden' by the noise. The mechanism for this effect to take place is explained, consisting of a combination of the structure of chaotic saddles on the basin boundary and the different sizes of the basins of attraction. This mechanism is pointed out to be distinct from the phenomenon of noise-induced selection of attractors in coupled systems (Kaneko, 1997), since the attractors in both cases have qualitatively different stability properties. In our case, the metastable states are surrounded by an open neighborhood of the basin of attraction, rendering the effect much more nontrivial. The problem of noise-induced escape out of a metastable state is examined in an elementary fashion, which was hitherto only executed for bistable systems (Kautz, 1988; Beale, 1989; Grassberger, 1989a). Finally, the relationship between the attractor-hopping process and chaotic saddles is investigated, which is done in much more detail in the next chapter for a different system.

Since for the dissipative standard map the attractor-hopping process and its connection to chaotic saddles is too involved to unveil the structure in detail, Chapter 3 introduces as a simpler, yet still complex, model two coupled logistic maps. The complexity of the hopping process is analyzed by employing symbolic dynamics and by computing the Shannon entropy and the topological entropy to provide a measure of complexity. With the variation of a parameter, a steep increase of the topological entropy at a certain parameter value suggests a change in the dynamics of the system. This change is due to a bifurcation of chaotic saddles. This novel bifurcation is explored in detail. The most prominent new feature is a merging of two chaotic saddles accompanied by the emergence of additional points filling the gap between the formerly separated saddles. This bifurcation is mediated by a snap-back repellor, whose properties are explained. Finally, scaling laws for the transient life-times on one chaotic saddle and the increase of the fractal dimension of the connected chaotic saddle slightly above the bifurcation point are presented, involving the eigenvalues of the mediating repellor in analogy to crisis. Both scaling laws should be observable in experiments.

Chapter 4 deals with noise-induced escape out of a metastable state. This question was already treated in Chapter 2 for the dissipative standard map in a preliminary way. Here we give a more detailed account of this problem and present in particular the new phenomenon of enhancement of noise-induced escape through the existence of chaotic saddles, as a parameter is varied. First, the noise-induced escape problem is exposed for nonequilibrium systems, and recent progress in this field is presented, with emphasis on the prehistory probability density and the most probable exit path. Then the theory of quasipotentials is introduced as a minimization method

and its main features are explained. After describing the Ikeda map, which is a basic model for a laser cavity with a delay, the new phenomenon of enhancement of noise-induced escape through the existence of chaotic saddles is shown to occur for this system. The effect can be explained utilizing the theory of quasipotentials, which is demonstrated in detail. This effect is of importance for optical systems with delay described by the Ikeda map. It should be detectable in experiments and is supposed to occur in other systems of physical relevance as well.

Finally, in Chapter 5, the results of this work are summarized, discussed and some directions for future work are proposed.

Chapter 2

A basic model of multistable behavior under the influence of noise

In this Chapter a prototype model of a multistable system under the influence of noise is investigated. The basic model without noise exhibits not only a very large number of coexisting states, where the specific number depends on the choice of the parameters, but also a fractal basin boundary separating these states. Thus, there exist two distinct sources of complex behavior in the system: The accessibility to many different states because of the multistability and the final state sensitivity due to the fractal basin boundary.

The addition of noise has several consequences, which are described in this Chapter. In Section 2.1 the dissipative standard map as a basic model is introduced and the most relevant properties are presented. Section 2.2 deals with the most important consequences through the addition of noise to the system, namely noise-induced chaos and attractor-hopping. Both effects are treated quantitatively with the help of Lyapunov exponents in Section 2.2.1, where also finite-time Lyapunov exponents are considered, and the noise-induced transition into chaos is elucidated. In Section 2.2.2 the existence of spectra with a $1/f$ divergence is shown, and necessary conditions for their occurrence are discussed. The next Section 2.2.3 establishes the effect of noise-induced preference of attractors, while in 2.2.4 the problem of noise-induced escape out of a metastable state is studied in an elementary fashion. A more detailed account of this topic is given in Chapter 4. Finally, Section 2.2.5 is dedicated to the relationship between the attractor-hopping process and chaotic saddles. The content of this Chapter has been published in (Kraut et al., 1999)

2.1   The dissipative standard map

As our basic model of multistable behavior, we investigate a two-dimensional map, which describes the time evolution of a mechanical pendulum, with no gravity and friction at the pivot (Zaslavskii, 1978; Ott, 1993). There is a bar of moment of inertia E and length l, which is fastened at one end to a frictionless pivot. The other end is subjected to a periodic impulsive force of impulse strength f_0/l applied at discrete times $t = 0, \tau, 2\tau, ...$ and from a fixed direction. The system is regarded to be without gravity. Using canonically conjugate variables p_θ (representing the angular momentum) and θ (the angular position of the rotor), we have that the Hamiltonian for this system and the corresponding equations of motions obtained from Hamilton's equations

$$
\begin{align}
d\mathbf{p}/dt &= -\partial H(\mathbf{p}, \mathbf{q}, t)/\partial \mathbf{q} \tag{2.1}\\
d\mathbf{q}/dt &= \partial H(\mathbf{p}, \mathbf{q}, t)/\partial \mathbf{p} \tag{2.2}
\end{align}
$$

are given by

$$
\begin{align}
H(p_\theta, \theta, t) &= p_\theta^2/(2E) + f_0 \, \cos(\theta) \sum_k \delta(t - k\tau) \tag{2.3}\\
d(p_\theta)/dt &= f_0 \, \sin(\theta) \sum_k \delta(t - k\tau)\\
d(\theta)/dt &= p_\theta/E,
\end{align}
$$

where $\delta(...)$ denotes the Dirac delta function. From Eqs. (2.3) we see that p_θ is constant between the kicks but changes discontinuously at each kick. The position variable θ varies linearly with t between the kicks (since p_θ is constant) and is continuous at each kick. Examining the values p_θ and θ just after each kick builds the surface of section. Let p_k and θ_k denote the values of p_θ and θ at times $t = k\tau + 0^+$, where 0^+ denotes a positive infinitesimal. By integrating the equation for $d(p_\theta)/dt$ through the delta function at $t = (k+1)\tau$, we then obtain

$$
p_{k+1} - p_k = f_0 \, \sin(\theta_{k+1}) \tag{2.4}
$$

and from the equation for $d(\theta)/dt$

$$
\theta_{k+1} - \theta_k = p_k \tau/E. \tag{2.5}
$$

Without loss of generality we can take $\tau/E = 1$ to arrive at the map

$$
\begin{align}
\theta_{k+1} &= \theta_k + p_k (\text{mod } 2\pi) \tag{2.6}\\
p_{k+1} &= p_k + f_0 \, \sin(\theta_k + p_k), \tag{2.7}
\end{align}
$$

where we have added a modulo 2π, since θ is an angle, and we wish to restrict its values to be between zero and 2π.

This is the well known standard map (Chirikov, 1979; Greene, 1979; Schmidt, 1980), which has been intensively studied (Lichtenberg & Liebermann, 1992), and plays a fundamental role in understanding the transition in Hamiltonian systems from regular to chaotic motion. The standard map is believed to possess infinitely many stable but nonattracting periodic orbits. The two eigenvalues of these periodic orbits are complex conjugate but their absolute values are exactly 1. In the vicinity of these marginally stable periodic orbits, there exists regular motion on the invariant Kolmogorov-Arnold-Moser (KAM) tori. Around these islands of stability there also exist regions in the phase space with persistent chaotic motion. Depending on the parameters, these areas of different dynamical behavior can be complexly interwoven. In Fig. 2.1 the phase portrait is shown for $f_0 = 3.5$. The dynamics takes
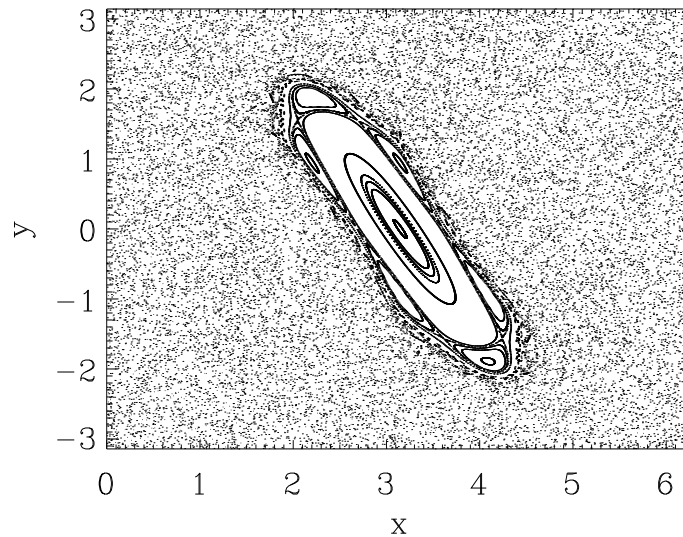

Figure 2.1: Phase portrait of the Hamiltonian standard map ($\nu = 0$) with $f_0 = 3.5$. Chaotic motion exists around the islands of stability.

place on the torus $[0, 2\pi] \times [-\pi, \pi]$. In particular, the family of period 1 orbits is given by $(x = \pi, y = m2\pi), m = 0, \pm1, ...$, which are, due to mod 2π also in the y coordinate, all mapped onto the one with $m = 0$. Orbits of higher periods, so-called secondary islands, are grouped around these period 1 orbits, which correspond to primary islands. These islands around islands build a highly intricate hierarchy.

However, we are interested in the dissipative form of the standard map, which we get by introducing a dissipation parameter ν, which corresponds to the consideration of

dissipation at the pivot. Doing this, and writing x for θ and y for p, results in

$$
\begin{aligned}
x_{k+1} &= x_k + y_k \,(\mathrm{mod}\,2\pi) \\
y_{k+1} &= (1-\nu)\,y_k + f_0 \sin(x_k + y_k).
\end{aligned}
\tag{2.8}
$$

The limit $(\nu = 0)$ corresponds to the Hamiltonian standard map, while the other limiting case $(\nu = 1\,)$ is also well understood (Schmidt & Wang, 1985; Wenzel et al., 1991). It results in a one-dimensional circle map with zero phase shift. If the damping lies between these two limiting cases $(0 < \nu < 1)$, the periodic orbits are turned into sinks (Lieberman & Tsang, 1985; Chen et al., 1986), with absolute values of both eigenvalues now slightly less than one and the chaotic motion is replaced by transient motion, before the trajectory settles eventually in one of these sinks. The motion is now located on a cylinder $[0, 2\pi] \times \mathbb{R}$ and the periodic orbits for different m values become discernible. The number of periodic orbits is in this case finite, but can be made arbitrarily large by reducing the damping. The mechanism for the creation of an arbitrarily large number of coexisting attractors is different from the Newhouse phenomenon in which infinitely many attractors can coexist (Newhouse, 1979; Robinson, 1983), but only for special sets of parameters (Tedeschini-Lalli & Yorke, 1986; Nusse & Tedeschini-Lalli, 1992).

Fixing the damping but varying the kick strength f_0, a complex bifurcation diagram is obtained. Periodic orbits of low periods are generated through saddle-node bifurcations and they eventually undergo a period doubling cascade that ends in chaos (Feudel et al., 1996). However, the chaotic intervals in, say, the parameter f_0 are extremely small and hardly detectable numerically, as chaotic attractors are generally rare in multistable systems (Feudel & Grebogi, 1997; 2000).

In the following, the parameters will be fixed at $\nu = 0.02$, which is a rather small damping, and $f_0 = 3.5$ for the kick strength. For these values no chaotic attractors are found and the period 1 orbits have not yet undergone the first period doubling. Numerically, we find 111 coexisting periodic attractors, the highest period being 32, by iterating 10^6 initial conditions on a grid in the state space $[0, 2\pi] \times [-\frac{f_0}{\nu}, \frac{f_0}{\nu}]$. This part of the cylinder is the trapping region in state space, where all attractors are located, as can be seen by

$$
|y_{k+1}| \leq (1-\nu)\,|y_k| + f_0.
\tag{2.9}
$$

Thus

$$
|y_k| < f_0/\nu \rightsquigarrow |y_{k+1}| < f_0/\nu.
\tag{2.10}
$$

More than 99.9% of all initial conditions converge to orbits of periods 1 and 3, so all other periods do not play an important role in the following. The basin for
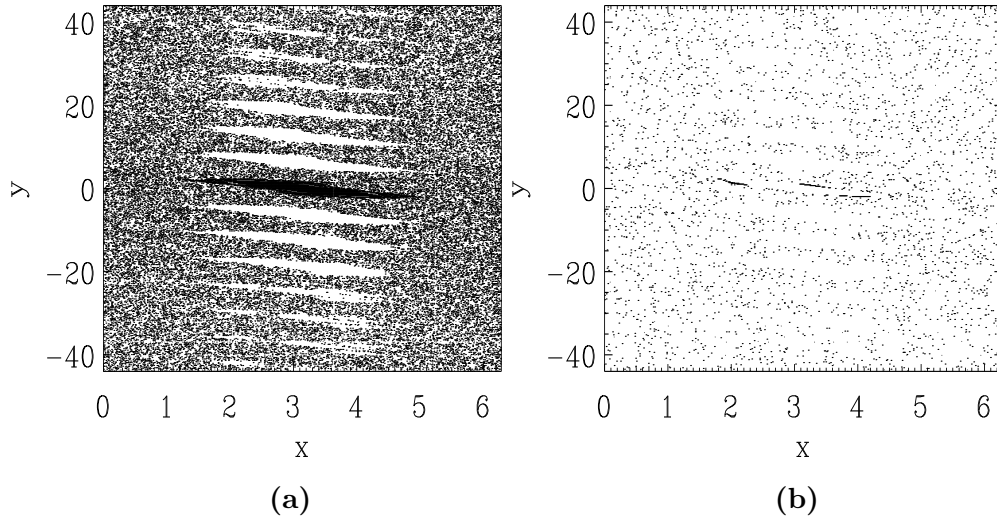
Figure 2.2: (a): Basin of attraction for the fixed point $(x = \pi, y = 0)$ and a fraction of the phase space in y-direction $y \in [-14\pi, 14\pi]$. (b): Same as in (a) but for the period 3 orbit located around the fixed point $(x = \pi, y = 0)$.

the fixed point $(x = \pi, y = 0)$ is shown in Fig. 2.2a. To gain more insight in the basin structure, in the y-direction not the complete phase space $[-\frac{f_0}{\nu}, \frac{f_0}{\nu}] = [-175, 175]$ is depicted, but only the fraction $[-14\pi, 14\pi]$. It is clearly visible, that the basin boundary extends over the whole phase space in a very intricate fashion, symmetrically with respect to $y = 0$. The horizontally stretched white regions correspond to basins of fixed points $y = m2\pi$ with $m = \pm 1, \pm 2, ...$. For $m \neq 0$ the basins have lost their symmetry with respect to $y = m2\pi$, as the number of initial conditions attracted below and above $y = m2\pi$ is not equal anymore. This question will be dealt with in Section 2.2.5. Fig. 2.2b shows for the same phase space region the basin for one of the two period 3 orbits around the period 1 fixed point $(x = \pi, y = 0)$. Again, the basin boundary extends over the whole area, but is much more sparse.

2.1.1 Fractal basin boundaries

The possibility of a basin boundary between two stable solutions of a dynamical systems to become *fractal* has been first pointed out in (Mira, 1979) and systematically explored in(Grebogi et al., 1983b). Fractal in these works means, that the curve separating the two basins of attraction is of noninteger *box-counting dimension*. The box-counting dimension is a simple measure for the dimension of fractal sets. It has integer values for ordinary sets (lines, surfaces, etc.) and noninteger val-

ues for fractal sets, see e.g. (Ott, 1993). If the fractal curve representing the basin boundary permeates large regions of the phase space, it might become increasingly difficult to predict the evolution of an initial condition accurately. This obstruction to predictability has been termed *'final state sensitivity'* and as a quantitative measure the *uncertainty exponent* has been introduced in (Grebogi et al., 1983a), where also a new form of fractal basin boundaries is discussed, which is a Cantor set and cannot be presented by a continuous curve anymore.

A schematic illustration for the motivation of the uncertainty exponent is given in Fig. 2.3. There are two possible final states, denoted by A and B. Initial conditions on one side of the boundary, Σ, eventually asymptote to B, while those on the other side of Σ eventually go to A. The regions to the left and right of Σ are the basins of attraction for A and B, respectively. Σ is the basin boundary. If the initial conditions are uncertain with respect to a perturbation of size ϵ, then for those initial conditions within ϵ on the boundary, we cannot predict a priori to which attractor the orbit will go. In Fig. 2.3 the point marked 1 will tend to B with certainty of
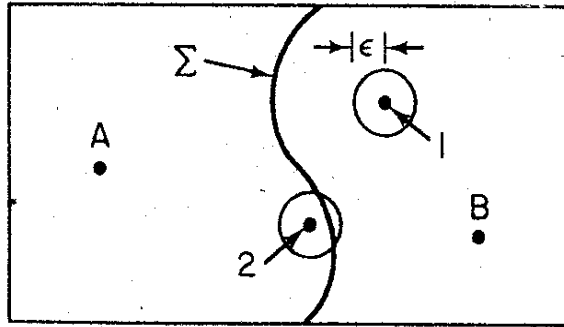

Figure 2.3: A region in phase space divided by the basin boundary Σ into basins of attraction for the two attractors A and B. 1 and 2 represent two initial conditions with uncertainty ϵ.

ϵ, while point 2 is uncertain within the resolution of ϵ, since it cannot be predicted, on which attractor it will terminate. The uncertainty exponent is defined as follows. Let f be the fraction of initial conditions in a well defined region in the phase space, which is uncertain with respect to ϵ, i.e. which terminate on another attractor if a perturbation of strength ϵ is applied. Then there exists typically a scaling relation

$$f \sim \epsilon^{\alpha} \tag{2.11}$$

with the resolution of ϵ. The scaling exponent α is the uncertainty exponent. If $\alpha < 1$ than there exists a final state sensitivity. In such cases, a substantial improvement

in the initial condition uncertainty, ϵ, yields only a relatively small decrease in the uncertainty of the final state. Furthermore, it has been proven in (Grebogi et al., 1988) that for a special class of systems (Axiom A) the relation

$$\alpha = D - d \qquad (2.12)$$

holds, where D is the dimension of the phase space and d is the dimension of the basin boundary. This relation is believed to hold for more general systems, like ours, as well. Thus, a small value of α implies that the dimension of the basin boundary is close to the dimension of the phase space. A generalization of the uncertainty exponent to parameter variations and noise has been undertaken in (Siapas, 1994).

For the dissipative standard map and our set of parameters, $f_0 = 3.5, \nu = 0.02$, the calculation of the uncertainty exponent is shown in Fig. 2.4. The scaling region extends over at least 8 orders of magnitude, showing very nicely where the scaling starts to hold and where it breaks down. We obtain an uncertainty exponent of $\alpha = 0.003$, which means, that the basin boundary has a dimension of $d = D - \alpha = 2 - 0.003 = 1.997$, very close the the phase space dimension.
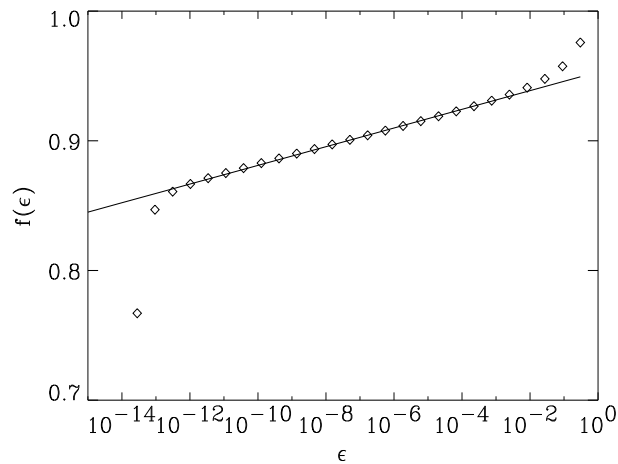
Figure 2.4: Log-log plot of the fraction of uncertain initial conditions f versus the resolution ϵ for $f_0 = 3.5, \nu = 0.02$. The slope yields an uncertainty exponent of $\alpha = 0.003$.

For cases, where α is close to 1, i.e. d is close to $D - 1$ and the basin boundary is only slightly fractal, the uncertainty method is very inefficient, as a extremely large number of initial conditions has to be considered to get a sufficiently good statistics, since only very few change with ϵ. This turns out to be computationally not feasible

if $\alpha > 0.5$. To overcome this difficulty, an improved method of output function evaluation has been proposed in (de Moura & Grebogi, 2001), which proves to be efficient.

Further investigations of basin boundaries yielded a distinction between locally connected and unconnected basin boundaries (McDonald et al., 1985) and *intertwined* basin boundaries, where the boundary has the property that in some regions it is smooth while in other regions it is fractal (has noninteger box-counting dimension). Furthermore, for any region where the boundary is fractal, one can find within that region a subregion where the boundary is smooth (Grebogi et al., 1987a). This has been extended to systems, where in spite of the basin boundary being smooth 'almost everywhere', its fractal dimension exceeds one for a two-dimensional system. These were termed 'sporadically fractal basin boundaries' (Hunt et al., 1999). The basin boundary of the dissipative standard map seems to be intertwined.

Another interesting property is that of a *Wada* basin (Kennedy & Yorke, 1991). A fractal basin boundary exhibits the Wada property, if each point that is on the boundary of one basin is also simultaneously on the boundary of at least two other basins. This has been found numerically for the driven damped pendulum and later explained with the concept of the basin cell (Nusse et al., 1995; Nusse & Yorke, 1996). This concept was applied to the mixing of chaotic flows (Nusse & Yorke, 2000). The Wada property has also been experimentally confirmed in a simple model of chaotic scattering (Sweet et al., 2000). It is not clear, if the dissipative standard map exhibits the Wada property, since numerical tests are not sufficient for establishing it and the construction of a basin cell has not been achieved up to now. However, numerical analysis shows, that zooming into the phase space and estimating the number of basins present in smaller and smaller parts of the phase space yields always the same number of basins of attraction. Therefore, the numerical result strongly hints on the basin boundary being of Wada type.

A new kind of basin was introduced in (Alexander et al., 1992) and called *riddled*. A basin of attraction is riddled if it is such that every point in the attractor's basin has pieces of another attractor's basin arbitrarily nearby. This is a very extreme case of fractality and renders predictability even more difficult if not impossible, as $\alpha \approx 0$. It is not only the basin boundary, which is riddled, but the whole basin of attraction. A riddled basin does not contain any open sets and can only occur in systems exhibiting a certain symmetry. The concept was further explored in (Sommerer & Ott, 1993), the scaling behavior was investigated in (Ott et al., 1993) and first experimental evidence has been provided in (Heagy et al., 1994). The basin of the dissipative standard map is clearly not riddled, as every periodic solution is surrounded by open neighborhoods.

2.2 Basic properties of the noisy dynamics

After the description of the basic properties of the system, we introduce noise to the dynamics, in the form

$$
\begin{aligned}
x_{k+1} &= x_k + y_k + \delta_x \,(\mathrm{mod}\,2\pi) \\
y_{k+1} &= (1-\nu)\,y_k + f_0 \sin(x_k + y_k) + \delta_y,
\end{aligned}
\tag{2.13}
$$

where δ_x and δ_y are the amplitudes of the uniformly distributed noise, restricted by $\sqrt{\delta_x^2 + \delta_y^2} \leq \delta$, with no temporal correlation. Thus δ serves as an overall noise strength. However, using noise with a Gaussian distribution does not change the findings in this Chapter. The trajectory of the noisy dynamics alternates between almost periodic motion in the neighborhood of an attractor and chaotic motion in the basin boundary region in a very complex way. This is illustrated in Fig. 2.5, where the x- and y-coordinates of the system are plotted for a large number of iterations and a noise level of $\delta = 0.1$. Clearly, there is almost periodic motion interspersed by random bursts.

Almost periodic motion takes place close to an attractor and the noise is not able to kick the trajectory out of the basin of attraction of this metastable state. The motion thus fluctuates around this attractor until the trajectory leaves the vicinity of the attractor and the motion takes place on the fractal basin boundary. These are the *random bursts*. After the trajectory has wandered around in an erratic fashion on the fractal basin boundary for some time, it is caught again from a metastable state (the same or another one as before). The whole process, consisting of an alternation of almost periodic motion and random bursts, which repeats itself forever, is called *attractor-hopping*.

This behavior has also been observed in numerical simulations of the Duffing oscillator (Arecchi et al., 1985) and the damped driven pendulum (Gwinn & Westervelt, 1985), where it was termed noise-induced intermittency. In both cases the fractal basin boundary is the origin of the behavior. Closely related is the effect of 'chaotic itinerancy' (Ikeda et al., 1989; Otsuka, 1990; Tsuda, 1991) in optical systems, where the phase of a laser is jumping between different solutions. However, the mechanism of the chaotic itinerancy is not caused by noise, but by the existence of unstable orbits localized around supermodes, which are called 'attractor ruins'. The latter phenomenon has also been confirmed in experiments (Arecchi et al., 1990).

Another typical feature can be seen by Fig. 2.6, where we use 1000 initial conditions, randomly distributed in the rectangle $[0, 2\pi] \times [-3\pi, 3\pi]$, and iterate each one for 10000 steps. This region of the state space is covered with a 300×300
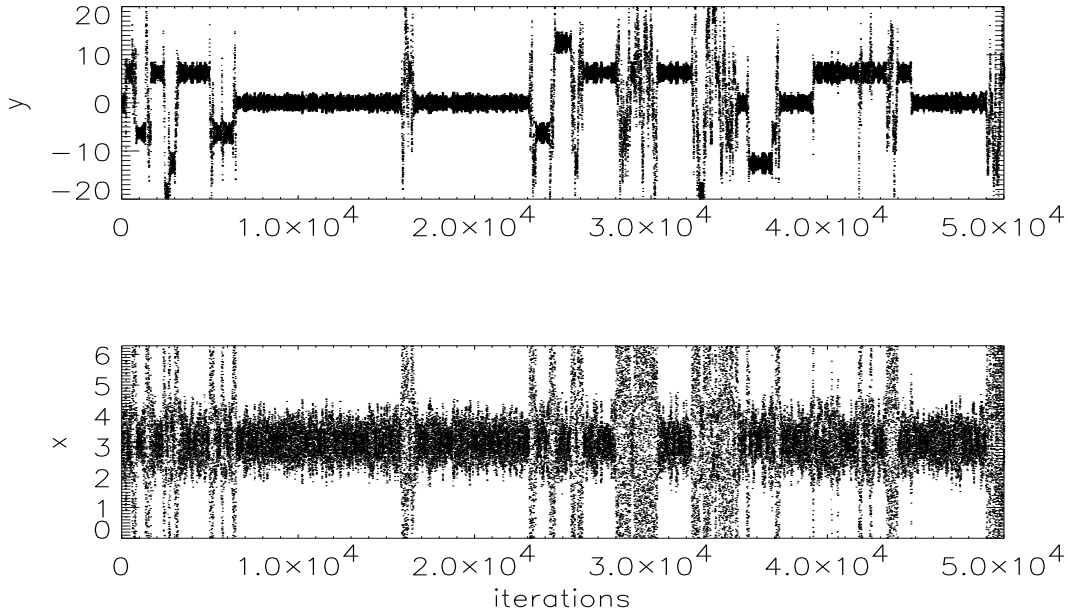
Figure 2.5: Dynamics of the dissipative standard map under the influence of noise with intensity $\delta = 0.1$. Top: angular velocity y; bottom: phase of the rotor x

grid and every visit of a grid cell is counted, creating thus numerically a probability density. As can be seen, the peaks of the 3 period 1 and corresponding period 3 orbits get increasingly broad (Fig. 2.6b and c) until almost no structure is present anymore (Fig. 2.6d), indicating the predominance of diffusion due to the noise.

The washing out of the fine structure of the invariant measure due to the noise has been investigated numerically for the logistic map in (Meyer-Kress & Haken, 1981; Crutchfield et al., 1982) and subsequently with semi-analytical methods using a matrix continued-fraction approach for solving the Fokker-Planck equation for a resistively shunted junction (Jung & Hänggi, 1990). It has been treated analytically in (Reimann & Talkner, 1991) with path integral methods for very simple one-dimensional maps and with an asymptotic expansion for a three-dimensional system in (Kuske & Papanicolaou, 1998). The invariant measure of a noisy system can also be found employing the theory of quasipotentials, as presented in Section (4.2). However, all these techniques are much too complicated for the highly multistable system presented here and the figure merely demonstrates the basic consequences of the noise.
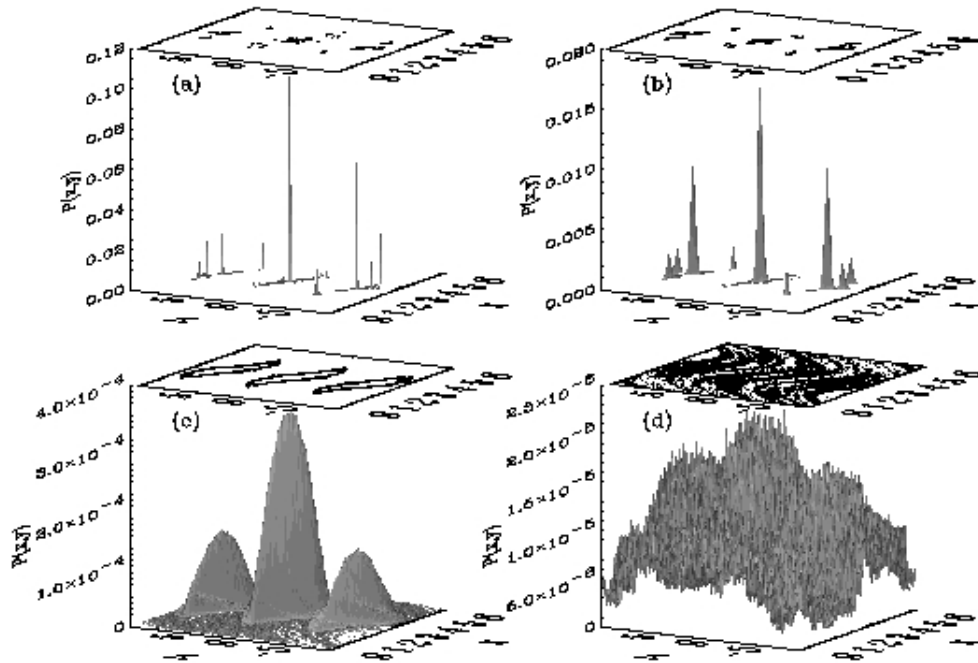
Figure 2.6: Probability density $P(x,y)$ in the rectangle $[0, 2\pi] \times [-3\pi, 3\pi]$ for increasing noise levels. (a) $\delta = 0.001$; (b) $\delta = 0.01$; (c) $\delta = 0.1$; (d) $\delta = 0.3$. On the top of each figure, a contour plot of a certain probability density $P_c(x,y)$ is shown. $P_c(x,y)$ has the values (a) 2.4×10^{-4}; (b) 2.5×10^{-5}; (c) 2.3×10^{-4}; (d) 2.2×10^{-5}.

It is also interesting to examine how the basins of attraction for different attractors change as we vary the noise level. For this purpose, we stop iterating the trajectory as soon as it reaches for the first time the neighborhood of an attractor. Hereby we disregard the fact that the trajectory can be kicked out of this neighborhood by the noise at a later time. The noisy dynamics is treated such, that we ascertain that the motion is in the vicinity of a given periodic orbit in the following way. Every initial condition is checked after each k (~ 30) iterations, whether the orbit stays for a certain number of time steps l ($\sim 5 * \text{period}$) close to the periodic orbit of the noiseless system, whereby closeness was specified by a maximum distance of about $j \approx 10 * \delta$. If these conditions are satisfied, the orbit is considered to be trapped in the neighborhood of the specific attractor. However, the exact numerical values of these choices (k, l, j) do not possess any crucial meaning and changing them by moderate amounts yields similar results.
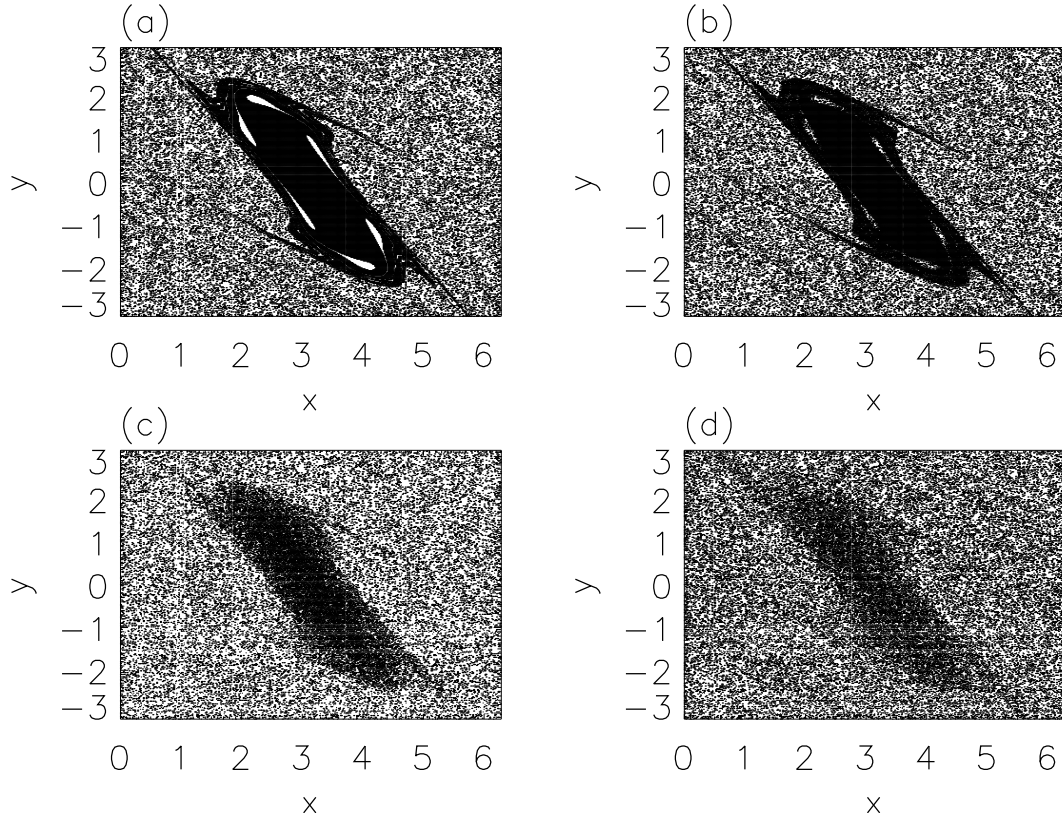
Figure 2.7: Basin of the fixed point $(x = \pi, y = 0)$ for increasing noise levels. (a) $\delta = 0$; (b) $\delta = 0.01$; (c) $\delta = 0.1$; (d) $\delta = 0.3$

The result is shown in Fig. 2.7 for the same noise levels as in Fig. 2.6, except for Fig. 2.7a, where we now can allow the zero noise limit, which wasn't possible for the natural measure because of the δ-peaked distribution. For a tiny noise amplitude ($\delta = 0.01$) a great similarity with the noiseless basin is seen, including the two embedded open neighborhoods of the two period 3 attractors. The fine structure becomes increasingly blurred with increasing noise intensity, e.g. ($\delta = 0.1$). For a large noise level ($\delta = 0.3$) the basic structure is still present, but it starts getting washed out. For each initial condition different noise realizations are used to create the picture of the basin of attraction. The size of the basins and the qualitative structure remain the same under other noise realizations.

Figures 2.7 and 2.6 also justify our numerical procedure. For instance, they show that the period 3 orbits are still present in the noisy dynamics as well as in the long-term behavior as approximated by the first visit to a periodic orbit. Both figure sequences, Fig. 2.7 and 2.6, illustrate qualitatively in the same way the process of loss of fine-scale structure of the basins of attraction with increasing noise intensity.

One might be interested in stabilizing one metastable state for a long time. While there is an immense literature on controlling a chaotic system, only recently the question of controlling a multistable system with noise has been addressed. It has been considered for the first time in (Poon & Grebogi, 1995), dealing with the double rotor map, which is a generalization to two rods of the dissipative standard map, employing a simple feedback scheme. For the noisy dissipative standard map, this method has been applied in (Feudel & Grebogi, 1997). Algorithms for reducing the number of control perturbations and the waiting time, at which the control can be switched on, have been devised in (Macau & Grebogi, 1999; Gadaleta & Dangelmayr, 2001).

2.2.1   Quantifying the dynamics with Lyapunov exponents

In the theory of chaotic systems, the *Lyapunov exponents* $(\lambda_j, j = 1, ..., d)$ for a d-dimensional system, are of crucial importance, as they give a measure for the stretching and contracting of distances between trajectories in the phase space and allow therefore to classify whether the motion is chaotic $(\max(\lambda_j) > 0)$, periodic $(\max(\lambda_j) < 0)$, or neutrally stable $(\max(\lambda_j) = 0)$. They are defined as

$$\lambda_j = \lim_{N \to \infty} \frac{1}{N} \sum_{i=1}^{N} \ln |(\frac{df}{dx})_i|, \tag{2.14}$$

where N is the length of the time interval and $(\frac{df}{dx})_i$ is the Jacobian matrix of the map at each time step i. For a numerical computation one can only use a finite time interval N, yet in general the computation of λ_j according to Eq. (2.14) should converge for 'sufficiently' large N, where the necessary minimum length depends on the system. In pathological cases, it might not be possible to decide, whether the computation has already converged or not, but in our system we did not encounter this problem. Also, in the general case, there should be no dependence on the starting point. For a d-dimensional system there are d Lyapunov exponents, but only the non-negative ones are relevant for the different dynamical regimes. In our case, like in most dynamical systems of low dimension, we will consider here only the largest Lyapunov exponent.
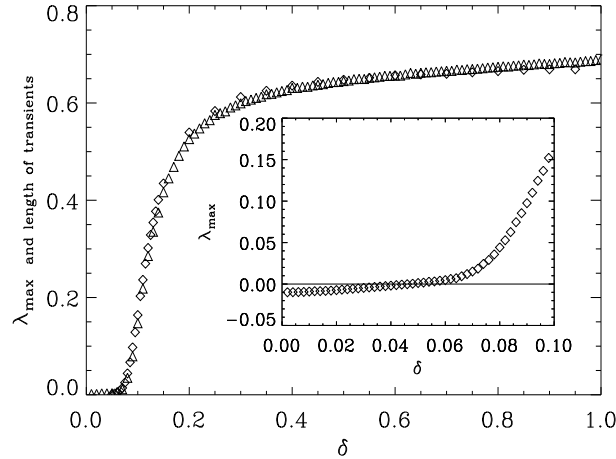
Figure 2.8: Maximum Lyapunov exponent ($\diamond$) and average ratio of the length of transients ($\triangle$) to laminar motion versus noise level. For each noise intensity, λ_{max} and the length of the transients are calculated by averaging over 50 trajectories with 10^6 iterations each. The inset shows the crossing of the Lyapunov exponent curve through zero. This takes place at $\delta_c \approx 0.047$ with a slope of 0.27.

The result of the computation is shown in Fig. 2.8, where also the average ratio of the length of the chaotic bursts to regular motion in the neighborhood of attractors (compare to Fig. 2.5) is plotted. We measure this length of the chaotic transients by splitting 50 trajectories of 10^6 iterations into blocks of 5 iterations and checking each of these blocks whether the motion is in the vicinity of an attractor or chaotic. The functional form of these averaged lengths of the chaotic bursts resembles very closely the behavior of the Lyapunov exponents, indicating that it is the motion on the fractal basin boundary during the bursts that gives rise to the chaotic component. The inset is a blow up of the region, where the Lyapunov exponent becomes positive, which happens at $\delta \approx 0.047$.

The effect of noise leading to a positive Lyapunov exponent of otherwise non-chaotic dynamics has been called 'noise-induced chaos' and was found for the first time in the logistic map (Meyer-Kress & Haken, 1981; Crutchfield et al., 1982) and later on in a variety of systems, like in experiments with Josephson junctions (Iansiti et al., 1985), SQUIDs (Bulsara & Jacobs, 1990), biological systems (Herzel et al., 1987), and the Kramers oscillator (Schimansky-Geier & Herzel, 1993). In all these cases a

smoothing of the Lyapunov exponent due to the noise has been observed. Also the opposite effect, namely stabilization by noise, has been reported (Herzel, 1988b). However, 'noise-induced chaos' is still to be discerned from truly chaotic dynamics, as it is only the interplay between a complex basin boundary between the stable states and the noise that is responsible for the positive Lyapunov exponent, and not a real divergence of nearby trajectories. A method to classify the complexity introduced by the noise with a refined Lyapunov exponent has been proposed in (Paladin et al., 1995).

To gain a better understanding of the noise-induced chaos transition, it is useful to consider finite-time Lyapunov exponents (Grassberger & Procaccia, 1984; Fujisaka, 1983), where the time interval T stays finite $\lambda_T = \frac{1}{T} \sum_{i=1}^{T} \ln |(\frac{df}{dx})_i|$. When we compute those λ_T for an ensemble of $L \, (L \gg 1)$ trajectories at a given time interval T, we obtain a set of positive finite-time exponents λ_i^+ and a set of negative ones λ_i^- corresponding to chaotic or almost periodic motion, respectively. Using this distribution of finite-time Lyapunov exponents, we can again estimate the noise intensity for which the asymptotic Lyapunov exponent λ becomes positive. This noise value δ_c satisfies

$$\lambda(\delta_c) = \frac{1}{K+L}(\sum_{i=1}^{K} \lambda_i^+ + \sum_{i=1}^{L} \lambda_i^-) \approx 0. \tag{2.15}$$

Here $K + L$ is the total number of trajectories, while $K(L)$ is the number of trajectories yielding positive (negative) finite-time Lyapunov exponents λ_i^+ (λ_i^-), respectively. It is also very interesting to look at the distribution of these finite-time Lyapunov exponents. They are computed for $T = 5000$, using 50 time series of length 1,000,000. It yields 10,000 Lyapunov exponents, a sufficiently high number to get good statistics. Smaller time intervals T do not yield good results, since the eigenvalues are complex and, by this fact, spurious peaks appear in the histograms, due to the rotation of the eigenvectors.

For the noiseless system, the motion is attractive and hence the finite-time Lyapunov exponents are negative, peaking about the maximum Lyapunov exponent, whose numerical value is $\lambda_{max} \approx -0.01$. As the noise intensity increases, the peak is shifted towards higher values of λ_{max} and starts to flatten out. At a noise level of $\delta = 0.075$, there is no negative Lyapunov exponent any longer and a second peak at a higher value begins to develop, see Fig. 2.9a. This second peak becomes increasingly dominant and develops into a Gaussian distribution, displayed in Fig. 2.9b and c. For $\delta = 0.125$ (Fig. 2.9e) the Gaussian part is fully developed and the peak associated with the periodic motion is not visible anymore. By increasing the noise further, it yields a single Gaussian distribution
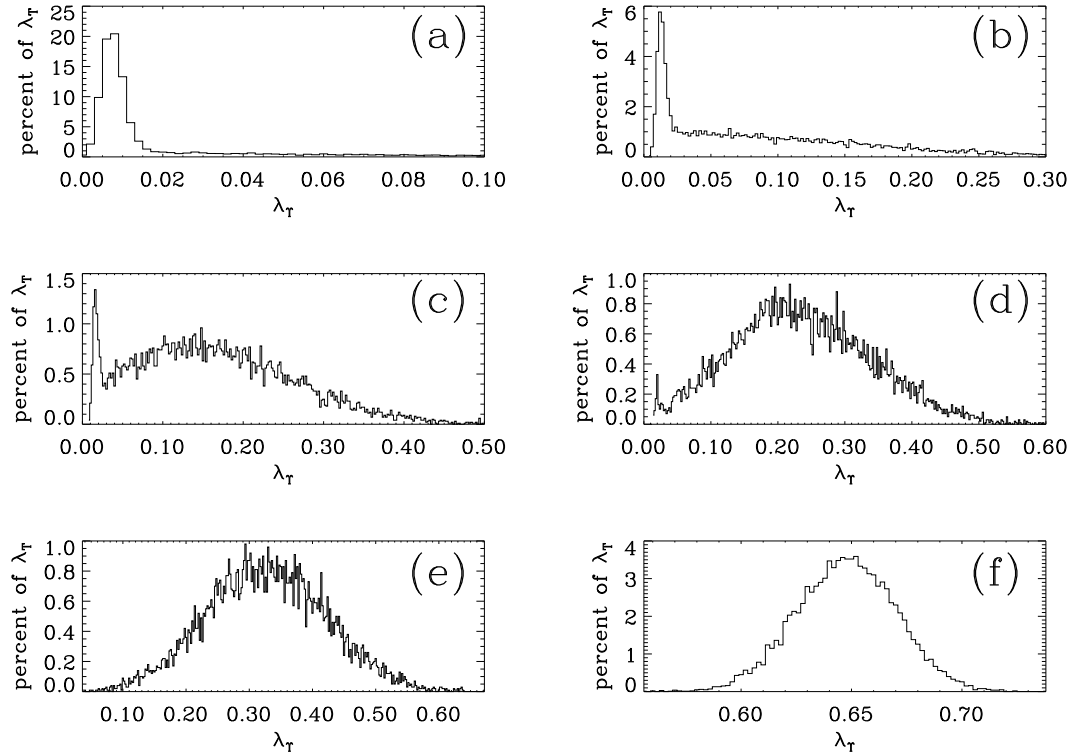
Figure 2.9: Histograms of finite-time Lyapunov exponents for different noise levels. The interval length is 5000, altogether 10,000 Lyapunov exponent values are computed for each picture, using 50 trajectories. The bin size is 0.002. (a) $\delta = 0.075$; (b) $\delta = 0.09$; (c) $\delta = 0.1$; (d) $\delta = 0.11$; (e) $\delta = 0.125$; (f) $\delta = 0.5$. Note the different scale in the y-axis.

(Fig. 2.9f), whose mean is in accordance with the maximal Lyapunov exponent of Fig. 2.8. The peak corresponding to the periodic motion has disappeared completely. This transition thus takes place around $0.08 < \delta < 0.11$. The features of the crossover behavior of Fig. 2.9b, consisting of a pronounced peak and an only weakly decaying tail, i.e. a significant departure from the Gaussian distribution, are also typical for intermittent dynamics, where, although without noise, an interplay between regular and chaotic motion is taking place (Benzi et al., 1985; Prasad & Ramaswamy, 1999).

2.2.2   1/f noise

The occurrence of $1/f$ *noise*, i.e. the divergence of the power spectrum S_f at low frequencies with a power law

$$S(f) \sim 1/f^\alpha, \; (\alpha \approx 1), \tag{2.16}$$

where the power spectrum is defined as the square of the Fourier transform, is ubiquitous in nature (Weissman, 1988; Press, 1978). It can be found in the current fluctuations of metal films, semiconductors, and various types of diodes (Dutta & Horn, 1981). It has also been detected in such disparate systems as water fluctuation in rivers (Mandelbrot & Wallis, 1969), human speech data (Voss & Clarke, 1978), music (Voss & Clarke, 1975), biological membranes (Derksen & Verveen, 1966), ion channels (Bezrukov & Winterhalter, 2000), Josephson junctions (Iansiti et al., 1985), traffic flows (Musha & Higuchi, 1976), granular flows (Schick & Vervear, 1974), heartbeat variability (Kobayashi & Musha, 1982), self-organized criticality (Bak et al., 1987; Rios & Zhang, 1999), DNA sequences (Voss, 1992), intermittent dissipative systems (Manneville, 1980) and non-integrable Hamiltonian dynamics (Geisel et al., 1987). Despite its ubiquity, *no universal mechanism* for its origin has been established so far.

We want to investigate, if the noisy dissipative standard map is generating $1/f$ noise, since it has been observed, that the hopping mechanism between different states can be responsible for $1/f$ noise. The original proposal, which used the Duffing oscillator with two states (Arecchi et al., 1982), has been questioned (Beasley et al., 1983; Voss, 1983) and refined in (Arecchi & Califano, 1987). As necessary conditions (i) at least two stable states, (ii) the presence of noise and (iii) a fractal basin boundary have been distilled. The last point guarantees, that the motion between the stable states is highly irregular and contributes a large variety of different time scales.
To check these conditions for the noisy dissipative standard map, we compute the power spectrum for three different noise levels, see Fig. 2.10, 2.11, and 2.12. In the first case (Fig. 2.10), the noise level is very small ($\delta = 0.01$) and not strong enough to kick the orbit out of the stable state. Therefore, the process is dominated by only one single correlation time τ and the spectrum can be fitted by a Lorentzian

$$S(f) \sim \tau/(a + \tau^2 f^2) \tag{2.17}$$

with a constant low frequency part and a high frequency part $S(f) \sim 1/f^2$. The same holds for Fig. 2.12, where the noise is very large ($\delta = 0.2$), and the motion diffuses over large parts of the phase space, without staying for a longer time close to a metastable state. However, for an intermediate noise level, Fig. 2.11 with ($\delta = 0.085$), the typical attractor-hopping occurs, with a broad distribution of residence times. These different time scales cause a low frequency part $S(f) \sim 1/f$
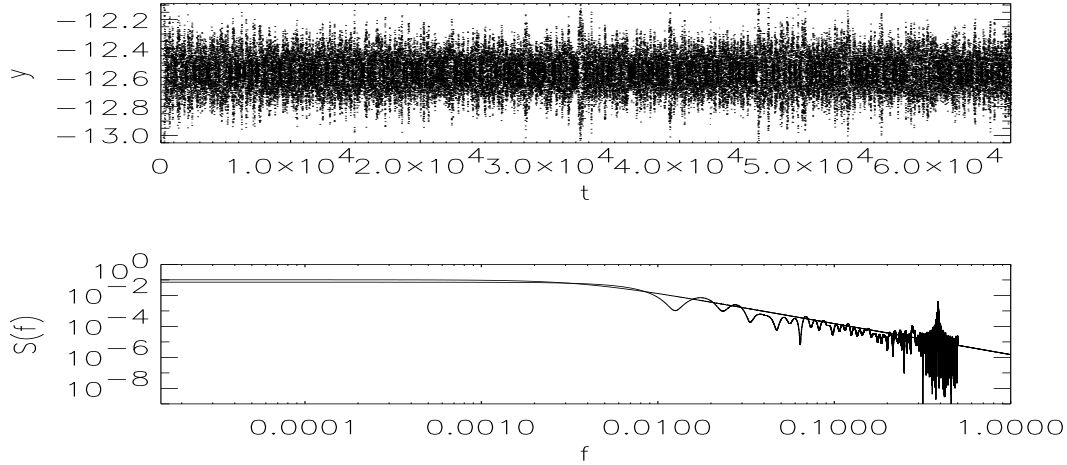
Figure 2.10: Time series of the angular velocity y (top) and the corresponding power spectrum $S(f)$ (bottom) for a noise level of $\delta = 0.01$ and a length of $2^{16} = 65536$. The noise is not strong enough to kick the orbit out of one of the attractors, therefore no hopping takes place and the whole spectrum follows a Lorentzian.
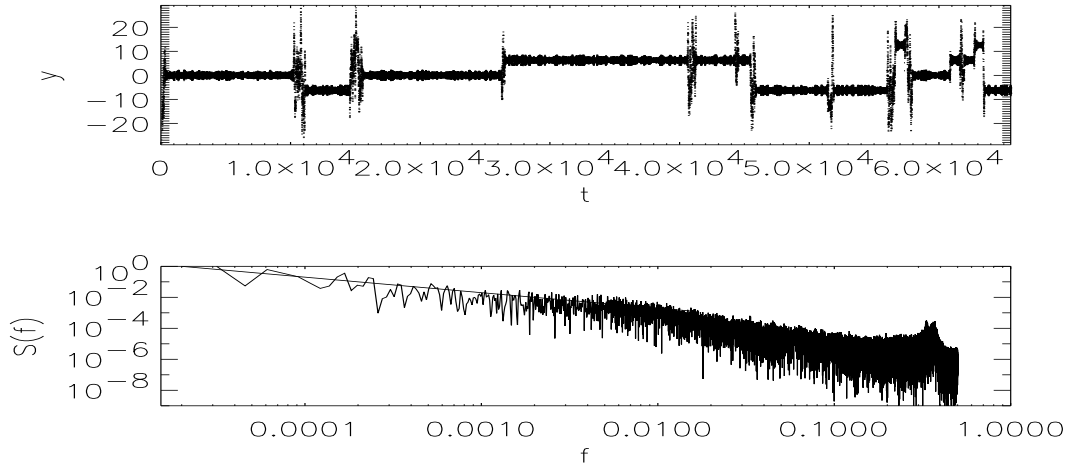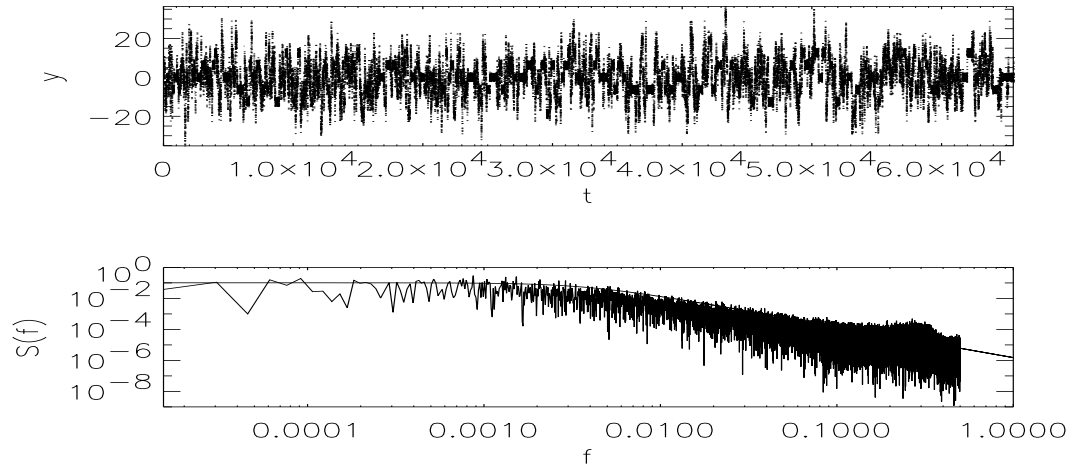

Figure 2.11: Time series of the angular velocity y (top) and the corresponding power spectrum $S(f)$ (bottom) for a noise level of $\delta = 0.085$. Here a competition between hopping and remaining in an attractor exists, which results in the low frequency part of the spectrum, which can be fitted by $S(f) \sim 1/f^{\alpha}$ for $f < 0.005$ (solid line).

Figure 2.12: Time series of the angular velocity y (top) and the corresponding power spectrum $S(f)$ (bottom) for a noise level of $\delta = 0.2$. For such a high noise intensity diffusive motion dominates and the trajectory does not remain for an appreciable length of time in the neighborhood of an attractor. The entire spectrum is again very well fitted by a Lorentzian.

for more than two orders of magnitude. Thus, the above mentioned three criteria are confirmed as sufficient conditions for the existence of $1/f$ noise. Moreover, in multistable systems with a fractal basin boundary $1/f$ noise is expected to be much more pronounced than in bistable systems, since not only two, but many metastable states coexist, with the consequence of many different average residence times and a much more complicated basin boundary.

2.2.3   Preference of attractors

As a consequence of the preceding analysis, there is a quite distinct behavior of the system for small and large noise levels, with the more interesting features for small noise. Accordingly, we will focus on this case. With the method described above, which has been applied to compute Fig. 2.7, we now explore the influence of the noise on the size of the basins. For this purpose, the number of initial conditions terminating (with the numerical criterion specified) on the period 1 orbits with different m is computed, where the fixed points with different m resulted from the introduction of the dissipation ν and the splitting of the phase space in a cylinder. The basin of the fixed points for different m is visualized in Fig. 2.2 for $m = 0$ in black and $m = \pm 1, \pm 2, ...$ in white. For higher m values the distance from the symmetry-axis $y = 0$ increases and the size of the basins decreases for increasing m.

(a)   (b)
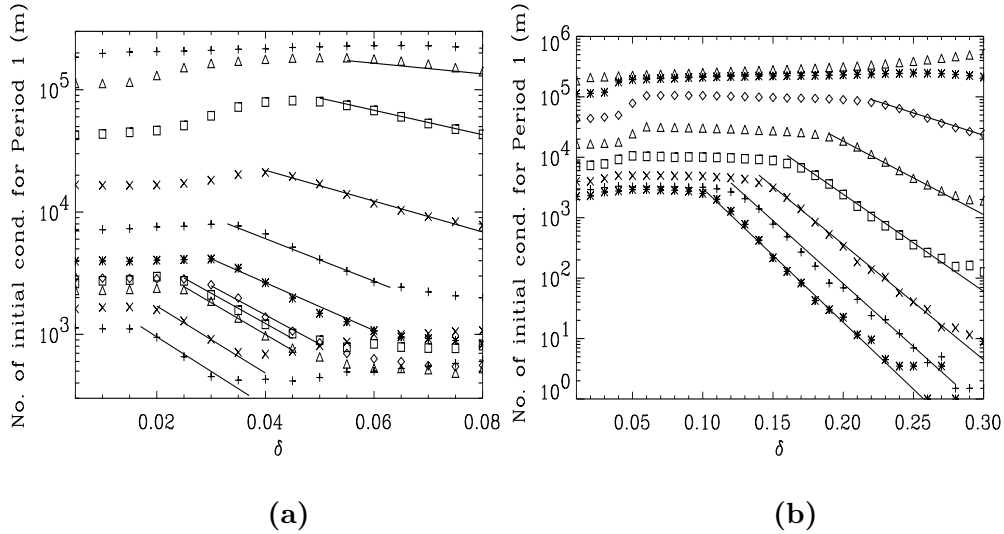
Figure 2.13: (a): Number of initial conditions converging to period 1 attractors with increasing m from top ($m = 0$) to bottom ($m = 10$). Because of the symmetry $m = +k$ and $m = -k$ are averaged. Altogether 10^6 initial conditions are iterated. (b): Same as in (a) for $m = 0$ (top) to $m = 7$ (bottom), but with multiplicative noise.

The computation of the number of initial conditions is depicted in Fig. 2.13a. It can be clearly seen that the curves for different m all possess roughly the same features, namely there is an increase up to a maximum value, followed by an exponential decrease taking place at lower noise intensity for higher m values. The starting points of the decrease versus m yields an exponential scaling, as can be seen in Fig. 2.14a. The determination of the slopes of these exponential decays reveals that they yield a logarithmic scaling in m (inset of Fig. 2.14a). These findings are robust against other forms of noise distributions, like Gaussian noise.

It is further interesting to investigate, if these results also hold when multiplicative noise is used. Generally, multiplicative noise is applied by perturbing the form of the function. In our case this amounts to altering the kick strength f_0 and we do that by introducing a noise-term via $f_0 \mapsto f_0 + \delta$ into the second of equations (2.8). This results in the additive term $\delta \sin(x_k + y_k)$ acting on the angular velocity only. The multiplicative noise reduces therefore to a special form of additive noise, whose strength depends on the location of the trajectory in the phase space and is always $\leq \delta$. Fig. 2.13b shows the result in analogy to Fig. 2.13a. The expected behavior

occurs at higher noise intensities as a consequence of the effective reduction of the influence of the noise by multiplying δ with the sin-term. In particular, for the fixed points $y = 2\pi m$, x is close to π and consequently the sin-term is very small. For multiplicative noise the exponential decay is even more pronounced. Again, the snap-off points scale exponentially and the slopes logarithmically with m, as depicted in Fig. 2.14b.

(a)   (b)
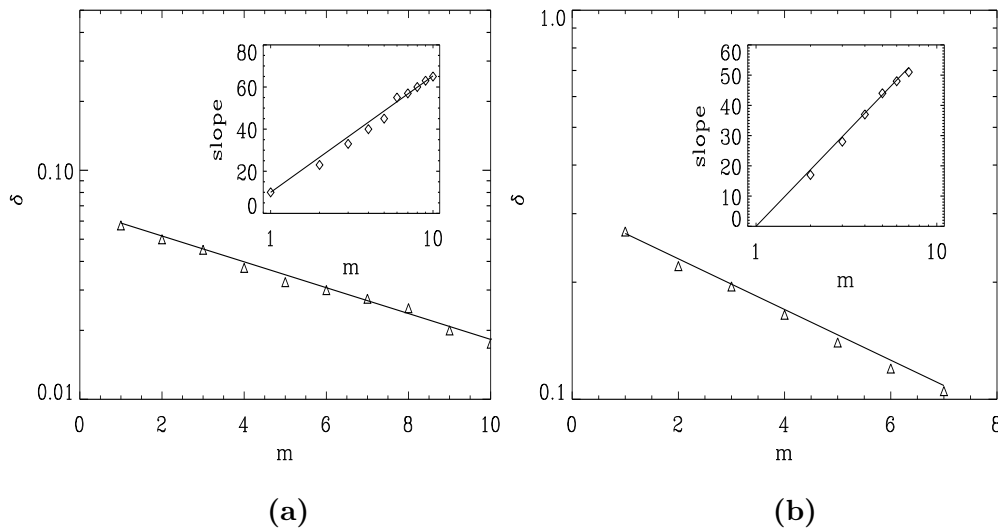
Figure 2.14: (a): Exponential scaling of the snap-off points, where the exponential decrease starts, of Fig. 2.13a versus m. The inset shows the logarithmic scaling of the slopes of the exponential decay versus m. (b) Same as (a), but for the case multiplicative noise in Fig. 2.13b.

For higher noise strengths the attractors with small basins lose part of their basins, while the ones with an already large basin are preferred. Thus the fine structure of the system is washed out due to the noise. This leads to an important consequence for the behavior of multistable systems. Even if the number of coexisting attractors is very high in a deterministic system, one observes only few of those attractors in the presence of noise. The behavior is dominated by a few preferred attractors, while the majority of them 'disappears'. Since in nature or in experimental systems noise is always inevitable, one can expect that only a tiny number of asymptotic states can be 'measured' while the majority remains 'hidden'.

On the other hand, if the noise level corresponds to the maxima in Fig. 2.13a and b, the opposite effects occurs, namely attractors with a small basin gain more initial conditions, the basins of many of them become even larger as compared with the noiseless basin. This is especially true in the case of the period 3 attractors as can be seen in Fig. 2.15. In Fig. 2.15a the number of initial conditions terminating

(a)   (b)
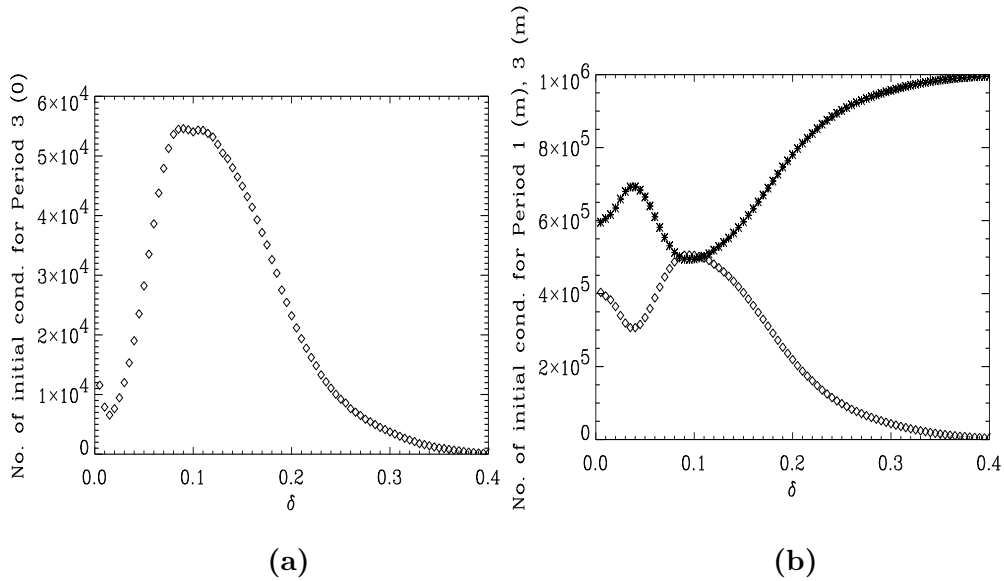
Figure 2.15: (a): Number of initial conditions terminating on the period 3 ($m = 0$) attractor versus the noise level. A clear maximum at $\delta \approx 0.1$ is visible. (b): Number of initial conditions terminating on the sum of all period 1 (stars) and period 3 (diamonds) attractors.

on the period 3 attractor for $m = 0$ is shown versus the noise level. There is a clear maximum at $\delta \approx 0.1$. This phenomenon is similar to the effect of stochastic resonance, where the signal to noise ratio of a periodically driven system reaches some maximum at a special noise value, originally observed in a bistable system (Benzi et al., 1981), and subsequently found in a large variety of different fields, reviewed in (Gammaitoni et al., 1998). In contrast to the general case, in our system no forcing is present. However, even in such systems stochastic resonance can occur (Gang et al., 1993). For higher noise values the period 3 attractors become extinct. Fig. 2.15b depicts the sum of all period 1 and 3 basins, with the same result.

The remarkable effect of the preference of period 3 attractors may be explained by the fact, that the eigenvalues of the period 3 orbits are slightly smaller than those of the period 1 fixed points. Additionally, the open neighborhoods of the period 3 attractors are located within the open neighborhood of the fixed points, see Fig. 2.7. For $f_0 = 4$, this is not the case and the effect cannot be observed. This effect of a noise-induced increase in the size of the basin of attraction has also been found in coupled map lattices (Kaneko, 1997; 1998) and in a bistable system (Yang et al., 1995). The bistable system exhibits two coexisting periodic orbits with a fractal basin boundary and the condition, that one basin has to be 'inside' the other one is therefore trivially fulfilled. In the coupled map lattice case, the attractors possess riddled basins of attraction. This riddling also provides intertwined basins of attraction as a necessary condition for the appearance of noise-induced selectivity of certain attractors. Furthermore, the attractors studied in this coupled map lattice are chaotic, which makes them to *Milnor attractors* (Milnor, 1985), i.e. they are intrinsically unstable against perturbations, and the system leaves the attractor with certainty at a finite time, even if only an *arbitrarily small amount of noise* is applied. It is the coexistence of Milnor and stable attractors, which causes the noise-induced selectivity of attractors in the coupled map lattice. By contrast, in the dissipative standard map for our set of parameters only periodic orbits are present, with basins consisting of open sets. The preference of certain attractors in our system originates thus from a different mechanism as a *finite* noise level is required for the phenomenon to occur.

2.2.4 Noise-induced escape

Let us now discuss the mechanism how the trajectory can leave the open neighborhood of a metastable state. This process corresponds to a noise-induced escape from a periodic orbit. The *escape rate W* over a barrier of a metastable potential, often referred to as *Kramers' law*, has been successfully derived by Kramers in his seminal work (Kramers, 1940), leading to an expression

$$W = \kappa \exp(-\Delta U/\delta^2), \tag{2.18}$$

where the escape rate is the product of the *Arrhenius factor* $\exp(-\Delta U/\delta^2)$ (Arrhenius, 1889) and a pre-exponential term κ, that depends only weakly on the noise, the friction and the details of the potential, with $\delta^2 \ll \Delta U$. The derivation is valid for the underdamped and overdamped limit. The *mean first passage time $\langle \tau \rangle$* of the barrier crossing is the inverse of the escape rate

$$\langle \tau \rangle = \frac{1}{\kappa} \exp(\Delta U/\delta^2). \tag{2.19}$$

Since in our system no potential exists, and furthermore not only one metastable but a large number of metastable states, it is interesting to see, whether Kramers' law is still applicable.

To gain a better understanding of the effect of noise and the relation to the eigenvalues of the system, we study as a preliminary step a trivial linear system with noise given by

$$
\begin{aligned}
x_{k+1} &= \alpha\, x_k + \delta_x \\
y_{k+1} &= \beta\, y_k + \delta_y,
\end{aligned}
\tag{2.20}
$$

where α and β are less than 1. A stable fixed point exists at $(x = 0, y = 0)$, from which the orbit cannot escape. The maximum distance $D = \max(|x|, |y|)$ of the orbit from the fixed point is related to the eigenvalues and given by

$$
D = \sum_{i=0}^{\infty} \max(|\alpha|, |\beta|)^i \delta = \frac{\delta}{1 - \max(|\alpha|, |\beta|)}.
\tag{2.21}
$$

m	$|\lambda|$	$\min(\delta_{escape})$	ΔU	$\frac{\Delta U}{\min(\delta_{escape})^2}$
0	0.98994952	0.061	0.034	9.14
1	0.98994952	0.05	0.022	8.80
2	0.98994952	0.041	0.015	8.92
3	0.98994952	0.031	0.0086	8.95
4	0.98994952	0.027	0.0065	8.92
5	0.98994952	0.021	0.0038	8.61

Table 2.1: The modulus of the eigenvalues, the minimal noise intensity necessary for escape, the height of the 'potential' ΔU from Kramers' law, and the ratio $\frac{\Delta U}{\min(\delta_{escape})^2}$.

In our nonlinear system, though, the norm of the maximal eigenvalues for the period-1 fixed points $|\lambda|$ is *identical* for all m, while the minimum noise intensity $\min(\delta_{escape})$, for which the trajectories leave the attractors for the first time, decreases with m, as shown in Tab. (2.1).

This result underlines the importance of the nonlinearities in this model, as the escape rate has no connection to the eigenvalues of the metastable states whatsoever. Furthermore, it is important to note that the eigenvalues are close to the stability threshold $|\lambda| = 1$. For noise intensities larger than the minimum noise intensity $\min(\delta_{escape})$ the trajectories leave eventually the open neighborhood of the
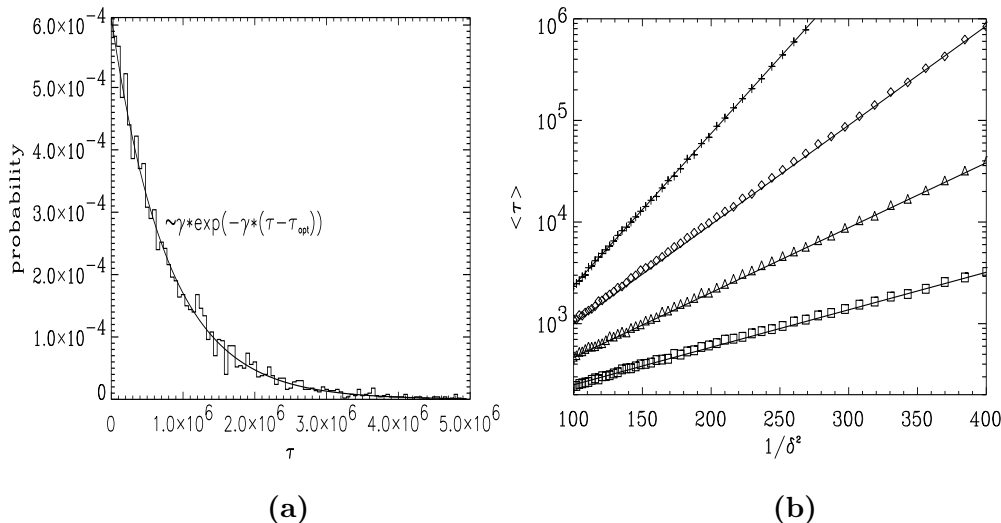
Figure 2.16: (a): Distribution of escape times $\langle \tau \rangle$ for the fixed point $m = 0$ (bin size = 50,000). (b): Escape times $\langle \tau \rangle$ for different fixed points in semi logarithmic plot ($m = 0, 1, 2, 3$) from top to bottom. The slopes ΔU correspond to the potential values of Kramers' law for the mean escape times $\langle \tau(\delta) \rangle \sim \exp(\frac{\Delta U}{\delta^2})$

attractor. This is clearly only true for our choice of the noise distribution; when using Gaussian noise, there does not exist a minimum noise intensity for escape. The escape times differ for each noise realization yielding an exponential distribution $P(\tau) \sim \gamma \exp(-\gamma[\tau - \tau_{opt}])$, as shown in Fig. 2.16a for $m = 0$. In principle, by using the relation $\langle \tau - \tau_{opt} \rangle = \frac{1}{\gamma}$, the optimal escape time can be determined. However, we get numerically only the approximate result $\tau_{opt} \leq 300$. In Fig. 2.16b the scaling of the mean escape times with increasing noise level for different m values is depicted. They follow Kramers' law (2.19) very well, which is far from trivial in cases where, like here, no potential U exists (Kautz, 1988; Beale, 1989; Grassberger, 1989a). The ratio $\frac{\Delta U}{\min(\delta_{escape})^2}$ for all m is roughly constant, which suggests that, in first order, the stability of each attractor can be approximated by a parabolic potential. This can be seen by the equation

$$\Delta U = U_{sp} - U_{fp} = \frac{1}{2} M \sum_{\alpha,\beta=1}^{2} Q^{\alpha\beta} \rho r_\alpha \rho r_\beta, \tag{2.22}$$

where sp denotes the saddle point on the basin boundary, across which the escape takes place, fp is the fixed point ($x = \pi, y = 0$), M is a constant, Q is the curvature matrix, and ρr are the displacements from the fixed point. Eq. (2.22) has been used

for the first time for the escape from a multidimensional potential in (Brinkman, 1956; Landauer & Swanson, 1961). Assuming, that there is a linear relation between the displacement and the minimal noise strength for escape (we were using bounded noise)

$$\rho r \sim \min(\delta_{escape}) \tag{2.23}$$

we arrive at

$$\frac{\Delta U}{\min(\delta_{escape})^2} = M. \tag{2.24}$$

The problem of noise-induced escape for systems without a potential and the role of a fractal basin boundary and the implications of chaotic saddles will be treated in much more detail in Chapter 4. There we report an enhancement of noise-induced escape caused by the existence of a chaotic saddle embedded in the open neighborhood of a metastable state.

2.2.5   Phase space and attractor-hopping

As described above, the periodic orbits in the dissipative standard map are located in the state space in a hierarchical structure. Therefore, it is an interesting question, whether this hierarchy is reflected in the transition probabilities of the jumps between the attractors. Furthermore, it is noteworthy that a typical noisy trajectory is not exploring the whole phase space uniformly, but seems to be confined to a much smaller interval in the y direction than the entire trapping region. This can be seen in Fig. 2.5 and Fig. 2.11 with a small noise level and even in Fig. 2.12, where a much larger noise amplitude was applied. Thus this phenomenon seems to be robust against different noise levels.

As the transition from one metastable state to another occurs via the fractal basin boundary, its properties are relevant for the attractor-hopping process, as explained in Section 2.2. To review briefly, a fractal basin boundary entails saddle points, i.e. points whose tangent spaces are direct sums of stable and unstable subspaces. The union of these saddle points forms a geometrically strange, invariant, and non-attracting set. It is called a chaotic saddle, where the term 'chaotic' refers to the fact, that the motion on this invariant set exhibits a positive Lyapunov exponent. A much more refined account of the importance of chaotic saddles for the attractor-hopping dynamics, the exact definitions of the terms involved, and the numerical algorithms will be presented in the following Chapter.

The chaotic saddle for various forcing strengths f_0 is shown in Fig. 2.17. As is clearly visible, the chaotic saddle evolves with increasing forcing f_0, exploring a
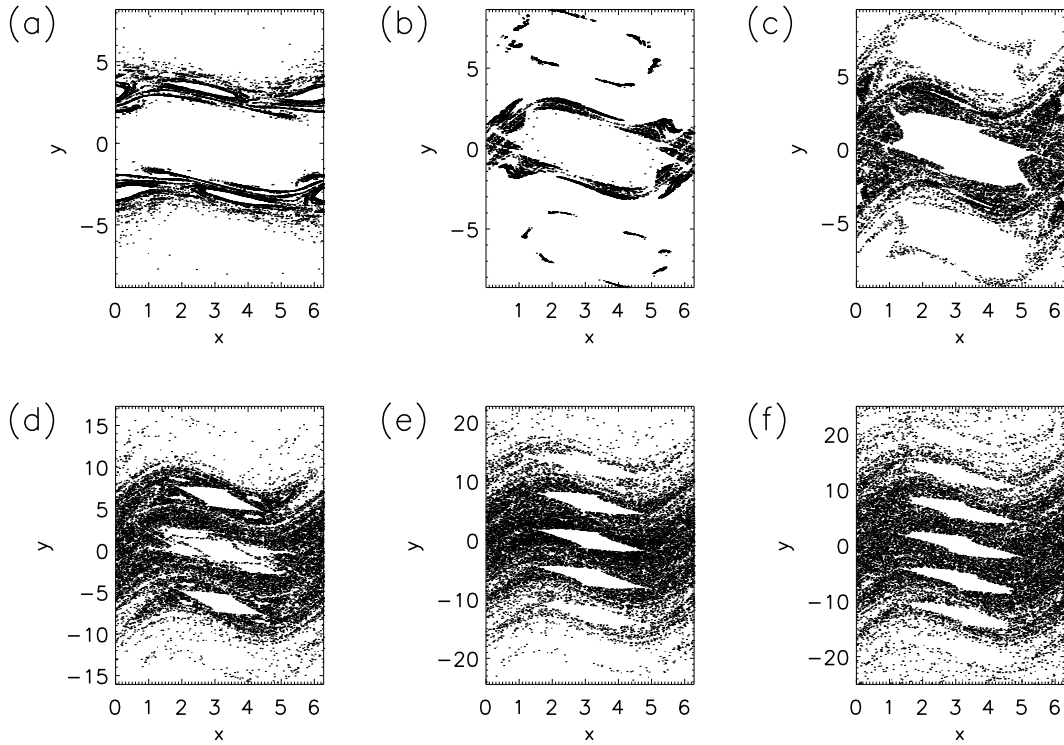
Figure 2.17: Chaotic saddle for the dissipative standard map. The values of the forcing strength f_0 are (a) 1.0, (b) 1.5, (c) 2.0, (d) 2.5, (e) 3.0 and (f) 3.5.

growing part of the phase space (note the different scale of the y-axis), yet never covering the whole trapping region $-f_0/\nu \leq y \leq f_0/\nu$. At the maximum value of $f_0 = 3.5$ in Fig. 2.17f the chaotic saddle covers exactly that region in phase space, which is also found in the noisy timeseries Fig. 2.5, Fig. 2.11 and Fig. 2.12. The same applies for all other values of the forcing f_0 in Fig. 2.17, which has been confirmed numerically, with the exception of Fig. 2.17b. Here, the chaotic saddle consists of non-connected, separate parts and no jumps between the period 1 solutions $m = 0$ and $m = 1$ are possible. In all other cases, the chaotic saddle is one large connected strange set and all connections between metastable states seem to be possible. However, this question can not be answered thoroughly for the dissipative standard map, since so many metastable states coexist. Moreover, the change in the topology of the chaotic saddle through parameter variation (f_0 in our case) and the resulting change in the hopping dynamics between the metastable states is a problem of high relevance for understanding the hopping process. Again, the dissipative standard map is too complicated for that purpose. Consequently we

investigate in the following Chapter a different prototype model to address these important questions.

2.3 Summary

In this Chapter the dissipative standard map as a prototype model of multistable behavior has been introduced. After describing its basic properties, noise was applied to the system. This resulted in the attractor-hopping process, in which long laminar-like motion is interrupted by sudden bursts. Another consequence is the washing out of the fine structure of the system, which was visualized through the probability density and some noisy basins of attractions. With the help of Lyapunov exponents the effect of 'noise-induced chaos' was explained, and utilizing finite-time Lyapunov exponents we were able to determine this transition into chaos in detail. The phenomenon of $1/f$-noise has been reported and recent criteria for its occurrence in the attractor-hopping process were tested with the result, that multistable systems favor its occurrence over bistable ones. This is caused through the introduction of many different time scales and a more intertwined basin boundary. Using a specific numerical procedure, the phenomenon of preference of attractors was found, which implies, that for special noise levels the system is more likely to be steered to certain attractors than others. The relationship to similar findings in the literature was pointed out. Then, the noise-induced escape from a metastable state was presented in a preliminary fashion, and the applicability of Kramers' theory suggested. Finally, the importance of the chaotic saddle for the attractor-hopping dynamics was addressed. This point will be dealt with in the following Chapter.

Chapter 3

Noise-induced attractor-hopping and the crucial role of chaotic saddles

The result of the last Chapter revealed the importance of the chaotic saddles for the attractor-hopping process. Since the dissipative standard map exhibits a very complicated evolution in the phase space, we turn here to a more basic map to investigate the role of the chaotic saddles. Therefore, in this Chapter, the noise-induced attractor-hopping process is studied using a more elementary model, namely two coupled logistic maps. Yet this model exhibits still the main features necessary for a complex attractor-hopping process: (i) more than two stable states, to discriminate it from the bistable case and (ii) a fractal basin boundary separating the metastable states, giving rise to a final state sensitivity and to long chaotic transients, when the motion takes place far from the metastable states.

In Section 3.1 we introduce the model of two coupled logistic maps and choose parameters to gain a multistable system. Section 3.1.1 lists the main properties of the system when noise is applied to it, which are basically the same as for the dissipative standard map. The concept of symbolic dynamics is presented in Section 3.1.2, and in turn the complexity of the timeseries resulting from the noise-induced attractor-hopping process by transforming it into a string of symbols is studied utilizing the tools of symbolic dynamics. The Shannon entropy and the topological entropy are computed, which can both be regarded as measures of complexity for the attractor-hopping process. As a system parameter is varied, a sudden increase for both entropies at a certain parameter value is observed. After establishing the invariant quantity of a chaotic saddle with definitions and examples in Section 3.1.3, we explain this increase of the entropies with a novel bifurcation of the underlying

chaotic saddles in Section 3.1.4, namely a merging of two chaotic saddles accompanied by the emergence of additional points filling the gap between the formerly separated saddles. This bifurcation is mediated by a snap-back repellor, whose properties are explained in detail. Finally, a scaling law for the transient life-times on one chaotic saddle close to the bifurcation point is presented in Section 3.1.4, involving the eigenvalues of the mediating repellor in analogy to crisis. The results of this Chapter are summarized in (Kraut & Feudel, 2001b)

3.1   Two coupled logistic maps

As was mentioned at the end of the last Chapter, the noise-induced attractor-hopping process of the dissipative standard map is too involved to elucidate the basic mechanisms. Therefore, we focus in this Chapter on a model, which is more elementary, but still sufficiently complex. The basic presuppositions for the complex behavior are the existence of more than two metastable states and a fractal basin boundary between these states. The first point guarantees, in contrast to a bistable system, that there may exist attractors, between which no direct transitions are possible. The second point causes the trajectory far from the metastable states to wander erratically around in the phase space and introduces a final state sensitivity. Our basic prototype model of multistablity is given by the 10-fold iterate of two coupled logistic maps:

$$
\begin{aligned}
x_{k+1} &= 1.0 - \alpha x_k^2 + \gamma(y_k - x_k) \\
y_{k+1} &= 1.0 - \alpha y_k^2 + \gamma(x_k - y_k).
\end{aligned}
\tag{3.1}
$$

There are two parameters, the nonlinearity α and the coupling strength γ. The space spanned by these two parameters is shown in Fig. 3.1a. Inside the region marked with P10 stable solutions exist. Also shown is the line, above which the dynamics is homoclinic as hatched. We will fix the coupling strength at $\gamma = 0.29$ and vary α, the nonlinearity, in the range $\alpha \in [0.720, 0.785]$. For this parameter set, there exists a stable period 10-orbit for the two coupled logistic maps themselves. Since we consider the 10-fold iterate, our map exhibits 10 coexisting fixed point attractors, where each 5 lie above and below the symmetry axis $x = y$, respectively. Using only initial conditions below the symmetry axis, we can restrict our study to a system possessing 5 coexisting fixed point attractors; there are also 5 repellers with two unstable directions and 10 saddle points. Each of the 5 attractors is surrounded by an open neighborhood of different size, in which all initial conditions converge to the corresponding attractor inside this neighborhood.

The basin of attraction for one of these fixed point attractors is shown in Fig. 3.1b. In this figure also the location of the fixed points, saddle points and repellers

(a)   (b)
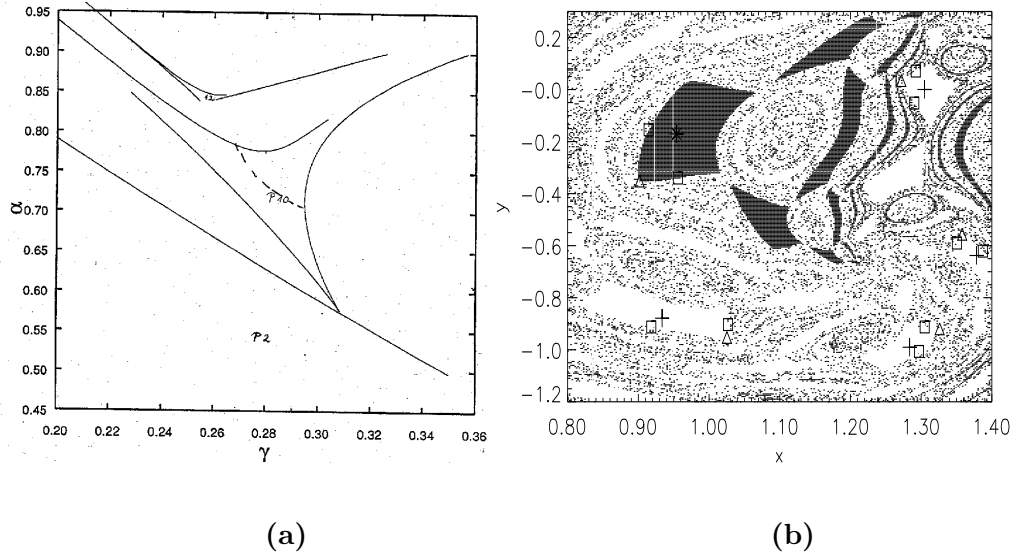
Figure 3.1: (a): Region of stable solutions in the $\gamma - \alpha$ plane. Also the line, above which homoclinic intersections occur, is shown hatched. P10 marks the region, where 10 fixed points for the 10th iterate exist. (b): Basin of attraction of map (3.1) for the fixed point marked with $*$, where $\alpha = 0.74$ and $\gamma = 0.29$. The other fixed points are marked with $+$, the saddle points with $\square$ and the repellers with $\triangle$.

is presented. Around each fixed point there exists an open neighborhood, about the attractor, in which all initial conditions converge to this attractor. The saddle points and repellers are located at the border of this open neighborhood.

3.1.1 Noisy dynamics

Since our investigation is focused on the attractor-hopping process, as a next step we apply noise to the system. We use Gaussian white noise with a standard deviation δ, added to the x and y component. Uniformly distributed noise does not change any of the results. Since we consider the 10-fold iterate of the map, the noise is consequently added only at every 10th iterate. The dynamics is depicted in Fig. 3.2. It exhibits, like the dissipative standard map, noise-induced chaos, which was first described for this system in (Anishchenko & Herzel, 1988). The characteristic features of the attractor-hopping process are present here as well, namely almost regular motion near a fixed point, and bursts similar to intermittent behavior, taking place on the chaotic saddles. However, in this system only 5 metastable states coexist and we can treat the question, in which way and by which mechanism the topology of the hopping dynamics changes as a system parameter is varied, in a much more
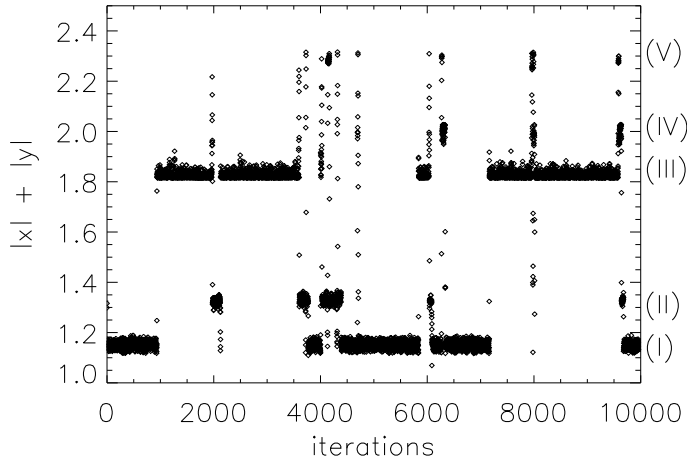
Figure 3.2: Noisy time series of equation (3.1) for $\alpha = 0.73, \gamma = 0.29$ and $\delta = 0.012$. There are clearly 5 distinct almost periodic states, marked with Roman numbers on the right hand side. These states are interrupted by bursts, where the motion takes place on a chaotic saddle.

systematic fashion. This will be done employing symbolic dynamics to the noisy time series.

3.1.2   Symbolic dynamics

For many purposes, it is possible and advantageous to describe the dynamics of a complex system with *symbolic dynamics*, see (Badii & Politi, 1997; Hao, 1989). The phase space $X \in \mathbb{R}^d$, where the motion takes place, is divided into a finite set of partitions $B = B_0, ... B_{b-1}$ consisting of b disjoint subsets: i.e., $\bigcup_{j=0}^{b-1} B_j = X$ and $B_j \cap B_k = 0$ for $j \neq k$. Under the action of the dynamics, the trajectory $x_{i=0}^n$ defines a sequence of visited partition elements. The set $A = 0, ..., b-1$ of labels of the partition elements is called the *alphabet*. Denoting with the symbol $s_i \in A$ the index of the domain $B_{s_i} \in B$ visited at time i, the trajectory is mapped to the symbolic sequence $S = s_0, s_1, ..., s_n$. This reduction of the real trajectory makes, of course, only sense, if the relevant features of the dynamics are still present in the symbolic description. It is equivalent to the real trajectory if every infinitely long symbol sequence corresponds to one single point (initial condition) x_0 in phase space: that is, if there is a map ϕ such that $\lim_{n\to\infty} S = \phi(x_0)$. If this is the case, the partition is called *generating*.

For one-dimensional maps, a generating partition is easily found and given by the coordinates of the critical points (maxima, minima, vertical asymptotes). As an example, the logistic map $x_{n+1} = r x_n(1 - x_n)$ can be transformed into a symbolic

representation with the two symbols **0** and **1**, according to whether $0 \leq x_n < x_c = 0.5$ or $x_c \leq x_n \leq 1$. For multidimensional non-hyperbolic maps, there is no clear rule for the construction of a generating partition. However, a method has been proposed (Grassberger & Kantz, 1985), consisting of connecting homoclinic tangencies together. This technique has been refined, using tangencies and finite pieces of invariant manifolds (Christiansen & Politi, 1995). Another approach is based on an algorithm involving unstable periodic orbits (Davidchack et al., 2000). The effect of a misplacement of the partition has been investigated in (Bollt et al., 2000).

For several reasons, we do not use the encoding scheme outlined above. First, our system is two-dimensional, which makes it quite hard to find the right partition, as described. Second, we have noise applied to our system, which blurs the borders between partitioning lines and makes it impossible to decide, which element the trajectory 'really' visited. Lastly, the trajectory stays often for a very large number of iterations close to a fixed point, which would result in a redundant number of identical symbols. Notwithstanding the fact, that methods have been developed to cope with the last problem (Abel et al., 2000), we use a different encoding scheme (Poon & Grebogi, 1995), which is more appropriate for our purpose, as we are mainly interested in the *topology* of the attractor-hopping process. Neglecting the number of iterations the trajectory spends close to a fixed point, a symbol is given to every fixed point and only after a jump out of an attractor a new symbol is bestowed, according to the attractor where the trajectory lands at. Thus, our alphabet consists of 5 elements, the number of attractors. No symbol is given to the motion far from any attractor. Using this scheme, we focus only on the structural properties of the jumps, not taking fully into account the complete temporal evolution in each iteration.

A measure for the complexity of the attractor-hopping process is now introduced via the *Shannon entropy* (Shannon, 1948)

$$
\begin{aligned}
h_n & = \lim_{n \to \infty} \frac{H_n}{n} = \lim_{n \to \infty} (H_{n+1} - H_n) \\
& = \lim_{n \to \infty} \frac{1}{n} \left(- \sum_{|S|=n} p(S) \log p(S) \right),
\end{aligned}
\tag{3.2}
$$

where $S = s_1 s_2 ... s_n$ denotes a finite symbol sequence consisting of n elements $s_i = 1, 2, ..., 5$, $p(S)$ its probability of occurrence and H_n the block entropy of block length n. If the symbols are given in accordance to the underlying generating partition, the Shannon entropy h_n is identical to the Kolmogorov-Sinai or metric entropy K_1 (Kolmogorov, 1958; Sinai, 1959). With the coding scheme used here, these two quantities differ, though. Yet both are a measure of unpredictability (Wackerbauer

et al., 1994). The difference $h_n = H_{n+1} - H_n$ between block entropies at consecutive hierarchy levels can be interpreted as the information needed to specify the symbol $n+1$, given the previous n symbols. If the process is Markovian of order k, i.e. the memory does extend only to the previous k iterations,

$$h_{k+l} = h_k \quad \forall \quad l \in \mathbb{N}. \tag{3.3}$$

If the process is not Markovian,

$$h_l > h_k \quad \forall \quad l < k. \tag{3.4}$$

In this case, the system is said to exhibit long-range correlations. To test, which class of process the attractor-hopping dynamics belongs to, the quantity $h_n = H_{n+1} - H_n$ is computed for different values of α, as shown in Fig. 3.3. For each case, a time
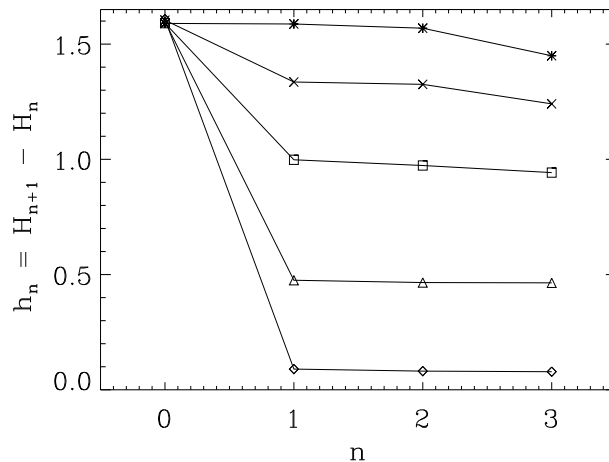
Figure 3.3: Shannon entropy h_n for $\gamma = 0.29$ and various values of α vs n. From bottom to top: $\alpha = 0.72, 0.73, 0.74, 0.75, 0.78$. For $n \geq 1$ h_n remains constant with respect to n, but increases with α.

series with $N = 1000$ symbols has been created and the noise level has been chosen in such a way, that the lengths of the original time series were of the same order of magnitude ($\sim 10^9$). However, it is important to note, that the specific noise level is of no relevance, as long as the dynamics is characterized by attractor-hopping and not by diffusion or trapping in the neighborhood of one attractor. All the findings remain unchanged for noise levels $10^{-5} < \delta < 10^{-2}$. Only the time series would become restrictively long by using a too small noise level. Furthermore, we stress that, although the *escape times* out of the stable states depend on the noise level, the *transition probabilities* remain constant for a wide range of noise values. Therefore,

the considered entropies are not affected by the noise amplitude for the interval of noise levels, which has been used.

As can be seen, for $n = 0$ all curves coincide. Equally obvious is the fact, that for all curves the values for $n = 1$ and $n = 2$ are identical, at least by taking the numerical error into account, which is about the size of the plot symbols. To cope with finite size effects, the first order correction $h_n = h_n + \frac{m(n)-1}{2N}$, derived by (Grassberger, 1988; Herzel, 1988a), has been used, where $m(n)$ is the number of blocks of length n occurring in the symbol sequence (out of 5^n possible ones), and N is the length of the symbol sequence. For $n = 3$ the finite size effects are for higher α even more pronounced. But because of equation (3.3), h_n has to be constant for all n for theoretical reasons and it is not necessary to care about the finite size effects.

The crucial point is, that the attractor-hopping dynamics is a Markov process of first order. This corresponds to the intuitive expectation, that the dynamics possesses only memory of the last state it was dwelling on, since higher correlations are suppressed by the long laminar-like motion. During this motion, the trajectory 'forgets' about the former states. Only for $\alpha \geq 0.755$ the dynamics changes into a Markov process of zeroth order, not even 'remembering' the last state. This transition will be explained in Section 3.1.3.

Another interesting quantity for the investigation of the symbol sequence is the *topological entropy* (Adler et al., 1965). It is defined as the exponential growth rate of the number $N(n)$ of allowed sequences as a function of their length n and thus classifies the 'richness' of a dynamical system mapped to a symbol sequence

$$\lim_{n\to\infty} N(n) \sim \exp(nh_T). \tag{3.5}$$

The strict inequality $h_T = K_0 > K_1$ applies. The most straightforward way to compute the topological entropy is using equation (3.5)

$$h_T = \lim_{n\to\infty} \frac{\log N(n)}{n}. \tag{3.6}$$

This might become a quite cumbersome computation, as the number of possible sequences $N(n)$ can become very large, but the result of quite a few n values is needed, to obtain a sufficiently large scaling region. Moreover, the topological entropy counts only the number of sequences independently of their probability of occurrence. Thus extremely long trajectories are needed to catch also sequences which are extremely rare. However, in our case there is a much more elegant way of computing the topological entropy. As was found above, we are dealing with a first order Markov process. Consequently it is possible to construct a 5×5 transition Matrix M, called the *Stefan*

transition matrix, entailing as entries **1** or **0**, depending on whether a transition between the corresponding states has taken place or not, respectively. The topological entropy is the logarithm of the largest eigenvalue of this matrix (Derrida et al., 1978; Hao, 1989).

In our numerical implementation, we use a certain very small cutoff limit of 10^{-3} for the transition probabilities, below which we regard the value as zero. Consequently, we neglect transitions, having extremely small probabilities compared to the other transitions, extinguishing by this procedure numerical artifacts. However, the exact value of this cutoff does not change the results significantly, as long as it is small enough. The topological entropy remains unchanged for cutoff limits between 10^{-2} to 10^{-4}. (For some control simulations $N = 10000$ was used to check, if these rare transitions depend on the length of the time series.) The Shannon entropy h_n can also be found using the Matrix representation, the entries are the actual transition probabilities. The result for both entropies is depicted in Fig. 3.4. The topological
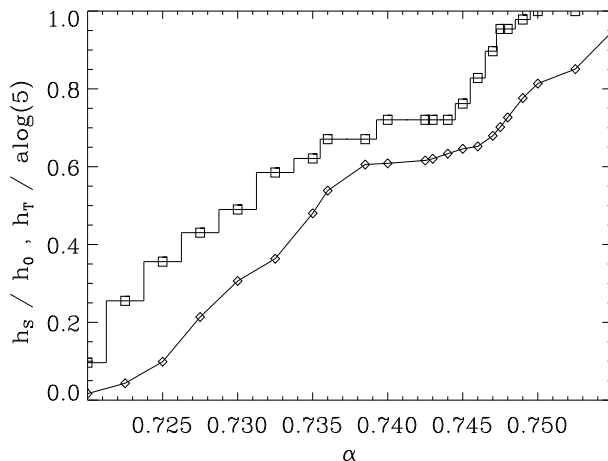
Figure 3.4: The Shannon entropy ($\Diamond$) and the topological entropy ($\Box$) of the symbol sequence under variation of the nonlinearity parameter α. Both quantities are normalized to 1.

entropy is always larger than the Shannon entropy, as it has to be. The Shannon entropy grows monotonically, in a smooth fashion, whereas the topological entropy seems to exhibit a *devil's staircase* behavior, which is defined as remaining constant for almost all values and increasing only at values of a Lebesgue measure zero (Ott, 1993). Devil's staircase behavior has for the first time been theoretically proposed in (Mandelbrot, 1977).

For physical systems, it was analyzed using a simple one-dimensional model with external pressure in (Aubry, 1978) and later in phase transitions of CeSb in (von Boehm & Bak, 1979). The first rigorous derivation of the existence of a devil's staircase was presented in (Bak & Bruinsma, 1982), dealing with the ground state of the Ising model with long-range interactions. It has also been discovered in the rotation numbers describing mode-locking in the circle map (Jensen et al., 1983) and was found experimentally in a variety of systems, like in a periodically driven pendulum with an additional constant external torque (Jensen et al., 1984) and in the voltage spectrum of a periodically driven Barium-Sodium-Niobate (BSN) crystal (Martin & Martienssen, 1986). Devil's staircase behavior has further been detected in the pressure dependence of the number of metastable configurations in a chain of particles (Häner & Schilling, 1989) and in chaotic scattering systems (Rückerl & Jung, 1994). Recently, it has been predicted to occur in the magnetoresistance of electron transport in two-dimensional periodic arrays of scatterers under the influence of a uniform magnetic field as well (Wiersig & Ahn, 2001).

The devil's staircase for the topological entropy was originally detected numerically in (Biham & Wenzel, 1989) and subsequently analytically investigated in (Breymann & Vollmer, 1997; Lai et al., 1999). The phenomenon occurs also in systems exhibiting chaotic scattering (Lai & Grebogi, 1994; Życzkowski & Lai, 2000) and in communication with chaos (Bollt et al., 1997). The general mechanism is the existence of forbidden words for certain parameter regions, which has been termed 'pruning' in the context of unstable periodic orbits (Cvitanovic et al., 1988).

In our case, this corresponds to the prohibited transitions between certain attractors. The matrix M changes only, if a new transition between hitherto unconnected attractors is created (turning a **0** into a **1**), which happens only at finitely many α values. Otherwise the matrix remains constant. Below the homoclinic bifurcation $\alpha < 0.72$, where the basin boundaries are smooth, only one transition per fixed point attractor is possible, as the fixed points are located on a closed curve formed by the unstable manifolds of the saddle points. These unstable manifolds impose a direction. Consequently, the topological entropy is zero. Above a value of $\alpha \approx 0.75$, all transitions can occur and the maximum of the topological entropy is reached. Besides the overall increase of both entropies, the plateau between $0.740 < \alpha < 0.744$ suggests, that there is a change in the dynamical behavior beyond it, as the entropies are rising steeply for $\alpha > 0.744$. This change is due to a change in the structure of the chaotic saddles of the system. Already at the end of Chapter 2 the importance of the chaotic saddle for the attractor-hopping process was mentioned. In the following, the crucial role of the chaotic saddles will be pointed out in detail.

3.1.3   Chaotic saddles

A chaotic saddle is a geometrically strange, invariant, non-attracting set. It resembles in some sense a strange attractor, yet missing the property of attractiveness. It is called 'chaotic', since it exhibits a positive Lyapunov exponent, if the motion is taking place strictly on the invariant set. It is geometrically strange, because it possesses a Cantor-like structure. If the motion is not exactly on the saddle, which will always be the case in numerics and experiments, the trajectory leaves the saddle after some time. The transient life-times decrease exponentially in time and can be expressed in terms of Lyapunov exponents (Kantz & Grassberger, 1985; Hsu et al., 1988). A trajectory starting from a random initial condition in a phase space region containing a chaotic saddle typically stays near the saddle exhibiting a chaotic-like dynamics for a finite amount of time before exiting the region eventually and asymptoting to a final stable state. Chaos in this case is only transient.

Necessary conditions for the occurrence of a chaotic saddle are homoclinic or heteroclinic intersections of manifolds of the system. A *homoclinic* intersection, where the stable and unstable manifolds of a periodic orbit of the system intersect, implies horseshoe type dynamics, which in turn makes the invariant set describable by symbolic dynamics (Smale, 1967). The horseshoe type dynamics consists of stretching and folding, which is the soul of chaotic dynamics. All points belonging to a chaotic saddle are direct sums of stable and unstable subspaces.

Mathematically, chaotic saddles are closed, bounded, invariant sets having a dense orbit. Physically, they play a fundamental role in fractal basin boundaries (McDonald et al., 1985), transient motion (Grebogi et al., 1983b; Jánosi et al., 1994), even superlong chaotic transients (Grebogi et al., 1985; Crutchfield & Kaneko, 1988; Lai & Winslow, 1995), chaotic scattering (Bleher et al., 1989), open hydrodynamic flows (Eckhardt & Aref, 1988; Péntek et al., 1995), fractal distribution of chemicals in environmental flows (Toroczkai et al., 1998), chaotic communication (Bollt et al., 1997), and the fluctuation of finite-time Lyapunov exponents in high-dimensional systems (Dawson, 1996; Moresco & Dawson, 1997). As will be demonstrated in Chapter 4, chaotic saddles are also of crucial importance in the noise-induced escape problem from a metastable state. Here we elucidate the role of the chaotic saddles for the hopping process.

Since a chaotic saddle is non-attracting, a special algorithm is needed for computing it. We use the *PIM-triple (proper interior maximum) method* of Nusse and Yorke (Nusse & Yorke, 1989). Two initial points of the phase space are chosen at the upper right and lower left corner, respectively. They are connected by a line, and on this line about $30 - 50$ equidistant points are selected. All these points are

iterated with respect to the dynamics of the system until they terminate in a stable state. The point, which needed the highest number of iterations is marked and the two neighboring points are taken as new initial conditions. This process is repeated, until a desired precision of the distance of the two points, say with a threshold of 10^{-12}, is reached. Thereby one saddle point has been found, at least in the frame of our numerical precision. This point is iterated, to generate more points pertaining to the saddle, until the threshold is crossed. Then the refinement procedure starts again and so on. Using this iterative scheme, in principle an infinitely long trajectory of points on the saddle can be created. At least in two dimensions this method works very well and is believed to typically generate the natural measure on the chaotic saddle (Jacobs et al., 1997). In higher dimensional systems the algorithm requires some modifications (Sweet et al., 2001).

3.1.4 Merging bifurcation of chaotic saddles

The result of the computation for the coupled logistic maps is shown in Fig. 3.5 for 4 values of α. In Fig. 3.5a slightly above the homoclinic bifurcation ($\alpha = 0.72$), there exist two separate saddles, which is graphically accentuated by the use of two different gray scales. Initial conditions starting exactly on one of the rings would stay there forever. Thus, there exist two disjoint invariant sets. Moreover, the saddles are very thin, since there are very few homoclinic intersections. Also, the structure of the manifolds imposes a clockwise direction on the dynamics on the rings, which makes only transitions to one nearest neighbor and some next nearest neighbors possible, hence both entropies are small (compare Fig. 3.4). For $\alpha = 0.740$ (Fig. 3.5b) the saddles have enlarged, causing more transitions in the hopping dynamics, yet the separation of the two rings is still present. Increasing α to 0.745 (Fig. 3.5c) results in a bifurcation, which leads to only one large chaotic saddle. Above the critical value, the connected piece of the chaotic saddle enables the trajectory to jump between the formerly separated parts, thereby causing a sharp increase in the number of the possible transitions, as can be seen from the topological entropy above $\alpha = 0.744$ in Fig. 3.4. The gaps of the former separated pieces are filled successively, until also the distinction between former gaps and saddle rings has vanished in Fig. 3.5d. This point will be discussed in more detail in Section 3.1.5.

For the value of $\alpha = 0.78$ both entropies have already attained their maxima, and the hopping dynamics has undergone a transition from a Markov process of first order to zeroth order. This means, that the trajectory is injected after an excursion on the chaotic saddle to an attractor without memory on the last attractor it was staying on before.
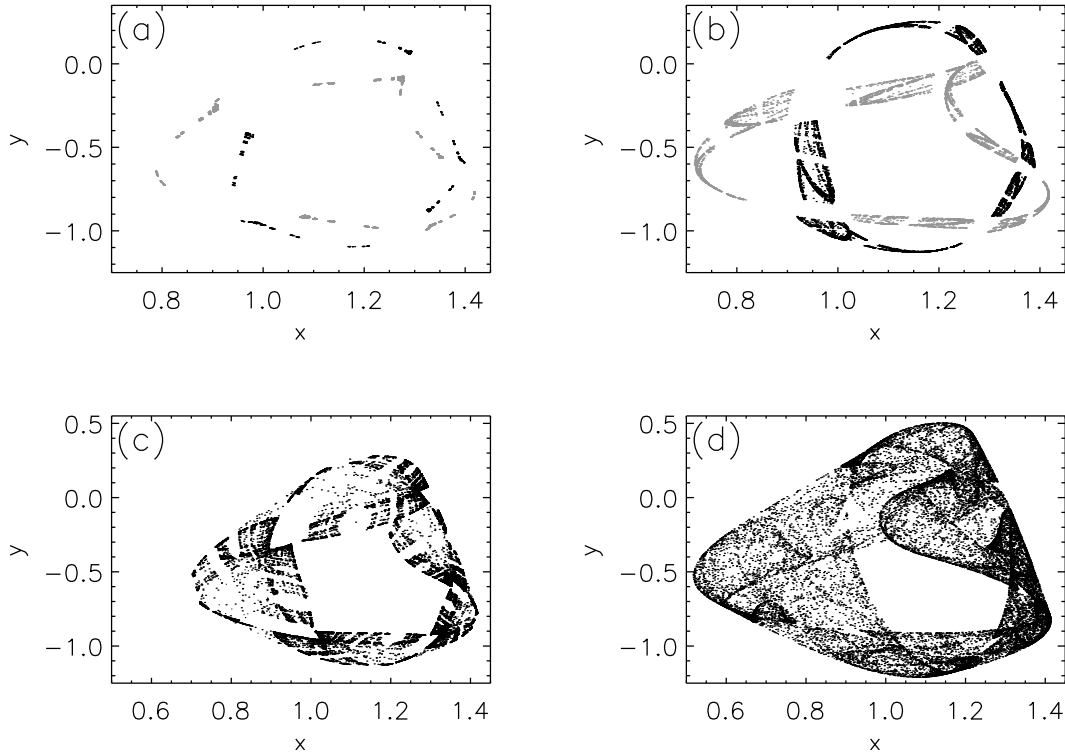
Figure 3.5: The chaotic saddles for the 10-fold iterates of equations (3.1).The values for α are (a) : 0.725, (b): 0.740, (c): 0.745 and (d): 0.780. In (a) and (b) the separate rings are depicted in a different gray scale. In (c) and (d) only one connected, large saddle is present.

To investigate the nature of the bifurcation more specifically, in Fig. 3.6 the chaotic saddle is shown again for 2 values of α below and above the bifurcation, together with the 4-fold preimages (marked +) of the repellor (marked □). It is clearly visible, that the repellor, formerly located outside of the saddles (like in Fig. 3.6a and for smaller α values), is now embedded in the large saddle (Fig. 3.6a and for larger α values). The same is true for the some preimages of the repellor, respectively. Hence, we have discovered a new merging crisis, mediated by a repellor. This can only take place because our system is non-invertible. That the repellor can be embedded in the chaotic saddle is at first sight counterintuitive, since it is repelling in both directions, while every point on the chaotic saddle has one stable direction. However, we
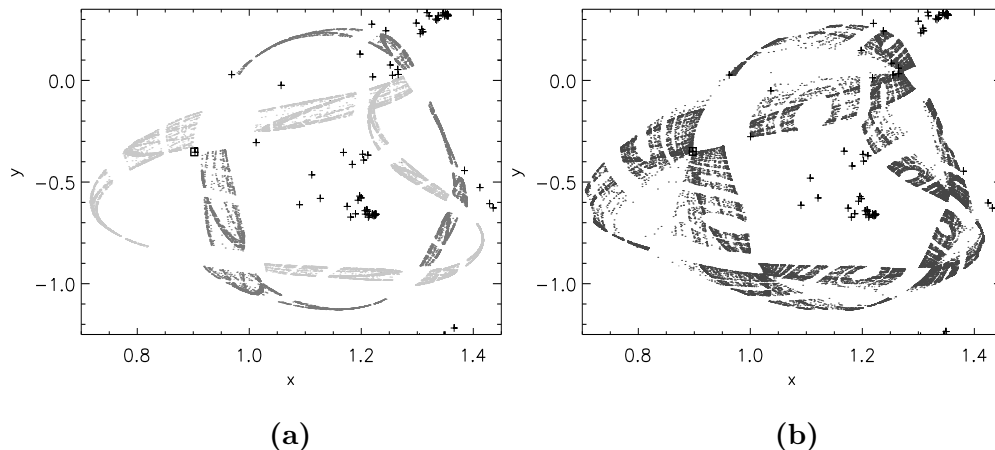
Figure 3.6: (a): Two chaotic saddle rings in different gray scale together with the 4-fold preimages (+) of the repellor R marked with a □ for $\alpha = 0.740$. (b): Chaotic saddle together with the 4-fold preimages (+) of the repellor R marked with a □ for $\alpha = 0.743$.

have encountered a special form of a repellor, namely a *snap-back repellor* (Marotto, 1978). A fixed point p is called a snap-back repellor, if

- all eigenvalues of p have absolute values larger than 1,

- there exists a $q \in W_{loc}^u(p)$, the unstable manifold of p, such that the M-fold iterate of the map $\mathcal{F}^M(q) = p$ for some positive integer M,

- $\det D\mathcal{F}^M(q) \neq 0$.

The first condition is obviously fulfilled, since p is a repellor. The third condition can also be checked explicitly, using the formalism of the critical lines for non-invertible discrete systems (Mira et al., 1996; Abraham et al., 1997). The critical curve of zeroth order

$$L_0 := \{(x,y) \mid \det D\mathcal{F}(x,y) = 0\} \tag{3.7}$$

marks the regions in the phase space, where the Jacobian is zero. With the iterates of this critical curve

$$L_k = \mathcal{F}^k(L_0), \tag{3.8}$$

the absorbing area $\mathcal{A}$ can be constructed with the properties (i) that once the trajectory has entered this area, it can never leave again, and (ii) all points from the

neighborhood will be mapped into the absorbing area in a finite number of itera-
tions. The absorbing area is analogous to the trapping region used in Section (2.1).
Its boundary $\partial\mathcal{A}$ can be generated by

$$\partial\mathcal{A} = \bigcup_{k=1}^{M} \mathcal{F}^k(L_0) \tag{3.9}$$

for some suitable M. With the help of the absorbing area, the bifurcation scenario
of the same system, Eqs. (3.1), has been successfully revealed in the context of
synchronization (Maistrenko et al., 1998). A numerical calculation shows, that the
critical curve L_0 does not coincide with any of the preimages of the repellor, confirm-
ing the last condition. Only the second criterion remains to be scrutinized, which is
done in Fig. 3.7b for $\alpha = 0.7428$, where the bifurcation takes place.
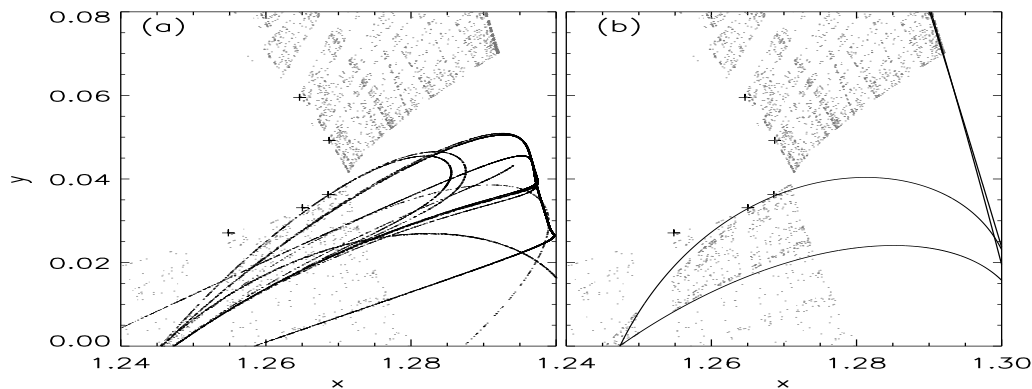
Figure 3.7: Saddle and preimages for $\alpha = 0.7428$. In (a) the unstable manifold of
the repellor is also shown, demonstrating the collision with some preimages of the
repellor. In (b) the same region is presented, indicating that the critical curves touch
some preimages, too.

3.1.5   Scaling laws of saddle merging bifurcation

The critical curves $L_k, k \neq 0$ are building the border of the saddle and collide with
some preimages of the repellor. The same holds for the unstable manifold, depicted
in Fig. 3.7a. Actually, only the one-dimensional projection in the most unstable
direction of the unstable manifold is shown, as it is clearly two-dimensional (orig-
inating from a repellor with two unstable directions). Both pictures confirm the
presented mechanism for the development of the snap-back repellor, which makes it
'attractive' for certain points.

One feature of the bifurcation is worth further discussion. Increasing the bifurcation parameter α slowly beyond the saddle merging value of $\alpha = 0.7428$, additional points between the two rings are created *smoothly*. This can be seen in Fig. 3.6b, where some points not belonging to one of the two rings are visible. Increasing α further results in more points (compare Fig. 3.5c), until the former gap is filled in such a way, that the two rings cannot be distinguished from it anymore (Fig. 3.5d).

Similar bifurcations of chaotic saddles have been reported recently. An *abrupt* filling of a chaotic saddle during the crisis has been investigated in (Szabó et al., 1996; 2000), where also a scaling law for the topological entropy close to the crisis has been derived. Explosions of non-attracting chaotic sets have been treated in (Robert et al., 1998; 2000), where the term explosion refers to the creation of new pieces of the invariant set located at a *finite distance*, when changing a bifurcation parameter. A scaling law describing the creation of unstable periodic orbits following such a bifurcation is provided as well. The merging of two chaotic saddles *without* the creation of additional points was found in a system of chaotic scattering (Lai et al., 1993; Lai & Grebogi, 1994).

However, in none of these cases an effect like in our system has been observed, namely that additional points are created (for $\alpha \geq 0.7428$) before the actual merging of the two invariant sets is taking place (the repellor becomes embedded in the chaotic saddle at $\alpha = 0.743$). This effect has been described in two-dimensional systems before, but only for the union of chaotic *attractors*. In (Chin et al., 1992) it has been termed 'spilling' and conditions for the occurrence have been established. In (Maistrenko & Sushko, 1998), also dealing with chaotic attractors, a contact bifurcation of the first kind was investigated and 'rare points' before the actual merging were found. The authors suspect a repellor responsible for this phenomenon, but did not elucidate its role in detail, as is done in the present work.

In the following, we want to motivate the application of a scaling law of the transient life-times in analogy to *crisis*. Sudden changes, caused by the collision of a chaotic attractor with an unstable periodic orbit or, equivalently, its stable manifold, have been called crisis (Grebogi et al., 1982). There exist three main types of crises: (i) A boundary crisis, where a chaotic attractor is suddenly destroyed, because the attractor collides with a periodic orbit on its basin boundary as the parameter passes through its critical value. (ii) An interior crisis, where the attractor is suddenly blown up in size, as it collides with a periodic orbit in the interior of its basin. (iii) A merging crisis, where two or more attractors merge caused by the collision with a periodic orbit on the basin boundary separating them.

After a boundary crisis, chaotic transients result (after which the trajectory leaves the former attractor), while in the latter two cases 'crisis-induced intermittency' can be observed, with sudden bursts away from the attractor, after which the trajectory returns to it. For all types, scaling laws, for the average transient life-times have been derived for the heteroclinic and the homoclinic case, respectively (Grebogi et al., 1986a; 1987b), and read

$$\tau \sim |p - p_c|^{-\epsilon}, \tag{3.10}$$

where p_c is the critical parameter at which the crisis occurs and ϵ is the universal exponent, given by an expression depending on the eigenvalues of the mediating saddle point for each case.

Experimentally, the transient life-times are an important quantity, as they are relatively easily measurable. The scaling laws have been experimentally observed for all the three types in various systems, e. g. the interior crisis for the homoclinic case in nonlinear oscillators (Jeffries & Perez, 1983), diodes (Rollins & Hunt, 1984) and a gravitationally buckled, parametrically driven, magnetoelastic ribbon (Ditto et al., 1989); for the heteroclinic case in NMR-lasers (Finardi et al., 1992). Boundary crisis have been found in CO_2-lasers (Dangoisse et al., 1986) and spin-wave experiments (Carroll et al., 1987), while a merging crisis was observed in a semiconductor in (Karakotsou & Anagnostopoulos, 1996).

When two parameters of a system are varied simultaneously, vertices in parameter space can be found, where sudden changes of both the chaotic attractor and of its basin boundary take place (Gallas et al., 1993). This can also cause the occurrence of a generalized crisis, at which an interior and a boundary crisis coincide (Stewart et al., 1995).

Also of interest is the effect of noise-induced crisis, where the existence of noise changes the scaling law into a generalized form. This phenomenon was examined numerically (Arecchi et al., 1984), analytically (Sommerer et al., 1991b), and has also been confirmed experimentally (Sommerer et al., 1991a). The noisy scaling law is given by

$$\tau \sim \delta^\epsilon g((p - p_c)/\delta). \tag{3.11}$$

Here δ is a measure of the strength of the noise, $g(.)$ is a non-universal function depending on the specific system under investigation and the distribution function of the noise, and ϵ is the universal critical exponent of the corresponding *deterministic* crisis. Noise near crisis has also been found to lead to stabilization of the transient motion (Franaszek, 1991; Reimann, 1994).

To establish the connection between crisis and the saddle merging bifurcation, we define the transient life-times in our system as the average number of iteration of points on the chaotic saddle calculated with the PIM-triple method and using as initial condition a point pertaining to one of the former rings, before the algorithm produces points on the other former ring. If these transient life-times obey any scaling relation, they should do so for values of the nonlinearity slightly above the bifurcation value of $\alpha = 0.7428$, at which the two rings become connected through the additional points. The calculation is shown in Fig. 3.8. The graph exhibits
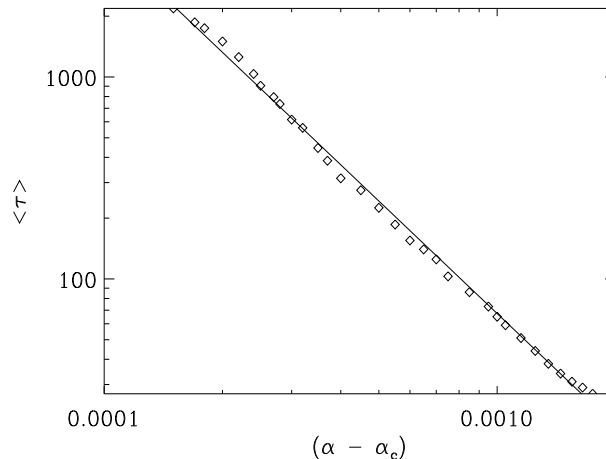
Figure 3.8: Scaling of the transient life-time to stay in one ring of the chaotic saddle with the nonlinearity α and $\alpha_c = 0.7428$. The slope of the log-log plot is $\epsilon = -1.86$.

clearly a power-law scaling of the form of Eq. (3.10). The best fit to the data yields an exponent $\epsilon = 1.86$. It is worth mentioning, that some oscillations are superimposed on the power-law scaling of Fig. 3.8. They are a direct consequence of the fractal structure of the basins of attraction (Kacperski & Holyst, 1999). While at a crisis a saddle point is the mediating link of the bifurcation, in our system a repellor mediates the merging. Although the bifurcation entailing a snap-back repellor is homoclinic (Devaney, 1989), the way the repellor is approached differs qualitatively from the way a stable fixed point or saddle point is approached, as is demonstrated in Fig. 3.9 for a one-dimensional map schematically. While in the first case, the distance of the trajectory and the fixed point decreases monotonically in size until the distance becomes infinitesimal, the snap-back repellor is approached with a jump of finite size from some distance. This behavior resembles more the heteroclinic tangency. Hence, we argue that the scaling of the transient life-times of the saddle
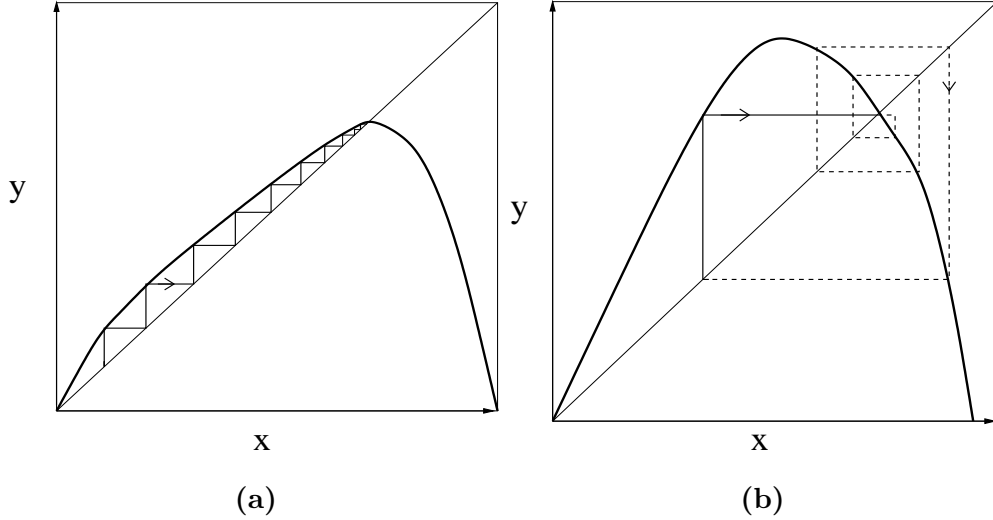
Figure 3.9: (a): Schematic presentation of a one-dimensional map with a stable fixed point. Every iteration comes closer to the fixed point, until the distances is infinitesimal. (b): Schematic presentation of a one-dimensional map with a snap-back repellor. At the dashed lines, the trajectory leaves the repellor, until (at solid lines) it jumps at the unstable fixed point from a finite distance.

merging can be described by the law of the heteroclinic case, given by

$$\epsilon = 1/2 + (\ln(\beta_1)/\ln(\beta_2)). \tag{3.12}$$

In the original derivation of this formula, β_1 and β_2 are the expanding and contracting eigenvalues of the mediating saddle point (Grebogi et al., 1986a). However, in our case both, β_1 and β_2, are expanding eigenvalues of the mediating repellor. When using the numerical values, we obtain

$$\epsilon = 1/2 + (\ln(2.45)/\ln(1.9)) = 1.85, \tag{3.13}$$

reproducing the exponent ϵ with a very good accuracy. To further verify the correctness of Eq. (3.12), we use other values of the coupling strength γ. For $\gamma = 0.292$ the result is shown in Fig. 3.10. The best fit to the data yields an exponent of $\epsilon = 1.93$, while Eq. (3.12) gives

$$\epsilon = 1/2 + (\ln(2.07)/\ln(1.66)) = 1.935, \tag{3.14}$$

which again is an excellent agreement. More values of γ have been tested, which all confirm the applicability of Eq. (3.12).
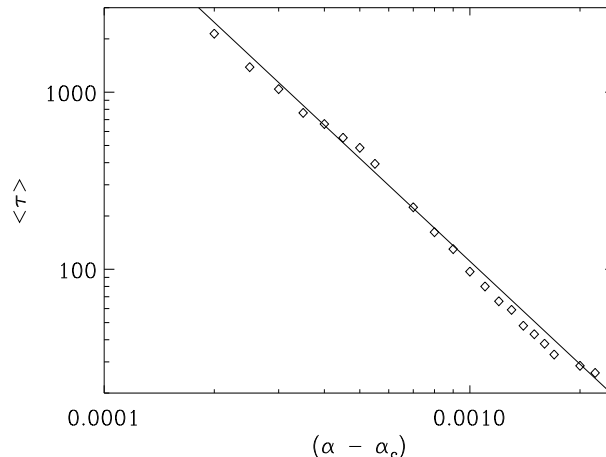
Figure 3.10: Scaling of the transient life-time to stay in one ring of the chaotic saddle with $\gamma = 0.292$, the nonlinearity α and $\alpha_c = 0.7353$. The slope of the log-log plot is $\epsilon = 1.93$.

The topological entropy has been computed in Section 3.1.2 only for the symbolic dynamics of the attractor-hopping process. It is also interesting to determine the topological entropy for the saddle itself, as the devil's staircase behavior was encountered there in a variety of systems, compare Section 3.1.2. Since no generating partition is known for our system, we computed the topological entropy employing an algorithm using stretching rates developed in (Jacobs et al., 1998). In our case, due to the nonhyperbolicity of the system, there exists a nonmonotonic behavior of the topological entropy versus the nonlinearity α (not shown). These fluctuations are also present in the graphs of the uncertainty exponent of the basin boundary and of the generalized dimensions D_0, D_1 and D_2 (box-counting dimension, information dimension and correlation dimension) of the saddle versus the nonlinearity α (not shown). Similar findings for a one-dimensional map have been reported in (Życzkowski & Lai, 2000). However, the box-counting dimension close to the value of the merging of the two saddle rings obeys a scaling relation, as depicted in Fig. 3.11. The plot $D_0(\alpha) - D_0(\alpha_{merge})$ versus $\alpha - \alpha_{merge}$ yields a straight line, extending over almost three orders of magnitude, whose slope is the exponent of the scaling relation

$$D_0(\alpha) - D_0(\alpha_{merge}) \sim (\alpha - \alpha_{merge})^\zeta \tag{3.15}$$

It is important to note, that in Eq. (3.15) the critical value of Eq. (3.10) is not the critical value $\alpha_c = 0.7428$, where the bifurcation takes place, but the value $\alpha_{merge} = 0.743$, where the actual merging of the two saddle rings occurs, since the
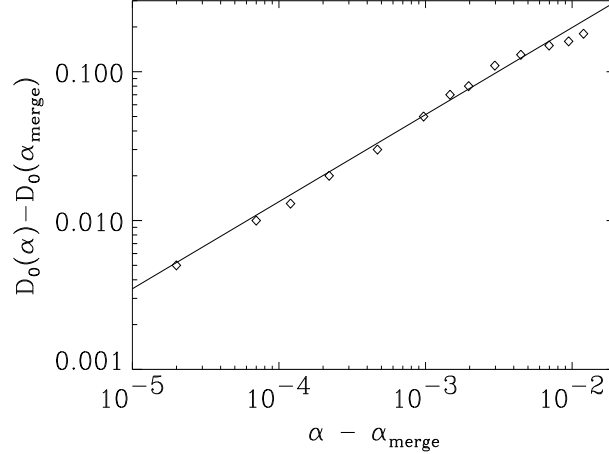
Figure 3.11: Scaling of the box-counting dimensions $D_0(\alpha) - D_0(\alpha_{merge})$ versus the nonlinearity $\alpha - \alpha_{merge}$ in a log-log plot, where $\alpha_{merge} = 0.743$ is the value of the actual merging. The slope of the log-log plot is $\zeta = 0.585$.

box-counting dimension is unaffected by the rare points and increases only after the merging occurred.

A similar scaling relation for fractal dimensions of the basin boundaries has been found for various types of intermittency in (Park et al., 1989). There the scaling exponent was $\zeta = 0.5$, while in our case it is $\zeta = 0.585$. We argue, that in our case the increase of the size of the chaotic saddle, described by the exponent ζ in Eq. (3.15) can be related to the expansion rates of the mediating repellor via the form

$$\zeta = \ln(\beta_1) \ln(\beta_2) \tag{3.16}$$

since the unstable manifolds build the border of the chaotic saddle and are determined by the stretching rates of the eigenvalues β_1, β_2. If we set in the eigenvalues, we get

$$\zeta = \ln(2.46) \ln(1.94) = 0.596, \tag{3.17}$$

which is a good agreement. Thus, the transient life-times on the saddle as well as the box-counting dimension of the saddle are determined by the eigenvalues of the repellor mediating the bifurcation.

3.2 Summary

This Chapter treated the role of chaotic saddles in the attractor-hopping process in detail. Two coupled logistic maps were used as a basic model. It was chosen

to be as simple as possible yet as complex as necessary, exhibiting more than two attractors and a fractal basin boundary. After introducing the basic concepts of symbolic dynamics, a special encoding procedure was utilized, which proved to be very adequate for our aims. The symbol string attained this way was found to reflect a Markov process of order 1. It was analyzed employing the Shannon entropy and the topological entropy. A sudden increase in both entropies with the variation of the nonlinearity parameter at a special value was observed. This increase was explained by a novel merging bifurcation of the underlying chaotic saddles involving a snap-back repellor. The bifurcation was further highlighted with a scaling relation of the transient life-times on one separated part of the chaotic saddle before the merging took place, in analogy to crisis. For the increase of the size of the chaotic saddle after the merging, a scaling relation has been presented as well. The bifurcation and the scaling law for the transient life-times should in principle be observable performing experiments with such systems.

Chapter 4

Enhancement of noise-induced escape through chaotic saddles

This Chapter deals with noise-induced escape out of a metastable state. This question was already treated in Section 2.2.4 for the dissipative standard map in a preliminary way. Here we give a more detailed account of this problem and present in particular the new phenomenon of enhancement of noise-induced escape through the existence of chaotic saddles, as a parameter is varied. Our findings are explained employing the theory of quasipotentials. In Section 4.1 the noise-induced escape problem is exposed for nonequilibrium systems and recent progress in this field is presented, with emphasis on the prehistory probability density and the most probable exit path. Section 4.2 introduces the theory of quasipotentials as a minimization method and explains its main features. After describing the Ikeda map, which is a basic model for a laser cavity, the novel phenomenon of enhancement of noise-induced escape through the existence of chaotic saddles is shown to occur for this system in 4.3. The effect can be explained, when the theory of quasipotentials is applied to the problem, as is done in Section 4.3.1. The results obtained in this Chapter will be published in (Kraut & Feudel, 2001a).

4.1 Noise-induced escape: Recent developments

Since the seminal treatment of the noise-induced escape problem by Kramers, culminating in the escape rate given by Eq. (2.18) (Kramers, 1940), major progress has been made by Onsager and Machlup, who realized, that the escape process consists of large fluctuations, which are very rare, and peaks sharply around some *optimal (most probable) escape trajectory* (Onsager & Machlup, 1953a; 1953b). Thus, despite the stochastic nature of the escape process, caused by the noise, the escape path is of almost deterministic nature, as other paths than the most probable one have an ex-

ponentially smaller probability. That theory was derived for a small noise level $\delta \to 0$ and systems in thermal equilibrium. For multidimensional potential wells, the theory has been generalized in (Landauer & Swanson, 1961), including also the prefactor of Eq. (2.18). A measurement confirming the scaling behavior in a three-dimensional bistable optical trap has been conducted in (McCann et al., 1999). The whole topic with the most important advancements is reviewed in (Hänggi et al., 1990; Mel'nikov, 1991)

In the last decade, one has realized, that systems that are not in thermal equilibrium or are lacking the property of detailed balance, can give rise to a large variety of interesting phenomena in the noise-induced escape problem. Only in the last years experiments on this problem have been conducted, utilizing Josephson junctions (Vion et al., 1996), electronic circuits (Luchinsky & McClintock, 1997) and an electron in a Penning trap (Lapidus et al., 1999). Some of the most interesting novel theoretical findings include a pre-exponential factor of the Kramers rate (2.18) (Maier & Stein, 1992), a symmetry breaking bifurcation of the optimal escape path (Maier & Stein, 1993) and a critical broadening of the distribution of the escape paths originating from a cusp point singularity (Dykman et al., 1996). Further, the very intriguing phenomenon of saddle-point avoidance in noise-induced escape for a particular bistable system has been discovered (Luchinsky et al., 1999), which is remarkable, since the trajectory in general always leaves the metastable state via a saddle point located at a local maximum of the potential (at the basin boundary). For systems where the escape occurs over a fluctuating barrier the effect of resonant activation has been theoretically predicted (Doering & Gadoua, 1992) and experimentally confirmed in a tunnel diode (Mantegna & Spagnolo, 1996). The question of short time scales in the Kramers problem has also been addressed, leading to a stepwise growth of the escape rate, if the quasistationary distribution within the wells has not been achieved (Soskin et al., 2001b). Recently, also the escape from a multiwell potential has been considered. An oscillation of the escape rate in dependence of the friction has been demonstrated (Soskin, 1999; Arrayás et al., 2000). For periodically driven systems a number of interesting results has been obtained as well, like a resonantly decrease in the activation energy (Dykman et al., 1997), a logarithmic susceptibility of the fluctuation probability (Smelyanskiy et al., 1997), time oscillations of escape rates (Smelyanskiy et al., 1999) and enhancement of escape due to transient chaos (Soskin et al., 2001a).

Since the escape process is governed by large fluctuations, which occur, however, very rarely, numerical and experimental investigations are very timeconsuming, because the theoretical results are only valid for the noise strength $\delta \to 0$ and the time scales exponentially with the inverse noise strength. One way to overcome these

difficulties consists in the construction of the *prehistory probability density*. This approach exploits the fact, that the tail of the probability density distribution must be formed by large occasional outbursts of noise that push the system far from the metastable state. The probabilities of such outbursts are small, and the chance to reach a given remote point in phase space will actually be determined by the probability of the *most probable* outburst among those bringing the system to this point. This particular realization is just the optimal fluctuation.

This method has been introduced in (Dykman et al., 1992) and made it possible to conduct experiments with analogue electrical circuits (Dykman et al., 1996; Luchinsky & McClintock, 1997), and semiconductor lasers (Hales et al., 2000). It has also been employed to study in detail the escape process from chaotic attractors, namely for a nonlinear oscillator (Luchinsky & Khovanov, 1999) and the Lorenz attractor (Anishchenko et al., 2001). The most probable exit path plays an important role in control problems as well. If an additive function is sought, which minimizes the energy necessary to steer the system out of a metastable state, the optimal function is found to evolve the system exactly along the most probable exit path (Khovanov et al., 2000).

4.2 Theory of quasipotentials

An approach, conceptually similar to the most probable escape path, to describe systems not in thermodynamic equilibrium, which are under the influence of noise, has been established with the theory of *quasipotentials*, also referred to as *nonequilibrium potentials*. In the mathematical literature, they have been introduced by Freidlin and Wentzell for time-continuous systems (Freidlin & Wentzell, 1984) and transferred to the discrete time case by Kifer (Kifer, 1988). For systems of physical interest, they were first proposed in (Graham & Tél, 1984) and extended to systems with coexisting attractors in (Graham & Tél, 1986). Discrete systems with strange invariant sets were for the first time treated in (Graham et al., 1991).

With the help of quasipotentials, invariant densities, mean first exit times, and the noise scaling behavior of invariant probabilities can be calculated. The nonequilibrium potential can exhibit discontinuities along certain surfaces in the configuration space, which are created by the coexistence of attractors (Graham & Tél, 1986; Reimann & Talkner, 1991). These discontinuities may have intriguing consequences on measurable quantities, such as mean first passage times. Also noise scaling of golden critical circle maps (Hamm & Graham, 1992b) and noise-induced attractor explosions have been investigated (Hamm et al., 1994). A detailed account for noise scaling properties in discrete systems can be found in (Hamm, 1993), which also

treats the scaling for non-Gaussian noise distributions. Good reviews can be found in (Graham, 1989; Graham & Hamm, 1992; Hamm & Graham, 1992a).

One derivation for the quasipotential is as follows. Let a dynamical system be described by a set of differential equations

$$\dot{q}^\nu = K^\nu(q) \tag{4.1}$$

and let some positive-definite 'transport matrix' $Q^{\nu\mu}(q)$ be given. A nonequilibrium potential $\Phi(q)$ may be introduced as a continuous but not necessarily continuously differentiable solution of

$$K^\nu(q) = r^\nu(q) - \frac{1}{2}Q^{\nu\mu}(q)\partial_\mu\Phi(q) \tag{4.2}$$

$$r^\mu(q)\partial_\mu\Phi(q) = 0 \tag{4.3}$$

with the constraint that Φ should be minimal in attractors. Here the drift $K^\nu(q)$ has been split in two parts

$$K^\nu(q) = d^\nu(q) + r^\nu(q), \tag{4.4}$$

in such a way that $r^\nu(q)$ conserves the quasipotential Φ and $d^\nu(q)$ is given by

$$d^\nu(q) = -\frac{1}{2}Q^{\nu\mu}(q)\partial_\mu\Phi(q). \tag{4.5}$$

The conditions (4.2) and (4.3) combined determine nonequilibrium potentials locally as solutions of a Hamilton-Jacobi equation

$$K^\nu\partial_\nu\Phi + \frac{1}{2}Q^{\nu\mu}\partial_\nu\Phi\partial_\mu\Phi = 0. \tag{4.6}$$

Using in the first step the sum rule, in the second (4.1) and in the third (4.2) together with (4.3), we find that Φ decreases like

$$\dot{\Phi}(q(t)) = \partial_\nu\Phi\,\dot{q}^\nu = \partial_\nu\Phi\,K^\nu(q) = -\frac{1}{2}Q^{\nu\mu}\partial_\nu\Phi\partial_\mu\Phi \le 0. \tag{4.7}$$

The dynamics may be interpreted as a relaxation in the potential Φ subject to the Φ-conserving part $r^\nu(q)$ of the drift $K^\nu(q)$. Under the dynamics $\dot{q}^\nu = K^\nu(q)$ the quasipotential Φ decreases monotonically and takes a minimum value on attractors.

Φ can equivalently be determined by solving a set of Hamiltonian differential equations or by minimizing the action integral

$$S[q] = \frac{1}{2}\int_0^T Q_{\nu\mu}(q)[\dot{q}^\nu - K^\nu(q)][\dot{q}^\mu - K^\mu(q)]d\tau \tag{4.8}$$

where $Q_{\nu\mu}$ is the matrix inverse of $Q^{\nu\mu}$. Among different coexisting local minima of the action integral the infimum is chosen. The Hamilton-Jacobi formalism is of fundamental importance, which confirms, that the theory of quasipotentials is dealing with least actions and a minimization procedure. For escape problems, this establishes the connection with the most probable escape path of Section 4.1.

Another way of motivating the quasipotential is the noisy equation

$$\dot{q}^\nu = K^\nu(q) + g^{\nu i}\xi_i(t), \tag{4.9}$$

where ξ_i is Gaussian white noise of infinitesimal intensity with no temporal correlations

$$\langle \xi_i(t)\xi_j(0)\rangle = \sigma^2 \delta_{ij}(t) \tag{4.10}$$

and with a 'diffusion' matrix $\sum_i g^{\nu i}g^{\mu i} = Q^{\nu\mu}(q)$.

Now, two central quantities can be derived. The probability density $W_{\sigma^2}(q)$ in the steady state is given by

$$W_{\sigma^2}(q) \sim \exp[-\Phi(q)/\sigma^2]. \tag{4.11}$$

Eq. (4.11) must be a time-independent solution $\partial W/\partial t = 0$ of the Fokker-Planck equation corresponding to (4.9)

$$\frac{\partial W}{\partial t} = \frac{\partial}{\partial q_\nu}\left[-K_\nu(q) + \frac{1}{2}\frac{\partial}{\partial q_\mu}Q^{\nu\mu}(q)W\right], \tag{4.12}$$

leading to the Eq. (4.6) and the conditions (4.2) and (4.3).

The mean first passage time $\langle \tau_{\sigma^2}\rangle$ out of the basin of attraction G of an attractor A with basin boundary ∂G can be written as

$$\langle \tau_{\sigma^2}\rangle \sim \exp[\Delta\Phi(q)/\sigma^2]. \tag{4.13}$$

In both cases Φ is a solution to the Hamilton-Jacobi equation with diffusion matrix $Q^{\nu\mu}$ and

$$\Delta\Phi := \min\{\Phi(y) - \Phi(a) : a \in A, y \in \partial G\}. \tag{4.14}$$

Eq. (4.13) is a generalization of Eq. (2.19). In Eq. (2.19) we only *assumed* a potential-like quantity, while in Eq. (4.13) the quasipotential Φ was rigorously derived. The quasipotential approach is especially useful for systems having strange sets, like attractors or chaotic saddles. For both quantities, the quasipotential is constant along the closure of unstable manifolds of some periodic orbits or the unstable manifold itself, respectively. This property will be exploited in the next Section.

Since we are interested in studying maps, we need a formulation of quasipotentials for the discrete time case. This was done in (Kifer, 1988; Graham et al., 1991; Hamm, 1993). Most of the derivation is completely analogous to the time-continuous case and will thus not be presented in the following. The underlying equation has the form

$$q_{n+1} = f(q_n) + \sqrt{\sigma^2 Q}\xi_n, \tag{4.15}$$

where f is a map characterizing the system and Q can be set to 1 for simplicity. The action S of a sequence $\{q_j\}_{0 \leq j \leq N}$ is defined, in analogy to (4.8), as

$$S[(q_j)] = \frac{1}{2} \sum_{j=0}^{N-1} [q_{j+1} - f(q_j)]^2. \tag{4.16}$$

Let $V_x^N(y)$ be its minimal values for fixed N and given initial and final points $q_0 = x, q_N = y$. The infimal action from x to y is defined by $V_x(y) := \inf\{V_x^N(y) : N \geq 1\}$. In systems with only one attractor A the quasipotential $\Phi(x)$, satisfying the relations (4.11) and (4.13), is

$$\Phi(x) = V_a(x), \ a \in A. \tag{4.17}$$

For systems with two attractors, the global quasipotential is a combination of the two local ones. However, the construction of the global quasipotential for systems with a high number of coexisting states becomes prohibitively difficult, as the number of combinations scales exponentially with the number of coexisting states (Hamm, 1993). This is the reason, why the theory could not successfully be applied to the dissipative standard map in Chapter 2 and the two coupled logistic maps in Chapter 3. By contrast, in this Chapter we investigate the noise-induced escape of a bistable system, where the theory proves to be very useful.

4.3   Noise-induced escape in the Ikeda map

Here we want to analyze the noise-induced escape process in the Ikeda map (Ikeda, 1979; Hammel et al., 1985). This is an idealized model of a laser pulse in an optical cavity. With complex variables it has the form

$$z_{n+1} = a + bz_n \exp\left[i\kappa - \frac{i\eta}{1 + |z_n|^2}\right], \tag{4.18}$$

where z_n is a complex quantity $z_n = x_n + iy_n$ related to the amplitude and phase of the nth laser pulse exiting the cavity. The parameter a is the laser input amplitude and corresponds to the forcing of the system. The damping $(1 - b)$ accounts for the reflection properties of mirrors in the cavity. The empty cavity detuning is given

by κ and the detuning due to the nonlinear dielectric medium by η. The Ikeda map gives rise to rich dynamical behavior, exhibiting for some parameters even highly multistable behavior (Feudel & Grebogi, 1997). When transformed into a two-dimensional map with real variables and additive Gaussian white noise added, it reads

$$
\begin{aligned}
x_{n+1} &= a + b\,(x_n \cos(w) - y_n \sin(w)) + \delta_x \\
y_{n+1} &= b\,(x_n \sin(w) + y_n \cos(w)) + \delta_y,
\end{aligned}
\tag{4.19}
$$

where $w = \kappa - \eta/(1 + x_n^2 + y_n^2)$.

We fix the parameters at $a = 0.85, b = 0.9$ and $\kappa = 0.4$ and vary only η in the range $2.6 < \eta < 12$. For these values for the noiseless system, two stable states are present, one fixed point (state A), that undergoes a period doubling scenario and becomes a chaotic attractor at $\eta \approx 5.5$ and another fixed point (state B), that stays a fixed point over the whole range considered. The noise-induced escape from state A is investigated. The basin boundary separating these two stable states is a smooth curve. For some very small intervals, there exist additional stable periodic orbits, but they can be neglected in the following.
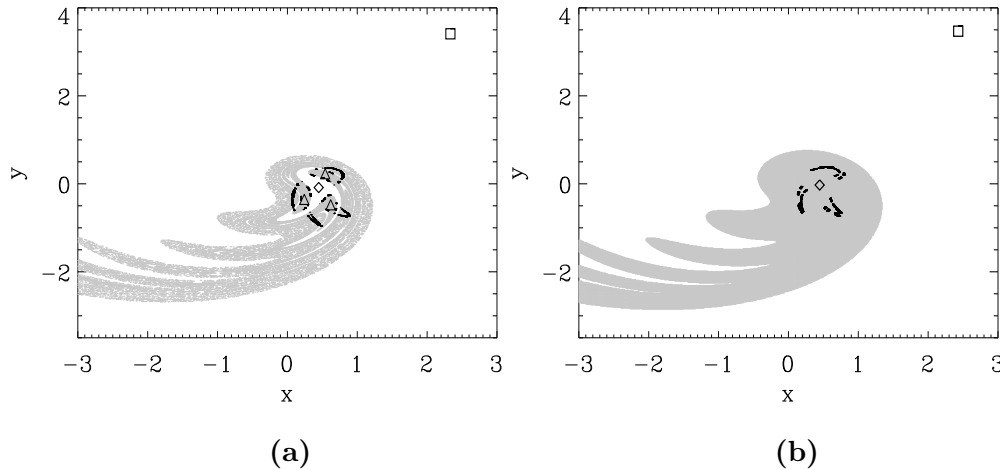
Figure 4.1: (a): Grey dots represent the basin of attraction for the period 3 orbit marked with a $\triangle$ for $\eta = 3.8$. The two fixed points are also depicted ($\diamond$ and $\square$). The chaotic saddle is shown with black dots. (b): Grey dots represent the basin of attraction for the fixed point marked with a $\diamond$ for $\eta = 4.1$. The other fixed point is also depicted ($\square$). The chaotic saddle is shown with black dots.

With the above mentioned features of the system, there are no unusual effects expected in the noise-induced escape problem. However, for a critical value of

$\eta_c = 3.5686$ an additional period 3 solution close to the fixed point (state A) comes into existence, with a fractal basin boundary between these two solutions and a chaotic saddle embedded in this fractal basin boundary. This is shown in Fig. 4.1a for $\eta = 3.8$. It is important to note, that the basin boundary between the two fixed points remains smooth over the whole parameter range considered here. Increasing η further, the period 3 solution becomes unstable, yet a chaotic saddle is *still* present, completely embedded in the open neighborhood of the basin of the stable solution, as can be seen in Fig. 4.1b for $\eta = 4.1$. It is this chaotic saddle, which has a remarkable effect on the escape times out of the stable fixed point.
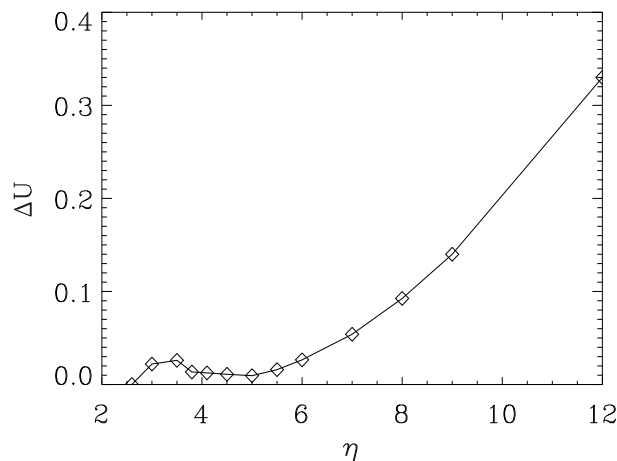
Figure 4.2: Average potential height according to Eq. (2.19) for the Ikeda map versus η. For each value of η 100 runs have been averaged over. Error bars are smaller than the size of the plot symbol.

As a preliminary treatment, we compute the mean first passage time out of the stable fixed point in the same fashion as in Section 2.2.4. The result for the potential height, computed according to Eq. (2.19), corresponding to the escape energy, is depicted in Fig. 4.2. There is a pronounced non-monotonic behavior of the potential height ΔU for values $3.5 \leq \eta \leq 6$.

In the linear approximation, the stability of a fixed point is determined by its eigenvalues. The eigenvalues are found to be $\lambda = 0.9$ for the whole range, where periodic solutions exist. Consequently, the *linear approximation* is of *no relevance* to the noise-induced escape problem whatsoever, as its range of validity is much smaller than the region for the escape, which is the whole open set of the basin of attraction shown in Fig. 4.1. The same situation has been encountered in Section 2.2.4.
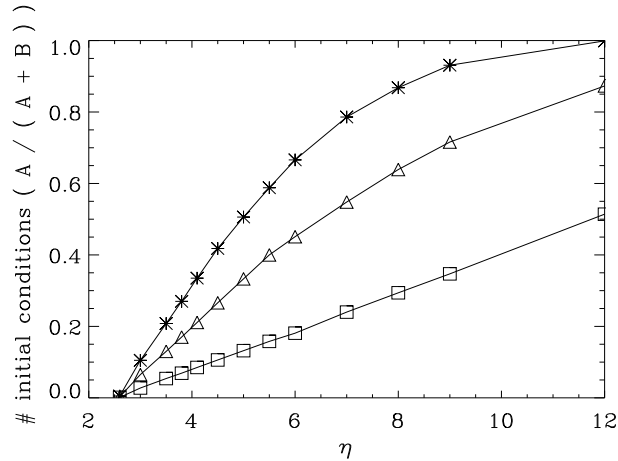
Figure 4.3: Scaling of the ratio of the size of the basin of attraction of state A. The curves correspond to a larger frame of reference from top to bottom, with the values $x \in [-3.0, 2.0], y \in [-3.5, 4.0]$ (marked with $*$) ; $x \in [-5.0, 5.0], y \in [-7.0, 7.0]$ (marked with $\triangle$); $x \in [-10.0, 10.0], y \in [-10.0, 10.0]$ (marked with $\square$), respectively.
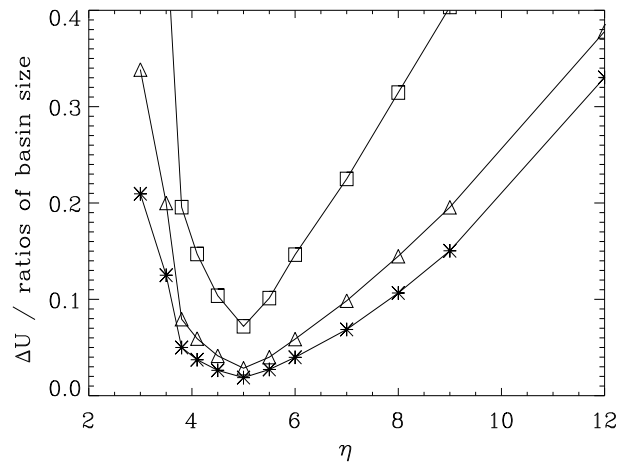
Figure 4.4: Average potential height (= escape energy) divided by the ratios of the sizes of the basins of attraction (curves of Fig. 4.3 with the same plot symbols).

As a next step, it seems to be reasonable to consider the relative size of the basin of attraction. It is obvious, that the relative size of the basin plays a role in the stability of the metastable state located in the basin, although we are not aware of

any theoretical work dealing with this relation directly. In Fig. 4.3 the ratio of the relative sizes of the basin of attraction of state A to the overall area is shown for 3 different areas. The sizes of the area increase from top to bottom. For the largest one, an almost linear increase takes place. The most important fact is, however, that the increase is monotonic. Therefore the non-monotonic behavior of Fig. 4.2 can not be explained by the scaling of the basin of attraction of state A. On the contrary, a combination of the two quantities, potential height and basin size, yields a pronounced minimum at $\eta \approx 5.0$ for all 3 curves of Fig. 4.3, as highlighted in Fig. 4.4.

4.3.1 Application of quasipotentials for the noise-induced escape in the Ikeda map

Now we employ the theory of quasipotentials, to treat the problem of noise-induced escape in greater detail. In Fig. 4.5, 4.6, 4.7, 4.8, the quasipotentials are computed for the values $\eta = 3.0, \eta = 4.1, \eta = 5.0$ and $\eta = 7.0$. For details of the numerical code, see (Hamm, 1993; 1999). In Fig. 4.5, there is a single peak, generated by the fixed point. There are no other dynamically relevant properties, hence the quasipotential decreases in every direction. In Fig. 4.6, as a new feature, a plateau region of a practically constant quasipotential emerges, which reflects the existence of the chaotic saddle. For $\eta = 5.0$ the fixed point (state A) has period doubled two times, exhibiting 4 peaks of a stable period 4 solution, surrounded by a large chaotic saddle. Finally, in Fig. 4.8 the fixed point has turned into a chaotic attractor, which is expressed in the quasipotential through a large number of peaks. Actually, every point on the chaotic attractor should be represented by a peak, not visible here through the finite spatial resolution. Again the plateau of the chaotic saddle is visible slightly below the attractor.

To demonstrate, how accurately the quasipotential describes the chaotic saddle, in Fig. 4.9 the chaotic saddle for $\eta = 5.0$ is compared with a contour plot of Fig. 4.7 at the height, where the chaotic saddle has fully developed, $-\log \Phi(x, y) = 7.5$. An excellent agreement is found, extending even to the fine structure and confirming the applicability of the nonequilibrium potentials to this investigation.

Utilizing the quasipotential for the noise-induced escape problem, the minimum value of $\Phi(x, y)$ has to be determined, where the quasipotential touches the basin boundary. This is exactly the minimum escape energy $\Delta\Phi(x, y)$, since the quasipotential at the stable solution (fixed point, periodic orbit or chaotic attractor) is zero. The point on the basin boundary, where this happens, is generally a saddle point of the system, which is also the case for the Ikeda map. This situation is depicted in Fig. 4.10a, for $\eta = 4.1$, where the contour of the quasipotential is drawn exactly
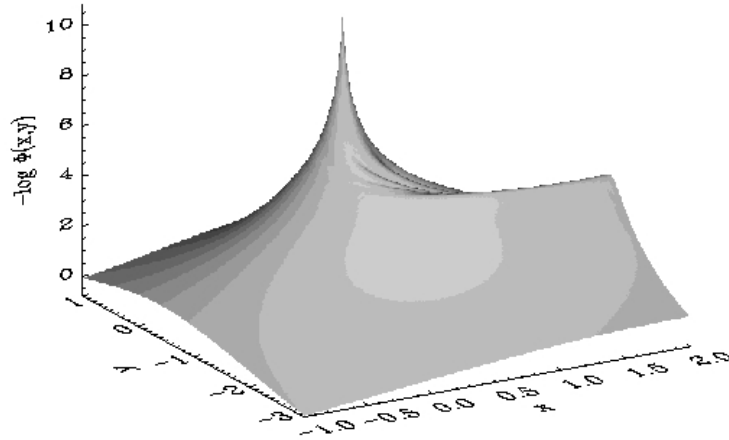
Figure 4.5: Quasipotential $\Phi(x, y)$ for the Ikeda map with $\eta = 3.0$ and a 300×300 grid. The single peak corresponds to the fixed point, which is the minimum of the quasipotential (the maximum of the graph, because of the minus operation). The form of $-\log \Phi(x, y)$ has been chosen to gain a better visual representation.
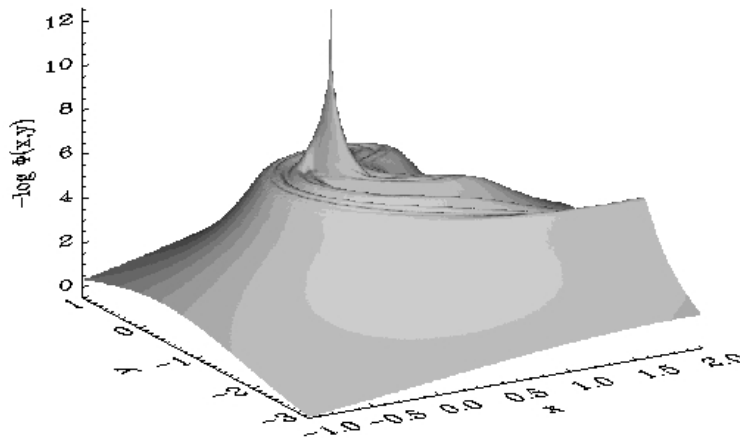
Figure 4.6: Quasipotential $\Phi(x, y)$ for the Ikeda map with $\eta = 4.1$ and a 300×300 grid. The single peak corresponds again to the fixed point. Also, an extended plateau at $-\log \Phi(x, y) \approx 5.0$ is visible, caused by the chaotic saddle.
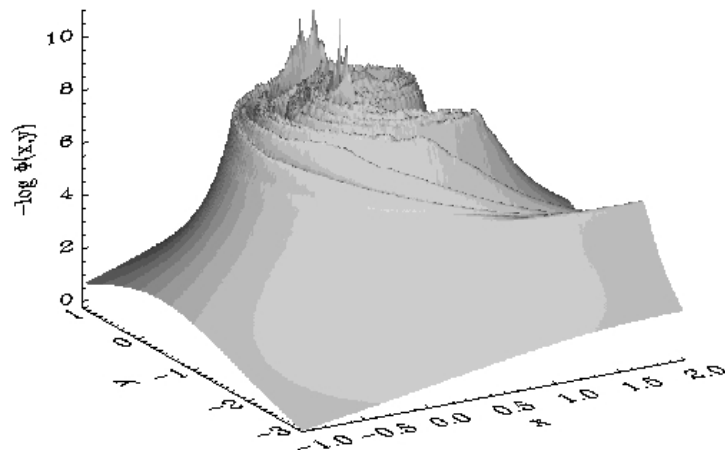
Figure 4.7: Quasipotential $\Phi(x, y)$ for the Ikeda map with $\eta = 5.0$ and a 300×300 grid. The 4 peaks correspond to a period 4 attractor. The plateau at $-\log \Phi(x, y) \approx$ 7.5 is due to a very large chaotic saddle.
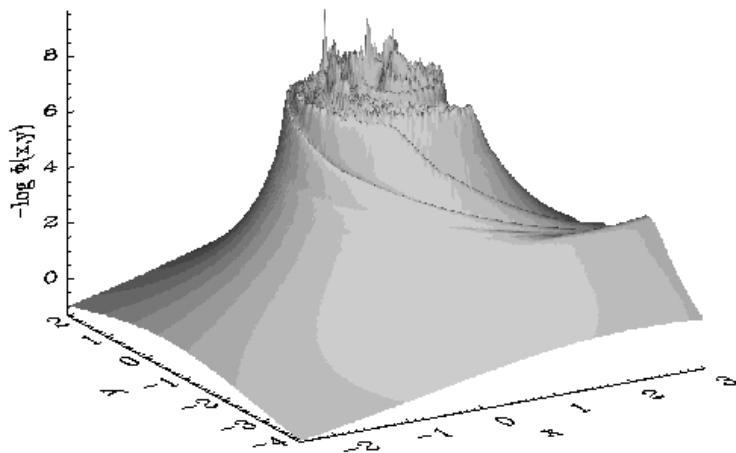
Figure 4.8: Quasipotential $\Phi(x, y)$ for the Ikeda map with $\eta = 7.0$ and a 300×300 grid. The complex peak structure corresponds to a chaotic attractor. Again, an extended plateau at $-\log \Phi(x, y) \approx 7.0$ slightly below the attractor is visible, caused by the chaotic saddle.
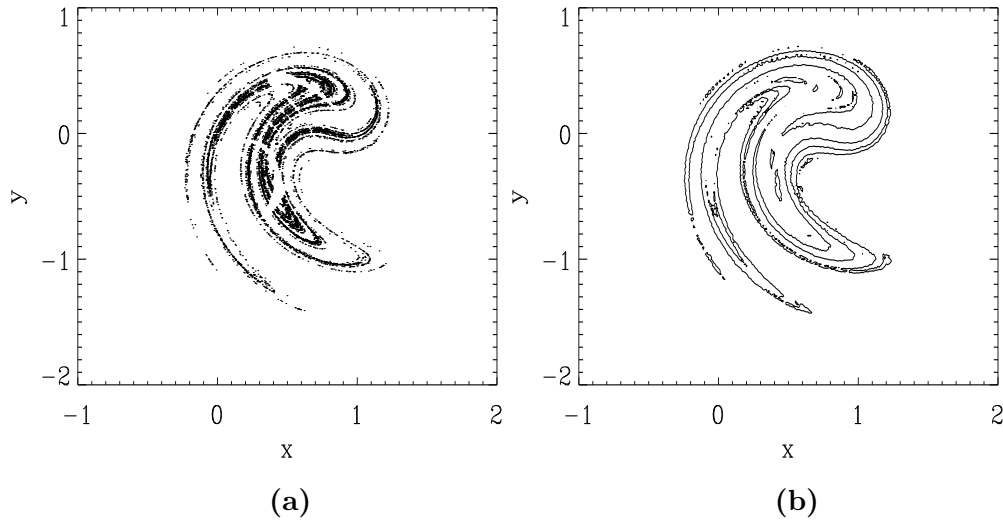
Figure 4.9: (a): Chaotic saddle for $\eta = 5.0$ computed with the PIM-triple method. (b): Contour plot of Fig. 4.7 at the height, where the chaotic saddle has fully developed, $-\log \Phi(x,y) = 7.5$.

at the minimum value of $\Phi(x,y)$, where the quasipotential touches the saddle point located at the basin boundary. The basin boundary is also shown in dark grey. In Fig. 4.10b, for a slightly higher value of $\Phi(x,y)$, a very narrow escape path emerges, located at the unstable manifold of the saddle point on the basin boundary, on which the trajectory can leave the metastable state and jump to the other solution of the system. This narrow path is equivalent to the most probable exit path of Section 4.1. For an infinitesimal noise strength, the system can only leave the metastable state along this path. However, at a slightly higher value, several tongues of the quasipotential touch the basin boundary, which is a typical situation. It is analogous to homoclinic or heteroclinic intersections at e. g. a basin boundary metamorphosis (Grebogi et al., 1986b). In that case also many tongues on the stable manifold segment accumulate through a period one saddle point.

To quantify the escape process with the quasipotential, we plot for every value of η the corresponding minimal escape energy $\Delta\Phi(x,y)$ in Fig. 4.11. To elucidate the role of the chaotic saddle as the origin of an *enhancement of noise-induced escape*, we include in the plot also the value of the height of the plateau in the quasipotential. In the framework of quasipotentials, the difference in *height* of the escape energy and the saddle plateau corresponds to the *distance* of the basin boundary and the chaotic saddle, whereas the height of the saddle is related to the distance between the attractor and the saddle.
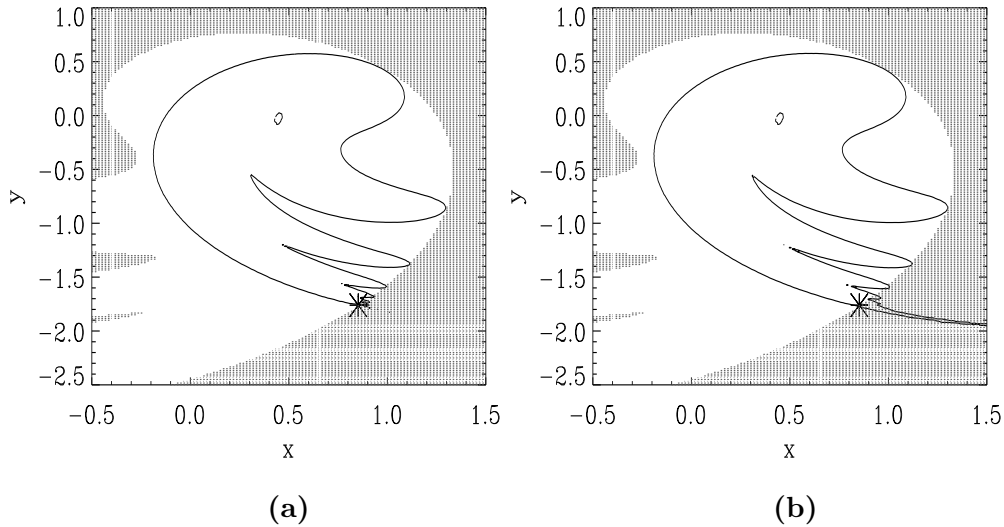
Figure 4.10: (a): Contour plot of Fig. 4.6 at the minimal value of the quasipotential $\Phi(x,y)$, where it touches the basin boundary, $-\log\Phi(x,y) = 4.915$, the latter shown in dark grey. The saddle point on the basin boundary is shown as $*$. (b) At a slightly higher value, $-\log\Phi(x,y) = 4.9$, it is clearly visible how a narrow escape path emerges along the unstable manifold of the saddle point on the basin boundary, again marked with a $*$.

Let us note, that for $\eta = 5.5$ it is not clear, if there exists a chaotic saddle, which is the case for all other values of $\eta \geq 3.5686$ we have tested. The PIM-triple method as well as the quasipotential yield for $\eta = 5.5$ no conclusive result, as a chaotic saddle may exist *very close* to the chaotic attractor, which can numerically not easily be resolved. The points evolved with the PIM-triple method converge very rapidly to the chaotic attractor, while an apparent plateau in the quasipotential (not shown) may simply be a numerical artifact of the insufficient spatial resolution, as discussed above. For this reason, in Fig. 4.11 the line, which is anyway only meant to guide the eyes, is shown broken at $\eta = 5.5$. In any case, the value of $\eta = 5.5$ does not possess any extraordinary meaning, and we can safely neglect this possible exception.

What is important to stress, is the mechanism of the escape process through the existence of an embedded chaotic saddle. It consists of two steps, namely of a noise-induced fluctuation from the attractor (state A) to the chaotic saddle, and then from the chaotic saddle via the saddle point on the boundary to the fixed point (state B). The escape can also be incomplete, as the trajectory may fall back from the
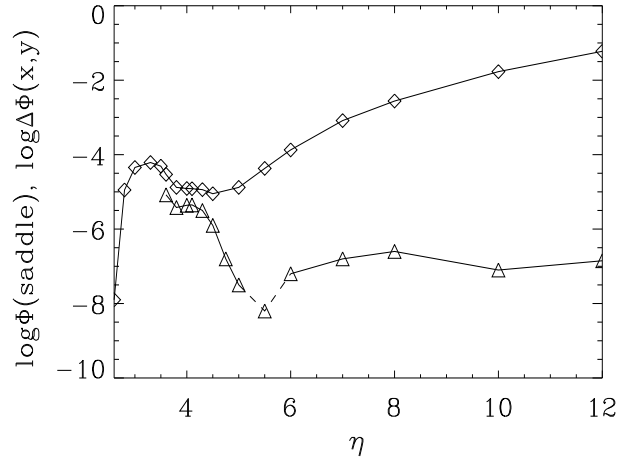
Figure 4.11: Minimal escape energy ($\Diamond$) and height of the saddle plateau ($\triangle$) in logarithmic scale versus η.

chaotic saddle to the attractor. In a successful escape, the chaotic saddle works as a 'shortcut', as its existence lowers the overall escape energy. This behavior seems to be especially pronounced, if the chaotic saddle is closer to the basin boundary than to the attractor, compare the region $3.6 \leq \eta \leq 4.5$ of Fig. 4.11.

Moreover, other values of the Ikeda map, where no chaotic saddle is present, have been investigated as well, and the effect could not be found, confirming, that the existence of the chaotic saddle is of crucial importance for the occurrence of the enhancement of noise-induced escape.

It is further important to note, that the reported mechanism of the lowering of the escape energy is of *qualitatively different nature* from a recently found effect, where also an enhancement of noise-induced escape through transient motion (typical for chaotic saddles) has been found (Soskin et al., 2001a). In this scenario, a nonadiabatically, periodically driven system exhibits a facilitation of noise-induced interwell transitions. This occurs, because the basin boundary becomes *fractal* and the distance between the two states is effectively reduced. In our case, we always have a smooth basin boundary between the two states and the chaotic saddle is embedded in the basin of one state, not in the basin boundary between the states.

Noise-induced escape over a fractal basin boundary has also been studied numerically in a two-dimensional system in (Grassberger, 1989a) and analytically with the help of the reactive flux method in (Reimann et al., 1994). For a noisy map with a smooth basin it was calculated in (Reimann & Talkner, 1995) with basically the

same result. However, the analytical treatment could only be performed for a very simple, piecewise linear one-dimensional map and no variation of a control parameter has been undertaken.

Since we obtain with the quasipotentials accurate escape energies, it is worthwhile to check, whether these results coincide with the 'naive' potential ΔU computed from the straightforward calculation of the average escape times, which was used in Fig. 4.2. In Fig. 4.12, we also include therefore the numerical estimates of ΔU in logarithmic scale. ΔU is shifted with a constant term, to give the best fit, as ΔU and $\Delta \Phi$ are only determined up to a constant value. The coincidence is striking.
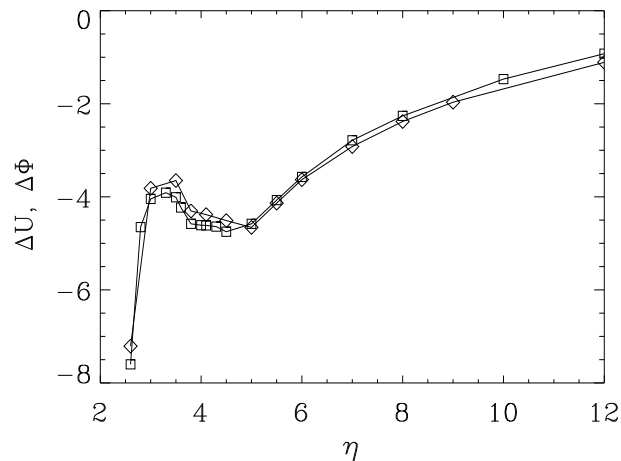
Figure 4.12: Escape energies from ΔU ($\Diamond$) and $\Delta \Phi$ ($\square$). A very good coincidence can be observed.

This justifies the use of the simple potential ΔU in Section 2.2.4. Nevertheless, the quasipotentials reveals much more details of the structure of the escape process, like the exact path or the height of plateaus through invariant sets (like chaotic saddles).

4.4   Summary

This Chapter dealt with the noise-induced escape problem out of a metastable state. The concept of the most probable escape path has been introduced and recent findings on the noise-induced escape problem for nonequilibrium systems were reported. Subsequently, the theory of quasipotentials was presented for the time continuous and for the time discrete case, and the most important properties were pointed out. These include the possibility to compute the noisy invariant density and the mean

escape time for an arbitrary noise distribution. The effect of enhancement of noise-induced escape through the existence of a chaotic saddle in the open neighborhood of the metastable state was shown to exist for the Ikeda map as a parameter is varied. Utilizing the theory of quasipotentials, it was possible to understand this lowering of the escape threshold. This was achieved through the ability of the quasipotentials to translate the location of the chaotic saddle in phase space to differences in escape energies. The reported new phenomenon is of general relevance for many physical and chemical problems, it is predicted to occur in a variety of systems, and should experimentally be observable.

Chapter 5

Conclusion

5.1 Summary and Discussion

The present work was devoted to an investigation of nonlinear multistable systems under the influence of noise. Several prototype models exhibiting multistability were analyzed, and three main new phenomena due to noise in multistable systems were discovered. Preference of attractors was found, meaning that for a certain noise level some attractors gain a higher probability to be observed than others. On the other hand, some attractors may be completely 'hidden' through the action of noise. The noise-induced attractor-hopping dynamics was analyzed in detail for two coupled logistic maps. It was found, that the structure of the underlying chaotic saddles embedded in the fractal basin boundary is of crucial importance for the complexity of the attractor-hopping process and that bifurcations of chaotic saddles cause a drastic change in the dynamics. The relevance of chaotic saddles was further highlighted in the study of the noise-induced escape problem. It was shown, that the mean first escape time out of one metastable state of the Ikeda map attains some pronounced nonmonotonic form as a parameter is varied. This phenomenon is caused by the existence of a chaotic saddle embedded in the open neighborhood of the metastable state, acting as a 'shortcut' in the escape process. The result was obtained utilizing the theory of quasipotentials.

Altogether the results stressed the importance of chaotic saddles in nonlinear multistable systems with noise. In the purely deterministic case without noise, only transient motion takes place on chaotic saddles and they don't need to be taken into account when investigating the long-term behavior of the system. By contrast, noise is able to kick the trajectory on a chaotic saddle and turns it into a dynamically relevant quantity. Thus, noise makes the saddle 'visible'.

The dissipative standard map as a prototype model of multistable behavior was introduced and noise was applied to the system. For a small noise level, the motion is taking place close to one of the stable states and the trajectory cannot leave the open neighborhood of the attractor. If the noise level is large, the trajectory diffuses over the whole phase space. We focused on an intermediate noise level. For this intermediate noise level we observed the attractor-hopping process, in which long laminar-like motion close to an attractor is interrupted by sudden bursts on a chaotic saddle. Another consequence is the washing out of the fine structure of the system, which was visualized through the probability density and some noisy basins of attractions. With the help of Lyapunov exponents the effect of 'noise-induced chaos' was explained, and utilizing finite-time Lyapunov exponents we were able to determine this transition into chaos in detail. The phenomenon of $1/f$-noise has been reported and criteria for its occurrence in the attractor-hopping process were scrutinized. As a result, $1/f$-noise should be more common in multistable systems than in bistable ones. This is caused by the introduction of many different time scales and a more intertwined basin boundary.

Employing a specific numerical procedure, the phenomenon of preference of attractors was found, which implies, that for special noise levels the system is more likely to be steered to some attractors than to others. For these attractors, their probability of occurrence starting with a random initial condition is considerably enhanced compared to the noiseless case. This effect bears some resemblance to stochastic resonance, albeit no external force is applied to the system. The mechanism of preference of attractors is highly relevant for experimental observations of multistable systems, since measurements, which are inevitably contaminated with noise, might reveal a much smaller number of stable states, as the noisefree system actually possesses. Many metastable states may simply be 'hidden' through the noise. On the other hand, a judiciously chosen external noise strength enhances the probability to obtain desirable states. The noise-induced escape from a metastable state was presented in a preliminary fashion and the applicability of Kramers' theory, originally developed for bistable systems, was suggested to hold also in multistable systems.

Using two coupled logistic maps, the role of chaotic saddles in the attractor-hopping process was analyzed in detail. This could be achieved through the concept of symbolic dynamics. Since no generating partition is known for this system, a special encoding procedure was chosen, which proved to be adequate for the examination of the attractor-hopping process. Each metastable state was given a symbol and only after this state has been left, a new symbol was bestowed, independent of the number of iterations the dynamics was residing on this state. The symbol string attained this way was found to reflect a Markov process of order 1. It was analyzed

using the Shannon entropy and the topological entropy. With the variation of the nonlinearity parameter at a special value of this parameter a sudden increase of the topological entropy was observed. This increase was explained by a novel merging bifurcation of the underlying chaotic saddles involving a snap-back repellor. This bifurcation is similar to the well known merging of chaotic attractors, except for the fact, that it is a bifurcation of saddles, not attractors, that the mediating periodic orbit is a repellor, with one additional unstable direction, not a saddle point, and that 'rare' points emerge in the gap of the formerly separated saddles. The bifurcation was further highlighted with a scaling relation of the transient life-times on one formerly separated part of the chaotic saddle before the merging took place, in analogy to crisis. For the increase of the size of the chaotic saddle after the merging, a scaling relation was presented as well. Both scaling laws are determined by the eigenvalues of the repellor mediating the bifurcation. It is an experimental challenge to observe the bifurcation and the scaling laws for the transient life-times and for the increase of the box-counting dimension of the chaotic saddle. Contrariwise, detecting a sudden change in the hopping-dynamics while varying a parameter of the system is a clear indication for a bifurcation of the underlying chaotic saddles.

An essential difference for the attractor-hopping process in bistable and multistable systems was found. Whatever the structure of saddles in a bistable system might be, the hopping dynamics is always trivial, as there is only the possibility to leave one state and then either jump to the other state or return to the state left and vice versa. In multistable systems, as was shown through the symbolic dynamics analysis, there might exist 'forbidden' transitions caused by the chaotic saddles. The 'accessibility' of the metastable state is determined through the structure of the chaotic saddles. As a consequence, the hopping-process can adopt a complex form.

The noise-induced escape problem out of a metastable state was investigated. The theory of quasipotentials was introduced for the time continuous and for the time discrete case, and the most important properties were pointed out. These include the possibility to compute the noisy invariant density and the mean escape time for an arbitrary noise distribution. The effect of enhancement of noise-induced escape through the existence of a chaotic saddle in the open neighborhood of the metastable state was shown to appear for the Ikeda map as a parameter is varied. Utilizing the theory of quasipotentials, it was possible to understand this lowering of the escape threshold. This was achieved through the ability of the quasipotentials to translate the location of the chaotic saddle in phase space into differences in escape energies. The reported new phenomenon is of general relevance for many physical and chemical problems and is predicted to occur in a variety of systems. It should experimentally be observable in optical systems with delay described by the Ikeda map and, due to the generality of the phenomenon, in other systems as well.

5.2 Outlook

Several interesting questions arise from the present level of understanding reached with this work, pointing to possible promising directions of future investigations in this field.

Noisy basins of attraction have been computed for the dissipative standard map for various noise values. An analysis of these basins using measures of complexity is an open task. Specifically, it is of interest, which amount of information can still be extracted out of a basin contaminated with noise, as this is a situation encountered in experiments.

For our purpose, it was not possible to give a symbol for every iteration in the symbolic analysis of the attractor-hopping process, for this would result in an extremely redundant symbol string and a prohibitively long timeseries would be required. Recently, a method to deal with such systems has been developed (Abel et al., 2000). The application of this method to the symbol string is currently under investigation, in order to employ the usual encoding procedure and to compare the results.

For the model of two coupled logistic maps, no dependence of the complexity of the hopping process on the noise strength has been found. Only the escape times changed, whereas the transition probabilities remained constant for a wide range of noise values. In the last years, there has been a controversy, whether noise has an influence on the length of chaotic transients. Some authors claim, that noise can indeed reduce the transient time (Franaszek, 1991; Gassmann, 1997), while others report no such effects (Blackburn et al., 1995; Lai, 1995). That question can probably be answered by investigating the structure of the chaotic saddle of the corresponding system.

The relevance of chaotic saddles for the attractor-hopping process is of general nature. Therefore, for many high-dimensional problems it is expected that bifurcations of the chaotic saddles are hitherto unnoticed, although they determine the dynamics in an essential way. With a recent modification of the PIM-triple algorithm for the computation of high-dimensional chaotic saddles (Sweet et al., 2001) these systems can be examined in detail and new and interesting bifurcations are believed to occur. This includes hydrodynamical and coupled systems.

The escape process in the Ikeda map consisted of two steps. First, the trajectory had to fluctuate from the metastable state (periodic orbit or chaotic attractor) to the chaotic saddle, and then from the chaotic saddle to the saddle point located

on the basin boundary. Since the application of symbolic dynamics proved to be successful for the attractor-hopping process, it might be equally interesting to use symbolic dynamics for the escape process. This was done in (Witt et al., 1997) for the usual Kramers problem and for the case with a fluctuating potential barrier. With one additional state (the chaotic saddle) the application of measures of complexity should reveal more details of the escape process.

Furthermore, the noise-induced escape in maps has been analyzed with Fokker-Planck equations (Reimann & Talkner, 1995), including the escape from a chaotic saddle (Reimann et al., 1994). However, this has only been undertaken for very simple one-dimensional maps, the chaotic saddle was located on the basin boundary, and no control parameter has been varied. It seems worthwhile to extend this approach to the case treated in this work, namely the escape from a map with a chaotic saddle embedded in the open neighborhood of the basin of attraction.

Finally, the relevance of the size of the basin of attraction for the escape process is still an unsolved problem. Although it is clear, that the eigenvalues of the periodic orbit to be left are only relevant as long as the linearization is valid, the limit of the validity of the linearization has not been determined so far. For this aim, quasipotentials might be the right tool, as they provide a global measure of stability for the whole basin of attraction.

Acknowledgment

List of Figures

81

Bibliography

ABEL, M., L. BIFERALE, M. CENCINI, M. FALCIONI, D. VERGNI, & A. VULPIANI (2000). Exit-time approach to ϵ-entropy. *Phys. Rev. Lett.*, **84**, 6002–6005.

ABRAHAM, R. H., L. GARDINI & C. MIRA (1997). *Chaos in Discrete Dynamical Systems.* Springer Verlag, Berlin.

ADLER, R. L., A. G. KONHEIM & M. H. MCANDREW (1965). Topological entropy. *Trans. Am. Math. Soc.*, **114**, 309–319.

AGARWAL, G. S. (1982). Existence of multistability in systems with complex order parameters. *Phys. Rev. A*, **26**, 888–891.

ALEXANDER, J. C., I. KAN, J. A. YORKE & Z. YOU (1992). Riddled basins. *Int. J. Bif. Chaos*, **2**, 795–813.

ANISHCHENKO, V. S. & H. HERZEL (1988). Noise induced chaos in a system with homoclinic points. *Z. angew. Math. Mech.*, **68**, 317–318.

ANISHCHENKO, V. S., I. A. KHOVANOV, N. A. KHOVANOVA, D. G. LUCHINSKY & P. V. E. MCCLINTOCK (2001). Noise-induced escape from the Lorenz attractor. *Fluct. Noise Lett.*, **1**, L27–L33.

ARECCHI, F. T., R. BADII & A. POLITI (1984). Scaling of first passage times for noise induced crises. *Phys. Lett. A*, **103**, 3–7.

ARECCHI, F. T., R. BADII & A. POLITI (1985). Generalized multistability and noise-induced jumps in a nonlinear dynamical system. *Phys. Rev. A*, **32**, 402–408.

ARECCHI, F. T. & A. CALIFANO (1987). Noise-induced trapping at the boundary between two attractors: A source of 1/f spectra in nonlinear dynamics. *Europhys. Lett.*, **3**, 5–10.

ARECCHI, F. T., G. GIACOMELLI, P. L. RAMAZZA & S. RESIDORI (1990). Experimental evidence of chaotic itinerancy and spatiotemporal chaos in optics. *Phys. Rev. Lett.*, **65**, 2531–2534.

ARECCHI, F. T., R. MEUCCI, G. PUCCIONI & J. TREDICCE (1982). Experimental evidence of subharmonic bifurcations, multistability, and turbulence in a q-switched gas laser. *Phys. Rev. Lett.*, **49**, 1217–1220.

ARNOLD, L. (1998). *Random Dynamical Systems*. Springer, Berlin, Heidelberg.

ARRAYÁS, M., I. KH. KAUFMAN, D. G. LUCHINSKY, P. V. E. MCCLINTOCK & S. M. SOSKIN (2000). Kramers problem for a multiwell potential. *Phys. Rev. Lett.*, **84**, 2556–2559.

ARRHENIUS, S. (1889). Über die Reaktionsgeschwindigkeit bei der Inversion von Rohzucker durch Säuren. *Z. Phys. Chem.*, **4**, 226–248.

AUBRY, A. (1978). The new concept of transitions by breaking of analyticity in a crystallographic model. In A. R. BISHOP & T. SCHNEIDER (Eds.), *Solitons and Condensed Matter Physics*, pp. 264–278. Springer Verlag, New York.

BADII, R. & A. POLITI (1997). *Complexity: Hierarchical structures and scaling in physics.* Cambridge University Press, Cambridge.

BAK, P. & R. BRUINSMA (1982). One-dimensional Ising model and the complete devil's staircase. *Phys. Rev. Lett.*, **49**, 249–251.

BAK, P., C. TANG & K. WIESENFELD (1987). Self-organized criticality: An explanation of the 1/f noise. *Phys. Rev. Lett.*, **59**, 381–384.

BARBÉROSHIE, A. E., I. I. GONTSYA, Y. N. NIKA & A. K. ROTARU (1993). Noise-induced optical multistability. *JETP*, **104**, 2655–2667.

BEALE, P. (1989). Noise-induced escape from attractors in one-dimensional maps. *Phys. Rev. A*, **40**, 3998–4003.

BEASLEY, M. R., D. D'HUMIERES & B. A. HUBERMAN (1983). Comment on "Hopping mechanism generating 1/f noise in nonlinear systems". *Phys. Rev. Lett.*, **50**, 1328.

BENZI, R., G. PALADIN, G. PARISI & A. VULPIANI (1985). Characterisation of intermittency in chaotic systems. *J. Phys. A*, **18**, 2157–2165.

BENZI, R., A. SUTERA & A. VULPIANI (1981). The mechanism of stochastic resonance. *J. Phys. A*, **14**, L453–L457.

BEZRUKOV, S. M. & M. WINTERHALTER (2000). Examining noise sources at the single-molecule lecel: 1/f noise of an open maltoporin channel. *Phys. Rev. Lett.*, **85**, 202–205.

BIHAM, O. & W. WENZEL (1989). Characterization of unstable periodic orbits in chaotic attractors and repellers. *Phys. Rev. Lett.*, **63**, 819–822.

BLACKBURN, J. A., N. GRØNBECH-JENSEN & H. J. T. SMITH (1995). Stochastic noise and chaotic transients. *Phys. Rev. Lett.*, **74**, 908–911.

BLEHER, S., E. OTT & C. GREBOGI (1989). Routes to chaotic scattering. *Phys. Rev. Lett.*, **63**, 919–922.

BOLLT, E., Y.-C. LAI & C. GREBOGI (1997). Coding, channel capacity, and noise resistance in communication with chaos. *Phys. Rev. Lett.*, **79**, 3787–3790.

BOLLT, E. M., T. STANFORD, Y.-C. LAI & K. ŻYCZKOWSKI (2000). Validity of threshold-crossing analysis of symbolic dynamics from chaotic time series. *Phys. Rev. Lett.*, **85**, 3524–3527.

BRAMBILLA, M., L. A. LUGIATO, V. PENNA, F. PRATI, C. TAMM & C.O. WEISS (1991). Transverse laser patterns. II. Variational principle for pattern selection, spatial multistability, and laser hydrodynamics. *Phys. Rev. A*, **43**, 5114–5120.

BREYMANN, W. & J. VOLLMER (1997). Symbolic dynamics and topological entropy at the onset of pruning. *Z. Phys. B*, **103**, 539–546.

BRINKMAN, H. C. (1956). Brownian motion in a field of force and the diffusion theory of chemical reactions. II. *Physica*, **22**, 149–155.

BULSARA, A. R. & E. W. JACOBS (1990). Noise effects in a nonlinear dynamic system: The rf superconducting quantum interference device. *Phys. Rev. A*, **42**, 4614–4621.

CARROLL, T. L., L. M. PECORA & F. J. RACHFORD (1987). Chaotic transients and multiple attractors in spin-wave experiments. *Phys. Rev. Lett.*, **59**, 2891–2894.

CHEN, G., G. GYÖRGY & G. SCHMIDT (1986). Universal transition between Hamiltonian and dissipative chaos. *Phys. Rev. A*, **34**, 2568–2570.

CHERN, C. S. & L. I (1991). Multiplicity of bifurcation in weakly ionized magnetoplasmas. *Phys. Rev. A*, **43**, 1994–1997.

CHIN, W., I. KAN & C. GREBOGI (1992). Evolution of attractor boundaries in two-dimensional non-invertible maps. *Rand. & Comp. Dynamics*, **1**, 349–370.

CHIRIKOV, B. V. (1979). A universal instability of many-dimensional oscillator systems. *Phys. Rep.*, **52**, 265–379.

CHRISTIANSEN, F. & A. POLITI (1995). Generating partition for the standard map. *Phys. Rev. E*, **51**, 3811–3814.

CRUTCHFIELD, J. P., J. D. FARMER & B. A. HUBERMAN (1982). Fluctuations and simple chaotic dynamics. *Phys. Rep.*, **92**, 45–82.

CRUTCHFIELD, J. P. & K. KANEKO (1988). Are attractors relevant to turbulence ? *Phys. Rev. Lett.*, **60**, 2715–2718.

CVITANOVIC, P., G. H. GUNARATNE & I. PROCACCIA (1988). Topological and metric properties of Hénon-type strange attractors. *Phys. Rev. A*, **38**, 1503–1520.

DANGOISSE, D., P. GLORIEUX & D. HENNEQUIN (1986). Laser chaotic attractors in crisis. *Phys. Rev. Lett.*, **57**, 2657–2660.

DAVIDCHACK, R., Y.-C. LAI, E. BOLLT & M. DHAMALA (2000). Estimating generating partitions of chaotic systems by unstable periodic orbits. *Phys. Rev. E*, **61**, 1353–1356.

DAWSON, S. P. (1996). Strange nonattracting chaotic sets, crises, and fluctuating Lyapunov exponents. *Phys. Rev. Lett.*, **76**, 4348–4351.

DE MOURA, A. P. S. & C. GREBOGI (2001). Output functions and fractal dimensions in dynamical systems. *Phys. Rev. Lett.*, **86**, 2778–2781.

DERKSEN, H. E. & A. A. VERVEEN (1966). Fluctuations of resting neural membrane potential. *Science*, **151**, 1388–1389.

DERRIDA, B., A. GERVOIS & Y. POMEAU (1978). Iteration of endomorphisms on the real axis and representation of numbers. *Ann. Inst. Poincaré A*, **29**, 305–356.

DEVANEY, R. L. (1989). *An Introduction to chaotic dynamical systems*. Addison-Wesley, Reading.

DITTO, W. L., S. RAUSEO, R. CAWLEY, C. GREBOGI, G.-H. HSU, E. KOSTELICH, E. OTT, H. T. SAVAGE, R. SEGNAN, M. L. SPANO & J. A. YORKE (1989). Experimental observation of crisis-induced intermittency and its critical exponent. *Phys. Rev. Lett.*, **63**, 923–926.

DOERING, C. R. & J. C. GADOUA (1992). Resonant activation over a fluctuating barrier. *Phys. Rev. Lett.*, **69**, 2318–2321.

DUTTA, P. & P. M. HORN (1981). Low-frequency fluctuations in solids: 1/f noise. *Rev. Mod. Phys.*, **53**, 497–516.

DYKMAN, M. I., D. G. LUCHINSKY, P. V. E. McCLINTOCK & V. N. SMELYAN-SKIY (1996). Corrals and critical behavior of the distribution of fluctuational paths. *Phys. Rev. Lett.*, **77**, 5229–5232.

DYKMAN, M. I., P. V. E. McCLINTOCK, V. N. SMELYANSKIY, N. D. STEIN & N. G. STOCKS (1992). Optimal paths and the prehistory problem for large fluctuations in noise-driven systems. *Phys. Rev. Lett.*, **68**, 2718–2721.

DYKMAN, M. I., H. RABITZ, V. N. SMELYANSKIY & B. E. VUGMEISTER (1997). Resonant directed diffusion in nonadiabatically driven systems. *Phys. Rev. Lett.*, **79**, 1178–1181.

ECKHARDT, B. & H. AREF (1988). Integrable and chaotic motions of four vortices. II. Collision dynamics of vortex pairs. *Phil. Trans. R. Soc. Lond. A*, **326**, 655–696.

FEUDEL, U. & C. GREBOGI (1997). Multistability and the control of complexity. *Chaos*, **7**, 597–604.

FEUDEL, U. & C. GREBOGI (2000). Why are chaotic attractors rare in multistable systems ? *Submitted to Phys. Rev. Lett.*

FEUDEL, U., C. GREBOGI, B. R. HUNT & J. A. YORKE (1996). Map with more than 100 coexisting low-period periodic attractors. *Phys. Rev. E*, **54**, 71–81.

FINARDI, M., L. FLEPP, J. PARISI, R. HOLZNER, R. BADII & E. BRUN (1992). Topological and metric analysis of heteroclinic crisis in laser chaos. *Phys. Rev. Lett.*, **68**, 2989–2991.

FOSS, J., A. LONGTIN, B. MENSOUR & J. MILTON (1996). Multistability and delayed recurrent loops. *Phys. Rev. Lett.*, **76**, 708–711.

FRANASZEK, M. (1991). Influence of noise on the mean lifetime of chaotic transients. *Phys. Rev. A*, **44**, 4065–4067.

FREIDLIN, M. I. & A. D. WENTZELL (1984). *Random perturbations of dynamical systems*. Springer Verlag, Berlin.

FUJISAKA, H. (1983). Statistical dynamics generated by fluctuations of local Lyapunov exponents. *Prog. Theor. Phys*, **70**, 1264–1275.

GADALETA, S. & G. DANGELMAYR (2001). Learning to control a complex multistable system. *Phys. Rev. E*, **63**, 036217–1–12.

GALLAS, J. A. C., C. GREBOGI & J. A. YORKE (1993). Vertices in parameter space: Double crises which destroy chaotic attractors. *Phys. Rev. Lett.*, **71**, 1359–1362.

GAMMAITONI, L., P. HÄNGGI, P. JUNG & F. MARCHESONI (1998). Stochastic resonance. *Rev. Mod. Phys.*, **70**, 223–287.

GANG, H., T. DITZINGER, C. Z. NING & H. HAKEN (1993). Stochastic resonance without external periodic force. *Phys. Rev. Lett.*, **71**, 807–810.

GASSMANN, F. (1997). Noise-induced chaos-order transitions. *Phys. Rev. E*, **55**, 2215–2221.

GEISEL, T., A. ZACHERL & G. RADONS (1987). Generic 1/f noise in chaotic Hamiltonian dynamics. *Phys. Rev. Lett.*, **59**, 2503–2506.

GRAHAM, R. (1989). Macroscopic potentials, bifurcations and noise in dissipative systems. In F. MOSS & P. V. E. MCCLINTOCK (Eds.), *Noise in nonlinear dynamical systems, 3 Volumes, Vol. 1*, pp. 225–278. Cambridge University Press, Cambridge.

GRAHAM, R. & A. HAMM (1992). Nonequilibrium potentials. In R. FRIEDRICH & A. WUNDERLICH (Eds.), *Evolution of dynamical structures in complex systems*, pp. 65–79. Springer, Berlin.

GRAHAM, R., A. HAMM & T. TÉL (1991). Nonequilibrium potentials for dynamical systems with fractal attractors and repellers. *Phys. Rev. Lett.*, **66**, 3089–3092.

GRAHAM, R. & T. TÉL (1984). Existence of a potential for dissipative dynamical systems. *Phys. Rev. Lett.*, **52**, 9–12.

GRAHAM, R. & T. TÉL (1986). Nonequilibrium potential for coexisting attractors. *Phys. Rev. A*, **33**, 1322–1337.

GRASSBERGER, P. (1988). Finite sample corrections to entropy and dimension estimates. *Phys. Lett. A*, **128**, 369–373.

GRASSBERGER, P. (1989a). Noise-induced escape from attractors. *J. Phys. A*, **22**, 3283–3290.

GRASSBERGER, P. (1989b). Randomness, information and complexity. In F. RAMOS-GÓMEZ (Ed.), *Fifth Mexican Summer School on Statistical Mechanics*, pp. 59–73. World Scientific, Singapore.

GRASSBERGER, P. & H. KANTZ (1985). Generating partition for the dissipative Hénon map. *Phys. Lett. A*, **113**, 235–241.

GRASSBERGER, P. & I. PROCACCIA (1984). Dimensions and entropies from a fluctuating dynamics approach. *Physica D*, **13**, 34–54.

GREBOGI, C., E. KOSTELICH, E. OTT & J. A. YORKE (1987a). Multi-dimensioned intertwined basin boundaries: Basin structure of the kicked double rotor. *Physica D*, **25**, 347–360.

GREBOGI, C., S. W. MCDONALD, E. OTT & J. A. YORKE (1983a). Final state sensitivity: An obstruction to predictability. *Phys. Lett. A*, **99**, 415–418.

GREBOGI, C., H. E. NUSSE, E. OTT & J. A. YORKE (1988). Basic sets: Sets that determine the dimensions of basin boundaries. In J. C. ALEXANDER (Ed.), *Lecture Notes in Mathematics, Vol.1342*, pp. 220–250. Springer Verlag, New York.

GREBOGI, C., E. OTT, F. ROMEIRAS & J. A. YORKE (1987b). Critical exponents for crisis-induced intermittency. *Phys. Rev. A*, **36**, 5365–5380.

GREBOGI, C., E. OTT & J. YORKE (1983b). Fractal basin boundaries, long-lived chaotic transients, and unstable-unstable pair bifurcation. *Phys. Rev. Lett.*, **50**, 935–938.

GREBOGI, C., E. OTT & J. YORKE (1985). Super persistent chaotic transients. *Ergod. Th. & Dynam. Sys.*, **5**, 341–372.

GREBOGI, C., E. OTT & J. A. YORKE (1982). Chaotic attractors in crisis. *Phys. Rev. Lett.*, **48**, 1507–1510.

GREBOGI, C., E. OTT & J. A. YORKE (1986a). Critical exponent of chaotic transients in nonlinear dynamical systems. *Phys. Rev. Lett.*, **57**, 1284–1287.

GREBOGI, C., E. OTT & J. A. YORKE (1986b). Metamorphosis of basin boundaries in nonlinear dynamical systems. *Phys. Rev. Lett.*, **56**, 1011–1014.

GREENE, J. M. (1979). A method for determining a stochastic transition. *J. Math. Phys.*, **20**, 1183–1201.

GWINN, E. G. & R. M. WESTERVELT (1985). Intermittent chaos and low-frequency noise in the driven damped pendulum. *Phys. Rev. Lett.*, **54**, 1613–1616.

HALES, J., A. ZHUKOV, R. ROY & M. I. DYKMAN (2000). Dynamics of activated escape and its observation in a semiconductor laser. *Phys. Rev. Lett.*, **85**, 78–81.

HAMM, A. (1993). *Quasipotentiale zur Beschreibung von stochastischen Störungen in zeitdiskreten dynamischen Systemen.* PhD thesis, Essen.

HAMM, A. (1999). Private communication.

HAMM, A. & R. GRAHAM (1992a). Quasipotentials for simple noisy maps with complicated dynamics. *J. Stat. Phys.*, **66**, 689–725.

HAMM, A. & R. GRAHAM (1992b). Scaling for small random perturbations of golden critical circle maps. *Phys. Rev. A*, **46**, 6323–6333.

HAMM, A., T. TÉL & R. GRAHAM (1994). Noise-induced attractor explosions near tangent bifurcations. *Phys. Lett. A*, **185**, 313–320.

HAMMEL, S., C. K. R. T. JONES & J. MALONEY (1985). Global dynamical behavior of the optical field in a ring cavity. *J. Opt. Soc. Am. B*, **2**, 552–564.

HÄNER, P. & R. SCHILLING (1989). Pressure dependence of the number of metastable configurations: a staircaselike behaviour for a chain of particles. *Europhys. Lett.*, **8**, 129–134.

HÄNGGI, P., P. TALKNER & M. BORKOVEC (1990). Reaction-rate theory: Fifty years after Kramers. *Rev. Mod. Phys.*, **62**, 251–341.

HAO, B.-L. (1989). *Elementary Symbolic Dynamics*. World Scientific, Singapore.

HEAGY, J. F., T. L. CARROLL & L. M. PECORA (1994). Experimental and numerical evidence for riddled basins in coupled chaotic systems. *Phys. Rev. Lett.*, **73**, 3528–3531.

HÉNON, M. (1976). A two-dimensional mapping with a strange attractor. *Commun. Math. Phys.*, **50**, 69–77.

HERZEL, H. (1988a). Complexity of symbolic sequences. *Syst. Anal. Model. Simul.*, **5**, 435–444.

HERZEL, H. (1988b). Stabilization of chaotic orbits by random noise. *Z. angew. Math. Mech.*, **68**, 582–583.

HERZEL, H., W. EBELING & T. SCHULMEISTER (1987). Nonuniform chaotic dynamics and effects of noise in biochemical systems. *Z. Naturforsch.*, **42a**, 136–142.

HORSTHEMKE, W. & R. L. LEFEVER (1984). *Noise-Induced Transitions*. Springer Ser. Syn. Vol 15, Berlin, Heidelberg.

HSU, G.-H., E. OTT & C. GREBOGI (1988). Strange saddles and the dimensions of their invariant manifolds. *Phys. Lett. A*, **127**, 199–204.

HUNT, B. R., E. OTT & E. ROSA JR. (1999). Sporadically fractal basin boundaries of chaotic systems. *Phys. Rev. Lett.*, **82**, 3597–3600.

HUNT, K. L. C., J. KOTTALAM, M. D. HATLEE & J. ROSS (1992). Multiple steady states in coupled flow tank reactors. *J. Chem. Phys.*, **96**, 7019–7033.

IANSITI, M., Q. HU, R. M. WESTERVELT & M. TINKHAM (1985). Noise and chaos in a fractal basin boundary regime of a Josephson junction. *Phys. Rev. Lett.*, **55**, 746–749.

IKEDA, K. (1979). Multiple-valued stationary state and its instability of the transmitted light by a ring cavity system. *Opt. Commun.*, **30**, 257–261.

IKEDA, K., K. MATSUMOTO & K. OTSUKA (1989). Maxwell Bloch turbulence. *Prog. Theor. Phys. Suppl.*, **99**, 295–324.

JACOBS, J., E. OTT & C. GREBOGI (1997). Computing the measure of nonattracting chaotic sets. *Physica D*, **108**, 1–11.

JACOBS, J., E. OTT & B. R. HUNT (1998). Calculating topological entropy for transient chaos with application to communication with chaos. *Phys. Rev. E*, **57**, 6577–6588.

JÁNOSI, I. M., L. FLEPP & T. TÉL (1994). Exploring transient chaos in an NMR-laser experiment. *Phys. Rev. Lett.*, **73**, 529–532.

JEFFRIES, C. & J. PEREZ (1983). Direct observation of crises of the chaotic attractor in a nonlinear oscillator. *Phys. Rev. A*, **27**, 601–603.

JENSEN, M. H., P. BAK & T. BOHR (1983). Complete devil's staircase, fractal dimension, and universality of mode-locking structures. *Phys. Rev. Lett.*, **50**, 1637–1639.

JENSEN, M. H., P. BAK & T. BOHR (1984). Transition to chaos by interaction of resonances in dissipative systems. *Phys. Rev. A*, **30**, 1960–1969.

JUNG, P. & P. HÄNGGI (1990). Invariant measure of a driven nonlinear oscillator with external noise. *Phys. Rev. Lett.*, **65**, 3365–3368.

KACPERSKI, K. & J. A. HOLYST (1999). Theory of oscillations in average crisis-induced transient lifetimes. *Phys. Rev. E*, **60**, 403–407.

KANEKO, K. (1997). Dominance of Milnor attractors and noise-induced selection in a multiattractor system. *Phys. Rev. Lett.*, **78**, 2736–2739.

KANEKO, K. (1998). On the strength of attractors in a high-dimensional system: Milnor attractor network, robust global attraction, and noise-induced selection. *Physica D*, **124**, 322–344.

KANTZ, H. & P. GRASSBERGER (1985). Repellers, semi-attractors, and long-lived chaotic transients. *Physica D*, **17**, 75–86.

KARAKOTSOU, C. & A. N. ANAGNOSTOPOULOS (1996). Crisis in electrical behavior of the TlInSe_2 semiconducting compound. *Physica D*, **93**, 157–164.

KAUTZ, R. L. (1988). Thermally induced escape: The principle of minimum available noise energy. *Phys. Rev. A*, **38**, 2066–2080.

KENNEDY, J. & J. A. YORKE (1991). Basins of Wada. *Physica D*, **51**, 213–225.

KHOVANOV, I. A., D. G. LUCHINSKY, R. MANNELLA & P. V. E. MCCLINTOCK (2000). Fluctuations and the energy-optimal control of chaos. *Phys. Rev. Lett.*, **85**, 2100–2103.

KIFER, Y. (1988). *Random perturbations of dynamical systems*. Birkhäuser, Boston.

KIM, S., S.H. PARK & C.S.RYU (1997a). Multistability in coupled oscillator systems with time delay. *Phys. Rev. Lett.*, **79**, 2911–2914.

KIM, S., S.H. PARK & C.S.RYU (1997b). Noise-enhanced multistability in coupled oscillator systems. *Phys. Rev. Lett.*, **78**, 1616–1619.

KITANO, M., YABUZAKI & T. OGAWA (1981). Optical tristability. *Phys. Rev. Lett.*, **46**, 926–929.

KOBAYASHI, M. & T. MUSHA (1982). 1/f fluctuation of heartbeat period. *IEEE Trans. of Biomed. Eng.*, **29**, 456–457.

KOLMOGOROV, A. N. (1958). A new metric invariant of transitive dynamical systems and automorphisms in Lebesque space. *Dok. Acad. Nauk SSSR*, **119**, 861–864.

KRAMERS, H. A. (1940). Brownian motion in a field of force and diffusion model of chemical reactions. *Physica*, **7**, 287–304.

KRAUT, S. & U. FEUDEL (2001a). Enhancement of noise-induced escape through the existence of chaotic saddles. *In preparation.*

KRAUT, S. & U. FEUDEL (2001b). Multistability, noise, and attractor-hopping: The crucial role of chaotic saddles. *Submitted to Phys. Rev. Lett.*

KRAUT, S., U. FEUDEL & C. GREBOGI (1999). Preference of attractors in noisy multistable systems. *Phys. Rev. E*, **59**, 5253–5260.

KUSKE, R. & G. PAPANICOLAOU (1998). The invariant density of a chaotic dynamical system with small noise. *Physica D*, **120**, 255–272.

LAI, Y.-C. (1995). Persistence of supertransients of spatiotemporal chaotic dynamical systems in noisy environment. *Phys. Lett. A*, **200**, 418–422.

LAI, Y.-C. & C. GREBOGI (1994). Crisis and enhancement of chaotic scattering. *Phys. Rev. E*, **49**, 3761–3770.

LAI, Y.-C., C. GREBOGI, R. BLÜMEL & I. KAN (1993). Crisis in chaotic scattering. *Phys. Rev. Lett.*, **71**, 2212–2215.

LAI, Y.-C. & R. L. WINSLOW (1995). Geometric properties of the chaotic saddle responsible for supertransients in spatiotemporal chaotic systems. *Phys. Rev. Lett.*, **74**, 5208–5211.

LAI, Y.-C., K. ŻYCZKOWSKI & C. GREBOGI (1999). Universal behavior in the parametric evolution of chaotic saddles. *Phys. Rev. E*, **59**, 5261–5265.

LANDAUER, R. & J. A. SWANSON (1961). Frequency factors in the thermally activated process. *Phys. Rev.*, **121**, 1668–1674.

LAPIDUS, L. J., D. ENZER & G. GABRIELSE (1999). Stochastic phase switching of a parametrically driven electron in a Penning trap. *Phys. Rev. Lett.*, **83**, 899–902.

LICHTENBERG, A. J. & M. A. LIEBERMANN (1992). *Regular and Chaotic Dynamics.* Springer, New York.

LIEBERMAN, M. A. & K. Y. TSANG (1985). Transient chaos in dissipatively perturbed near-integrable Hamiltonian systems. *Phys. Rev. Lett.*, **55**, 908–911.

LUCHINSKY, D. G. & I. A. KHOVANOV (1999). Fluctuation-induced escape from the basin of attraction of a quasiattractor. *JETP Lett.*, **69**, 825–830.

LUCHINSKY, D. G., R.S. MAIER, R. MANNELLA, P. V. E. MCCLINTOCK & D. L. STEIN (1999). Observation of saddle-point avoidance in noise-induced escape. *Phys. Rev. Lett.*, **82**, 1806–1809.

LUCHINSKY, D. G. & P. V. E. MCCLINTOCK (1997). Irreversibility of classical fluctuations studied in analogue electrical circuits. *Nature (London)*, **389**, 463–466.

MACAU, E. E. N. & C. GREBOGI (1999). Driving trajectories in complex systems. *Phys. Rev. E*, **59**, 4062–4070.

MAIER, R. S. & D. L. STEIN (1992). Transition-rate theory for nongradient drift fields. *Phys. Rev. Lett.*, **69**, 3691–3695.

MAIER, R. S. & D. L. STEIN (1993). Effect of focusing and caustics on exit phenomena in systems lacking detailed balance. *Phys. Rev. Lett.*, **71**, 1783–1786.

MAISTRENKO, Y. L., V. L. MAISTRENKO, A. POPOVICH & E. MOSEKILDE (1998). Role of absorbing area in chaotic synchronization. *Phys. Rev. Lett.*, **80**, 1638–1641.

MAISTRENKO, Y. L. & I. SUSHKO (1998). About two mechanisms of reunion of chaotic attractors. *Chaos, Solitons & Fractals*, **8**, 1373–1390.

MANDELBROT, B. (1977). *Fractals, Form, Chance, and Dimension.* Freeman, San Francisco.

MANDELBROT, B. & J. R. WALLIS (1969). Some long-run properties of geophysical records. *Water Resour. Res.*, **5**, 321–340.

MANNEVILLE, P. (1980). Intermittency, self-similarity, and 1/f-spectrum in dissipative dynamical systems. *J. Phys. (Paris)*, **41**, 1235–1243.

MANTEGNA, R. N. & B. SPAGNOLO (1996). Noise enhanced stability in an unstable system. *Phys. Rev. Lett.*, **76**, 563–566.

MARMILLOT, P., M KAUFMANN & J.-F. HERVAGAULT (1991). Multiple steady states and dissipative structures in a circular and linear array of three cells: Numerical and experimental approaches. *J. Chem. Phys.*, **95**, 1206–1214.

MAROTTO, F. R. (1978). Snap-back repellers imply chaos in $\mathbb{R}^2$. *J. Math. Anal. Appl.*, **63**, 199–223.

MARTIN, S. & W. MARTIENSSEN (1986). Circle maps and mode locking in the driven electrical conductivity of Barium Sodium Niobate crystals. *Phys. Rev. Lett.*, **56**, 1522–1525.

MATSUMOTO, K. & I. TSUDA (1983). Noise-induced order. *J. Stat. Phys.*, **31**, 87–106.

MCCANN, L. I., M. DYKMAN & B. GOLDING (1999). Thermally activated transitions in a bistable three-dimensional optical trap. *Nature (London)*, **402**, 785–787.

MCDONALD, S. W., C. GREBOGI, E. OTT & J. YORKE (1985). Fractal basin boundaries. *Physica D*, **17**, 125– 153.

MEL'NIKOV, V. I. (1991). The Kramers problem: Fifty years of development. *Phys. Rep.*, **209**, 1–71.

MEYER-KRESS, G. & H. HAKEN (1981). The influence of noise on the logistic model. *J. Stat. Phys.*, **26**, 149–171.

Mielke, A. (2000). Noise induced stability in fluctuating, bistable potentials. *Phys. Rev. Lett.*, **84**, 818–821.

Millonas, M. (Ed.) (1996). *Fluctuations and Order: The New Synthesis.* Springer-Verlag, New York.

Milnor, J. (1985). On the concept of attractor. *Commun. Math. Phys.*, **99**, 177–195.

Mira, C. (1979). Frontiére floue séparant les domaines d'attraction de deux attracteurs, examples. *C. R. Acad. Sci. Paris A*, **288**, 591–594.

Mira, C., L. Gardini, A. Barugolu & J.-C. Cathala (1996). *Chaotic Dynamics in Two-Dimensional Noninvertible Maps.* World Scientific, Singapore.

Moresco, P. & S. P. Dawson (1997). Chaos and crisis in more than two dimensions. *Phys. Rev. E*, **55**, 5350–5360.

Moss, F. & P. V. E. McClintock (Eds.) (1989). *Noise in nonlinear dynamical systems, 3 Volumes.* Cambridge University Press, Cambridge.

Musha, T. & H. Higuchi (1976). The 1/f fluctuation of a traffic current on an expressway. *Jap. Jour. Appl. Phys.*, **15**, 271–1275.

Newhouse, S. E. (1979). The abundance of wild hyperbolic sets and non-smooth stable sets for diffeomorphisms. *Publ. Math. Inst. Hautes Etude. Sci.*, **50**, 101–151.

Nusse, H. E., E. Ott & J. A. Yorke (1995). Saddle-node bifurcations on fractal basin boundaries. *Phys. Rev. Lett.*, **75**, 2482–2485.

Nusse, H. E. & L. Tedeschini-Lalli (1992). Wild hyperbolic sets, yet no chance for the coexistence of infinitely many KLUS-simple Newhouse attracting sets. *Commun. Math. Phys.*, **144**, 429–442.

Nusse, H. E. & J. A. Yorke (1989). A procedure for finding numerical trajectories on chaotic saddles. *Physica D*, **36**, 137–156.

Nusse, H. E. & J. A. Yorke (1996). Basins of attraction. *Science*, **271**, 1376–1380.

Nusse, H. E. & J. A. Yorke (2000). Fractal basin boundaries generated by basin cells and the geometry of mixing chaotic flows. *Phys. Rev. Lett.*, **84**, 626–629.

Onsager, L. & S. Machlup (1953a). Fluctuations and irreversible processes. *Phys. Rev.*, **91**, 1505–1512.

ONSAGER, L. & S. MACHLUP (1953b). Fluctuations and irreversible processes. II. Systems with kinetic energy. *Phys. Rev.*, **91**, 1512–1515.

OTSUKA, K. (1990). Self-induced phase turbulence and chaotic itinerancy in coupled laser systems. *Phys. Rev. Lett.*, **65**, 329–332.

OTT, E. (1993). *Chaos in dynamical systems.* Cambridge University Press, Cambridge.

OTT, E., J. C. SOMMERER, J. C. ALEXANDER, I. KAN & J. A. YORKE (1993). Scaling behavior of chaotic systems with riddled basins. *Phys. Rev. Lett.*, **71**, 4134–4137.

PALADIN, G., M. SERVA & A. VULPIANI (1995). Complexity in dynamical systems with noise. *Phys. Rev. Lett.*, **74**, 66–69.

PARK, B.-S., C. GREBOGI, E. OTT & J. A. YORKE (1989). Scaling of fractal basin boundaries near intermittency transitions to chaos. *Phys. Rev. A*, **40**, 1576–1581.

PÉNTEK, Á., Z. TOROCZKAI, T. TÉL, C. GREBOGI & J. A. YORKE (1995). Fractal boundaries in open hydrodynamical flows: Signatures of chaotic saddles. *Phys. Rev. E*, **51**, 4076–4088.

PIKOVSKY, A. S. & J. KURTHS (1997). Coherence resonance in a noise-driven excitable system. *Phys. Rev. Lett.*, **78**, 775–778.

POON, L. & C. GREBOGI (1995). Controlling complexity. *Phys. Rev. Lett.*, **75**, 4023–4026.

PRASAD, A. & R. RAMASWAMY (1999). Characteristic distributions of finite time Lyapunov exponents. *Phys. Rev. E*, **60**, 2761–2766.

PRENGEL, F., A. WACKER & E. SCHÖLL (1994). Simple model for multistability and domain formation in semiconductor superlattices. *Phys. Rev. B*, **50**, 1705–1712.

PRESS, W. H. (1978). Flicker noise in astronomy and elsewhere. *Comments Astrophys. Space Phys.*, **7**, 103–119.

RAHMSTORF, S. (1995). Multiple convection patterns and thermohaline flow in an idealized OGCM. *J. Climate*, **8**, 3028–3039.

REIMANN, P. (1994). Noisy map near crisis. *Z. Naturforsch.*, **49a**, 1248–1250.

REIMANN, P., R. MÜLLER & P. TALKNER (1994). Decay of metastable states with discrete dynamics. *Phys. Rev. E*, **49**, 3670–3682.

REIMANN, P. & P. TALKNER (1991). Invariant densities for noisy maps. *Phys. Rev. A*, **44**, 6348–6363.

REIMANN, P. & P. TALKNER (1995). Escape rates for noisy maps. *Phys. Rev. E*, **51**, 4105–4113.

RIOS, P. DE LOS & Y.-C. ZHANG (1999). Universal 1/f noise from dissipative self-organized criticality models. *Phys. Rev. Lett.*, **82**, 472–475.

RISKEN, H. (1989). *The Fokker-Planck Equation.* Springer Ser. Syn. Vol 18, Berlin, Heidelberg.

ROBERT, C., K. T. ALLIGOOD, E. OTT & J. A. YORKE (1998). Outer tangency bifurcation of chaotic sets. *Phys. Rev. Lett.*, **80**, 4867–4870.

ROBERT, C., K. T. ALLIGOOD, E. OTT & J. A. YORKE (2000). Explosions of chaotic sets. *Physica D*, **144**, 44–61.

ROBINSON, C. (1983). Bifurcation to infinitely many sinks. *Commun. Math. Phys.*, **90**, 433–459.

ROLLINS, R. W. & E. R. HUNT (1984). Intermittent transient chaos at interior crises in the diode resonator. *Phys. Rev. A*, **29**, 3327–3334.

RÜCKERL, B. & C. JUNG (1994). Scaling properties of a scattering system with an incomplete horseshoe. *J. Phys. A*, **27**, 55–77.

RYABOV, V. B. & H. M. ITO (1995). Multistability and chaos in a spring-block model. *Phys. Rev. E*, **52**, 6101–6112.

SCHEFFER, M. (1990). Multiplicity of stable states in freshwater systems. *Hydrobiologica*, **200**, 475–486.

SCHICK, K. L. & A. A. VERVEAR (1974). 1/f noise with a low frequency white noise limit. *Nature (London)*, **251**, 599–601.

SCHIFF, S., K. LERGER, D. H. DUONG, T. CHANG, M. L. SPANO & W. L. DITTO (1994). Controlling chaos in the brain. *Nature (London)*, **370**, 615–620.

SCHIMANSKY-GEIER, L & H. HERZEL (1993). Positive Lyapunov exponents in the Kramers oscillator. *J. Stat. Phys.*, **70**, 141–147.

SCHMIDT, G. (1980). Stochasticity and fixed-point transitions. *Phys. Rev. A*, **22**, 2849–2854.

SCHMIDT, G. & B. W. WANG (1985). Dissipative standard map. *Phys. Rev. A*, **32**, 2994–2999.

SHANNON, C. E. (1948). The mathematical theory of communication. *Bell Syst. Tech. J.*, **27**, 379–423.

SIAPAS, A. G. (1994). Quantifying the geometric sensitivity of attractor basins: Power law dependence on parameter variations and noise. *Phys. Rev. Lett.*, **73**, 2184–2187.

SINAI, YA. G. (1959). On the concept of entropy of a dynamical system. *Dok. Acad. Nauk SSSR*, **124**, 768–771.

SMALE, S. (1967). Differentiable dynamical systems. *Bull. Amer. Math. Soc.*, **73**, 747–817.

SMELYANSKIY, V. N., M. I. DYKMAN & B. GOLDING (1999). Time oscillations of escape rates in periodically driven systems. *Phys. Rev. Lett.*, **82**, 3193–3196.

SMELYANSKIY, V. N., M. I. DYKMAN, H. RABITZ & B. E. VUGMEISTER (1997). Fluctuations, escape, and nucleation in driven systems: Logarithmic susceptibility. *Phys. Rev. Lett.*, **79**, 3113–3116.

SOMMERER, J. C., W. L. DITTO, C. GREBOGI, E. OTT & M. L. SPANO (1991a). Experimental confirmation of the scaling theory for noise-induced crises. *Phys. Rev. Lett.*, **66**, 1947–1950.

SOMMERER, J. C. & E. OTT (1993). A physical system with qualitatively uncertain dynamics. *Nature (London)*, **365**, 138–140.

SOMMERER, J. C., E. OTT & C. GREBOGI (1991b). Scaling law for characteristic times of noise-induced crises. *Phys. Rev. A*, **43**, 1754–1769.

SOSKIN, S. M. (1999). Large fluctuations in multiattractor systems and the generalized Kramers problem. *J. Stat. Phys.*, **97**, 609–676.

SOSKIN, S. M., R. MANNELLA, M. ARRAYÁS & A. N. SILCHENKO (2001a). Strong enhancement of noise-induced escape by nonadiabatic periodic driving due to transient chaos. *Phys. Rev. E*, **63**, 051111–1–6.

SOSKIN, S. M., V. I. SHEKA, T. L. LINNIK & R. MANNELLA (2001b). Short time scales in the Kramers problem: A stepwise growth of the escape flux. *Phys. Rev. Lett.*, **86**, 1665–1669.

STEWART, H. B., Y. UEDA, C. GREBOGI & J. A. YORKE (1995). Double crises in two-parameter dynamical systems. *Phys. Rev. Lett.*, **75**, 2478–2481.

SWEET, D., H. E. NUSSE & J. A. YORKE (2001). Stagger-and-step method: Detecting and computing chaotic saddles in higher dimensions. *Phys. Rev. Lett.*, **86**, 2261–2264.

SWEET, D., E. OTT & J. A. YORKE (2000). Topology in chaotic scattering. *Nature (London)*, **399**, 315–316.

SZABÓ, K. G., Y.-C. LAI, T. TÉL & C. GREBOGI (1996). Critical exponent for gap filling at crisis. *Phys. Rev. Lett.*, **77**, 3102–3105.

SZABÓ, K. G., Y.-C. LAI, T. TÉL & C. GREBOGI (2000). Topological scaling and gap filling at crisis. *Phys. Rev. E*, **61**, 5019–5032.

TEDESCHINI-LALLI, L. & J. A. YORKE (1986). How often do simple dynamical processes have infinitely many coexisting sinks? *Commun. Math. Phys.*, **106**, 635–657.

THUAL, O. & J.C. MCWILLIAMS (1992). The catastrophe structure of thermohaline convection in a two-dimensional fluid model and a comparison with low-order box models. *Geophys. Astrophys. Fluid Dyn*, **64**, 67–95.

TOROCZKAI, Z., G. KÁROLYI, Á. PÉNTEK, T. TÉL & C. GREBOGI (1998). Advection of active particles in open chaotic flows. *Phys. Rev. Lett.*, **80**, 500–503.

TSUDA, K. (1991). Chaotic itinerancy as a dynamical basis of hermeneutics in brain and mind. *World Futures*, **32**, 167–184.

VAN DEN BROECK, C., J. M. R. PARRONDO & R. TORAL (1994). Noise-induced nonequilibrium phase transition. *Phys. Rev. Lett.*, **73**, 3395–3398.

VAN KAMPEN, N. G. (1983). *Stochastic Processes in Physics and Chemistry*. North-Holland, Amsterdam.

VILAR, J. M. G. & J. M. RUBÍ (2001). Noise suppression by noise. *Phys. Rev. Lett.*, **86**, 950–953.

VION, D., M. GÖTZ, P. JOYEZ, D. ESTEVE & M. H. DEVORET (1996). Thermal activation above a dissipation barrier: Switching of a small Josephson junction. *Phys. Rev. Lett.*, **77**, 3435–3438.

VON BOEHM, J. & P. BAK (1979). Devil's stairs and the commensurate-commensurate transitions in CeSb. *Phys. Rev. Lett.*, **42**, 122–125.

VOSS, R. F. (1983). Comment on "Hopping mechanism generating 1/f noise in nonlinear systems". *Phys. Rev. Lett.*, **50**, 1329.

Voss, R. F. (1992). Evolution of long-range fractal correlations and 1/f noise in DNA base sequences. *Phys. Rev. Lett.*, **68**, 3805–3808.

Voss, R. F. & J. Clarke (1975). 1/f noise in music and speech. *Nature (London)*, **258**, 317–318.

Voss, R. F. & J. Clarke (1978). 1/f noise in music: Music from 1/f noise. *J. Acoust. Soc. Am.*, **63**, 258–263.

Wackerbauer, R. (1995). Noise-induced stabilization of the Lorenz system. *Phys. Rev. E*, **52**, 4745–4749.

Wackerbauer, R., A. Witt, H. Altmanspacher, J. Kurths & H. Schein-graber (1994). A comparative classification of complexity-measures. *Chaos, Solitons & Fractals*, **4**, 133–173.

Weissman, M. B. (1988). 1/f noise and other slow, nonexponential kinetics in condensed matter. *Rev. Mod. Phys.*, **60**, 537–571.

Wenzel, W., O. Biham & C. Jayaprakash (1991). Periodic orbits in the dissipative standard map. *Phys. Rev. A*, **43**, 6550–6557.

Wiersig, J. & K.-H. Ahn (2001). Devil's staircase in the magnetoresistance of a periodic array of scatterers. *Phys. Rev. Lett.*, **87**, 026803–1–4.

Wiesenfeld, K., C. Bracikowski, G. James & R. Roy (1990). Observation of antiphase states in a multimode laser. *Phys. Rev. Lett.*, **65**, 1749–1752.

Wiesenfeld, K. & K. Hadley (1989). Attractor crowding in oscillator arrays. *Phys. Rev. Lett.*, **62**, 1335–1338.

Witt, A., A. Neiman & J. Kurths (1997). Characterizing the dynamics of stochastic bistable systems by measures of complexity. *Phys. Rev. E*, **55**, 5050–5059.

Yang, W., M. Ding & H. Gang (1995). Trajectory (phase) selection in multistable systems: Stochastic resonance, signal bias, and the effect of signal phase. *Phys. Rev. Lett.*, **74**, 3955–3958.

Zaslavskii, G. M. (1978). The simplest case of a strange attractor. *Phys. Lett. A*, **69**, 145–147.

Życzkowski, K. & Y.-C. Lai (2000). Devil-staircase behavior of dynamical invariants in chaotic scattering. *Physica D*, **142**, 197–216.